Development of leptin responses in the Magel2-null mouse model of Prader-Willi syndrome

by

Igor Pravdivyi

A thesis submitted in partial fulfillment of the requirements for the degree of

Master of Science

Medical Sciences - Medical Genetics
University of Alberta

Abstract

An individual's body weight is tightly regulated by balancing food intake with energy expenditure. This is accomplished in part by secretion of the hormone leptin by adipocytes, an excess of which signals to reduce appetite and increase activity through action in the hypothalamic region of the brain. This signalling pathway is disrupted in an obese and underactive mouse model of Prader-Willi syndrome (PWS), which lacks the gene *Magel2*. Although loss of several genes may result in PWS-like features, we have strong evidence that *MAGEL2* plays a vital role in the development of obesity in PWS. In *Magel2*-null mice, a population of anorexigenic hypothalamic cells, which make pro-opiomelanocortin (POMC), fail to respond to leptin stimulation. Consequently, mutant POMC neurons do not secrete a factor called alpha-melanocyte-stimulating hormone (alpha-MSH), resulting in their inability to effectively regulate energy balance. The aim of my project was to further characterize the nature of faulty leptin signalling in our mutant mice and to determine whether administration of an alpha-MSH-like agonist molecule, melanotan II (MTII) can restore the energy balance.

Through immunohistochemical analysis I discovered that unlike in adults, young mutant mice have a normal number of POMC neurons. These cells are able to sense leptin at the appropriate cell surface receptor and initiate a downstream signalling cascade through phosphorylation of the nuclear transcription factor, STAT3. Further examination of cellular function using electrophysiology and calcium imaging, revealed that POMC neurons of *Magel2*-null mice are responsive to leptin at a young age but lose this capability when the mice become adults. Peripheral injection of MTII into mutant mice revealed increased sensitivity to the compound as compared to wildtype mice, which manifested itself in significantly elevated food

intake. Although not apparent at 3 weeks of age, this effect was first detected in 4 week old mice. A pilot study testing the efficacy of long-term MTII treatment on adult mutant mice failed to produce diminished food intake or body weight in the long run.

These results indicate that mice lacking *Magel2* have leptin-responsive POMC neurons at birth but lose this functionality by adulthood. Thus, they are not resistant to leptin as neonates, but rather develop insensitivity during postnatal life. The existence of a period where POMC neurons are responsive to leptin may provide a window of opportunity for preventative treatment using therapeutic agents. PWS pathology seen in humans may follow closely what we observe in our mouse model in terms of progression of leptin signalling impairments. If such is the case, results from this study may be extended to better understand the causes and origins of PWS in humans and to design drugs that counteract obesity and other related clinical manifestations of PWS.

Preface

This thesis is an original work by Igor Pravdivyi. The research project, of which this thesis is a part, received research ethics approval from the University of Alberta Research Ethics Board, “Murine homologues of Prader-Willi Syndrome (PWS) Genes”, AUP00000359, July 30, 2014.

Acknowledgements

First and foremost, I wish to thank my supervisor, Dr. Rachel Wevrick, for welcoming me to Edmonton, for continual guidance on my research project, and for valuable contributions in helping me realize my full potential. I am very grateful for the freedom that you afforded me in completing my experiments, which allowed me to balance graduate school with extracurricular activities. Your guidance has been instrumental to steering my project in the right direction and helping me to stay on track. I am thankful for the effort you put forth in assisting me to sharpen my time management skills, the feedback that contributed to the development of my presentation abilities, and the advice on conflict resolution. I also appreciate your continued support of my endeavours into medicine.

I wish to thank Dr. William Colmers for constructive critique of my project during supervisory committee meetings and help with drafting abstracts and scholarship applications. I am very grateful for your teaching of electrophysiology principles and techniques to me and for your help in troubleshooting experiments. I also wish to thank Dr. Michael Walter for inspiring leadership qualities in me and for constantly supporting my medical interests.

Thanks also to Dr. David Eisenstat for his unfaltering support of my medical passions and encouragement throughout these past two years. I am immensely grateful that you took time out of your busy schedule to give me valuable career advice and help me assess my options. I also want to thank you for establishing a neurodevelopmental framework for my project through our graduate course, which helped me excel in journal club seminars and allowed me to better understand my own work. I appreciate your feedback on my grant writing proposal and your positive input during our supervisory committee meetings.

I am thankful for all of the technical expertise and project advice provided by Jocelyn Bischof, Sheldon Michaelson, Araya Ungpakawa, Klaus Ballanyi, Xiao Li, Rebecca Mercer, and Sebastien Bouret. I would also like to thank my friends and family for their tireless support of my academic endeavours and believing in my ability to succeed.

The work in this thesis was funded by a Foundation for Prader-Willi Research operating grant. I wish to thank the following agencies that helped fund my research: Department of

Medical Genetics (Medical Genetics Recruitment Award), the Faculty of Graduate Studies and Research (Queen Elizabeth II Graduate Scholarship; Profiling Alberta's Graduate Students Award), Faculty of Medicine & Dentistry (75th Anniversary Graduate Student Award; Medical Science Graduate Program Scholarship) and the Women & Children's Health Research Institute (WCHRI Trainee Travel Funds).

Table of contents

List of Tables

List of Figures

Abbreviations

ACTH	Adrenocorticotropic hormone
AgRP	Agouti-related protein
ARC	Arcuate nucleus
BSA	Bovine serum albumin
DAPI	4',6-diamidino-2-phenylindole
DIO	Diet-induced obesity
DMN	Dorsomedial nucleus
eGFP	Enhanced green fluorescent protein
ERK	Extracellular signal-regulated kinase
GABA	Gamma-Aminobutyric acid
ip	Intraperitoneal
Jak2	Janus kinase 2
LepRb	Leptin receptor long isoform
LHA	Lateral hypothalamic area
MAGE	Melanoma-associated antigen
MAGEL2	Melanoma antigen (MAGE)-like 2
MC3R	Melanocortin 3 receptor
MC4R	Melanocortin 4 receptor
MHD	MAGE homology domain
α-MSH	Alpha-melanocyte-stimulating hormone
MTII	Melanotan II
MFMR	Multifunctional mosaic region
NGS	Normal goat serum
NPY	Neuropeptide Y
NTS	Nucleus tractus solitarius
OCT	Optimal cutting temperature compound
PBS	Phosphate buffered saline
PFA	Paraformaldehyde
POMC	Pro-opiomelanocortin

PVN	Paraventricular nucleus
PWS	Prader-Willi syndrome
RING	Really interesting new gene
SCN	Suprachiasmatic nucleus
SHP2	Tyrosine-protein phosphatase non-receptor type 11
SmN	Small nuclear ribonucleoprotein N
snoRNA	Small nucleolar RNA
SOCS3	Suppressor of cytokine signalling-3
SON	Supraoptic nucleus
STAT3	Signal transducer and activator of transcription 3
UPD	Uniparental disomy
VCA	Verprolin homologous or WH2, central hydrophobic, and acidic
VMN	Ventromedial nucleus
WASH	Wiskott-Aldrich syndrome protein and scar homolog

Chapter 1. Introduction

1.1 Prader-Willi syndrome

1.1.1 Patient phenotype

Prader-Willi syndrome (PWS), less commonly known as Prader-Labhart-Willi syndrome, is named after the three physicians who documented similar clinical features among nine patients in 1956 (Prader et al., 1956). The disorder was originally called polysarcia when it was first documented by Langdon-Down (Down, 1887). He described a 13 year-old female patient who was 84 kg at only 1.32 m tall, had small hands and feet but remarkably long appendages, and showed cognitive impairment. At age 25 she had virtually no pubic or axillary hair and had never menstruated nor shown any sexual interest. These are only some of the characteristics found in PWS patients today.

Clinical features of PWS are now well-defined, although they change with age (Fig. 1). Holm et al. presented a set of diagnostic criteria compiled through the expert opinions of a group of healthcare professionals with many years of experience with PWS (Holm et al., 1993). These criteria are divided into three groups: major, minor and supportive. Major criteria comprise feeding problems in infancy, failure to thrive, characteristic facial features (narrow face, almond-shaped eyes, down-turned corners of mouth), hypogonadism, developmental delay/learning problems, and hyperphagia (Schulze et al., 1996). Minor criteria include characteristic behaviour (aggressive outbursts, rigid personality, perseveration), sleep disturbance, short stature, hypopigmentation, small hands/feet, eye abnormalities, and skin picking. Major criteria are awarded one point whereas minor criteria receive a half point. Since infants and children under the age of 3 years display fewer signs of PWS, historically they only needed five points in total (four of which must have come from major criteria) to be diagnosed with PWS; older children and adults had to accumulate at least 8 points (minimum of five points from major category). Supportive criteria include less frequent and nonspecific clinical features and when present, served to increase the confidence of diagnosis. However today, these criteria only serve to direct patient samples to molecular diagnostic facilities for definitive genetic testing. It has been suggested that the presence of unexplained hypotonia with poor suck may

Figure 1. Classic morphological features observed in patients with Prader-Willi syndrome. A) 2 ½ year old girl, and B) a 21-year-old male. Note the central obesity, typical facial appearance and skin picking lesions. Adapted from (Cassidy and Driscoll, 2009).

necessitate genetic testing, even in the absence of other clinical signs (Gunay-Aygun et al., 2001).

PWS is an intriguing disorder in that patients experience various nutritional phases throughout their lifespan. Miller et al. proposed that affected individuals progress through a series of five distinct phases that also include several subphases (Miller et al., 2011). Foetuses experience phase 0 *in utero*, showing decreased foetal movement and having a lower birth weight. From birth to 9 months of age, infants are in phase 1a, characterized by hypotonia and feeding difficulty. As they progress into phase 1b that lasts to about 25 months of age, babies no longer experience feeding difficulty and grow appropriately. Phase 2a manifests itself in increased body weight with no abnormalities in appetite or calorie intake and lasts until 4.5 years of age. Weight continues to increase throughout phase 2b, which lasts until 8 years of age, but is now accompanied by increasing appetite. As children progress into phase 3, they become hyperphagic and develop an insatiable appetite with an inability to feel full. Lasting into adulthood, phase 3 is the ultimate phase for the majority of PWS patients. Interestingly, adults may enter a rare phase 4, characterized by improved appetite control and an ability to feel full.

The hyperphagia and increased body weight are hallmarks of PWS that categorize it as a form of genetic obesity. With an estimated prevalence of 1 in 10,000 to 25,000 live births, PWS involves the most common genetic defect in human obesity (Butler, 1990), second only to genetically determined melanocortin 4 receptor (MC4R) deficiency (Farooqi et al., 2003). Individuals with PWS have a sixfold relative risk of death when compared to other developmentally disabled patients (Einfeld et al., 2006), which is attributed to obesity and related complications. Cardiovascular problems, gastric illness and sleep apnea are the most common causes of death in adults with PWS (Hertz et al., 1995, Schrander-Stumpel et al., 2004), whereas children are most likely to die from respiratory and febrile disorders (Stevenson et al., 2004, Tauber et al., 2008). Morbidity results from obesity-related diabetes mellitus, thrombophlebitis, and skin problems such as infections and chronic edema that result from skin picking (Schrander-Stumpel et al., 2004). The combination of high disease prevalence and gravity of complications related to obesity highlight the importance of studying PWS etiology.

1.1.2 Genetics of Prader-Willi syndrome

Although familial inheritance of PWS was previously reported (Hall and Smith, 1972, Jancar, 1971, Clarren and Smith, 1977), the vast majority of cases are sporadic. One of the first chromosomal analyses involving 39 PWS patients revealed that the majority had an interstitial deletion on chromosome 15 between breakpoints q11 and q13 while the remainder had an apparently normal karyotype (Butler et al., 1986). Other studies of PWS patients identified duplications and translocations (unbalanced as well as balanced) involving the 15q11-q13 region (Butler, 1990). This locus is particularly susceptible to such rearrangements because of its inherent instability due to flanking low-copy repeats that have ≥95% sequence identity (Sharp et al., 2006). The pathogenicity of these rearrangements labels PWS as a genomic disorder (Lupski, 1998). Angelman syndrome is another genomic disorder involving deletions within the 15q11-q13 region. The difference between PWS and the latter is whether the deletion resides on the paternal or maternal copy of chromosome 15, respectively. In a process known as genomic imprinting, epigenetic modifications (such as methylation and histone modification) tag certain regions of germline DNA, which either allows or forbids transcription from tagged parent-specific alleles in cells of the offspring. Thus, for imprinted genes, only one allele is ever expressed while the other is permanently silenced by the imprinting. The 15q11-q13 gene locus contains a maternally imprinted (silenced) PWS region, and deletions within this region on the paternal chromosome result in loss of function of genes contained therein (Horsthemke and Buiting, 2006).

Based on meta-analyses, it is estimated that 70% of PWS patients harbour deletions in 15q11-q13 involving one of two common proximal breakpoints (BP1 or BP2) and the common distal breakpoint BP3 (Cassidy et al., 2012). The 250-400 kb low-copy repeats that surround these breakpoints encourage nonhomologous recombination of 15q11-q13 during meiosis, resulting in the deletions, as well as other chromosomal rearrangements. Roughly 25% of individuals affected by PWS have two maternal copies of chromosome 15 but no paternal copies, known as uniparental disomy (UPD). The most likely explanation of UPD is that meiotic nondisjunction creates a disomic ovum. The ovum is then fertilized with normal sperm leading to trisomy but the paternal chromosome is lost as the blastocyst divides (Cassidy et al., 2012). A

third mechanism involving imprinting defects accounts for the remainder of PWS cases. In these patients random errors in imprinting during spermatogenesis are believed to silence the paternal allele, leaving offspring with a PWS region devoid of active non-imprinted genes (Glenn et al., 1997).

In addition to the three common breakpoints (BP1—3), chromosomal region 15q11-q13 contains two rare breakpoints (BP4 and BP5) and clusters of genes, some of which are under imprinting epigenetic regulation (Fig. 2). PWS patients typically harbour 5.3—6 Mb interstitial deletions in this region, with the smaller deletion corresponding to BP2—BP3 (type 2 deletion) and the larger one involving BP1—BP3 (type 1 deletion) (Kim et al., 2012). Both types share a 1.8 Mb segment dubbed the "PWS region", containing only maternally imprinted (silenced) genes. This region is regulated through an imprinting center that overlaps with the promoter and exon 1 of the *SNURF-SNURPN* gene. The imprinting center consists of *cis* acting CpG islands that are methylated on the maternally inherited silenced allele and unmethylated on the paternally inherited expressed allele. The *SNURF-SNURPN* gene itself produces small nuclear ribonucleoprotein N (SmN) from exons 4-10, which is involved in mRNA splicing (Glenn et al., 1996), and a polypeptide of unknown function from exons 1-3 (Gray et al., 1999). Identification of PWS patients with balanced translocations involving *SNURF-SNURPN* excluded this gene as a pathogenic candidate (Buiting, 2010). Interestingly, *SNURF-SNURPN* acts as a host gene to six C/D box small nucleolar RNAs (snoRNAs), thereby regulating their expression. These snoRNAs are: *SNORD107*, *SNORD64*, *SNORD109A*, *SNORD116*, *SNORD115* and *SNORD109B*, which are thought to be involved in alternative mRNA splicing and each may have more than one target (Kishore and Stamm, 2006). *SNORD115* is not a likely contributor to the PWS phenotype because a family was identified in which this gene was deleted in its entirety, yet paternal inheritance failed to produce a clinical phenotype (Runte et al., 2005). On the other hand, a patient with a microdeletion encompassing the entire length of *SNORD116* met diagnostic criteria for PWS (Sahoo et al., 2008). However, this patient also had tall stature as a child and a large head circumference—atypical findings for PWS. Furthermore, three other patients were reported with different microdeletions that also encompass the entire length of *SNORD116*; although they had PWS-like characteristics, they failed to meet PWS diagnostic criteria (de Smith et al., 2009, Duker et al., 2010, Bieth et al., 2014). This suggests that although

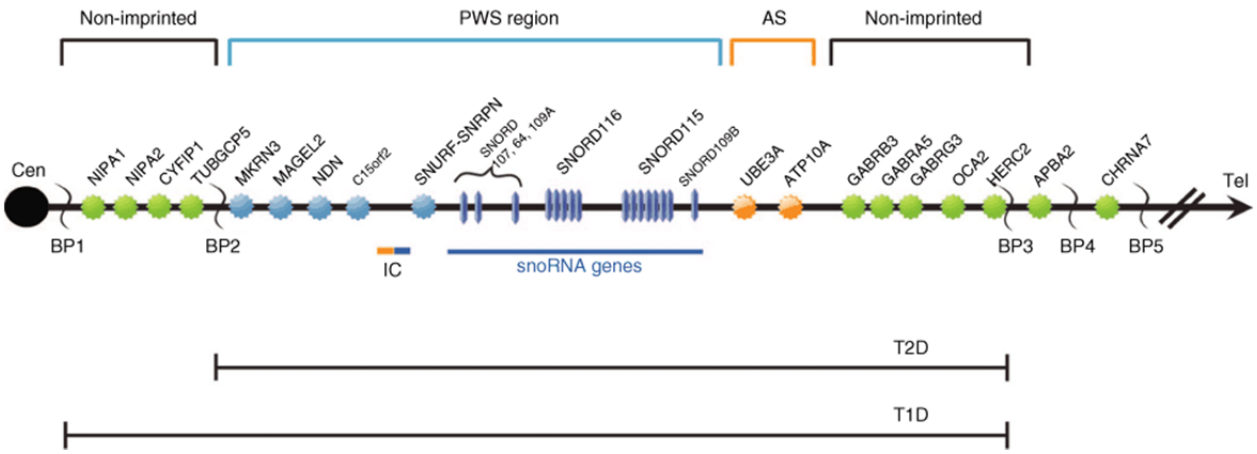

Figure 2. Genetic map of human chromosomal region 15q11-q13. Maternally imprinted (blue), paternally imprinted (orange) and non-imprinted (green) genes are found herein. The Prader-Willi syndrome (PWS) region contains the imprinting centre (IC). BP1-BP5, breakpoints; AS, Angelman syndrome region; T1D, type 1 deletion; T2D, type 2 deletion. Note that there are more copies of the *SNORD116* and *SNORD115* genes than depicted here and this map is not drawn to scale. Adapted from (Cassidy et al., 2012).

SNORD116 is an important contributor to the PWS phenotype, other genes also play an important role.

Four maternally imprinted genes are found centromeric to the PWS imprinting center on chromosome 15: *C15orf2*, *MKRN3*, *NDN* and *MAGEL2*. *C15orf2* (also known as *NPAP1*) is expressed in the testes and fetal brain but silenced via methylation in other tissues; it encodes a nuclear-pore-complex-associated protein (Farber et al., 2000, Wawrzik et al., 2010, Neumann et al., 2012). This gene has no murine ortholog and is specific to the primate lineage (Neumann et al., 2014). Its potential contribution to the PWS phenotype is not yet established. *MKRN3*, which is paternally expressed in the brain and germ cells, encodes a protein containing multiple zinc finger motifs suggestive of a ribonucleoprotein role (Jong et al., 1999). Recently, mutations in *MKRN3* were identified that disrupt protein function and correlate with an early pubertal onset (Abreu et al., 2013). Since early sexual maturation is a clinical finding of PWS patients, the loss of this gene may contribute in part to the PWS phenotype. *NDN* encodes necdin, and is paternally expressed in many tissues including the brain, placenta, skeletal muscle, pancreas, lungs, kidneys and liver (MacDonald and Wevrick, 1997). Necdin has been implicated in a variety of cellular roles: migration, differentiation and cell survival (Bush and Wevrick, 2010, Cypess et al., 2011, Lafontaine et al., 2012). In mice, a lack of necdin reduces the number of gonadotropin-releasing hormone neurons in the brain and impairs their migration, suggesting that loss of function of *NDN* may account for some of the hypogonadism and infertility seen in PWS patients (Muscatelli et al., 2000, Miller et al., 2009). Additionally, necdin deficiency impairs central respiratory drive and results in sleep apnea in mice—findings which mirror what clinicians see in some PWS patients (Zanella et al., 2008, Ren et al., 2003). *MAGEL2* is discussed in the following section.

1.1.3 *MAGEL2* and Prader-Willi syndrome

Recently, four patients were identified with point mutations in *MAGEL2* that result in truncated protein, either due to frame shift mutations or a premature stop codon (Schaaf et al., 2013). Three of these individuals displayed PWS-like characteristics but did not score high

enough on the diagnostic criteria established by Holm to be labelled as PWS patients. However, the fourth person having a heterozygous c.1802delC (p.Pro601fs) mutation met these diagnostic criteria, and represents the first case of PWS with a mutation/deletion in *MAGEL2* but no other genomic abnormalities. All four of these mutations occurred on the paternal (expressed) allele and are predicted to be causative factors for the phenotypes observed (Fig. 3). Thus, *MAGEL2* contributes to the clinical phenotype characteristic of PWS patients.

MAGEL2 (Gene ID: 54551) is an intronless gene that spans 4298 bp and contains a single exon. Bases 105-3854 encompass the coding region for the MAGEL2 protein (NP_061939), which is 1249 aa long. The protein contains three conserved domains: proline-rich domain (aa 53 → 225), G-box binding protein multifunctional mosaic region (MFMR) (112 → 224), and MAGE homology domain (aa 1027 → 1197). Since several protein-protein interaction domains prefer proline-rich ligands (Kay et al., 2000), the proline-rich domain (which contains the G-box binding protein MFMR domain) of MAGEL2 may interact with yet unidentified proteins. The details of molecular interactions involving the MAGE homology domain (MHD) are better understood.

The MHD is a common element of MAGE class genes named after human melanoma antigen A1 (*MAGE-A1*), the first member of this gene family to be discovered. Originally precursors of tumour antigens presenting on melanomas, these genes are now classified into types I and II (van der Bruggen et al., 1991). Type I MAGE genes are localized to the X chromosome and only expressed in the testes, trophoblast, and placenta (Chomez et al., 2001); elsewhere they are silenced through methylation, but epigenetic reprogramming that sometimes occurs in tumours can lead to their ectopic expression (Simpson et al., 2005). In contrast, type II MAGE genes, including *MAGEL2*, are widely expressed in many tissues and are not restricted to the X chromosome (Ohman-Forslund and Nordqvist, 2001). The unravelling of molecular function of the MHD that is common to all MAGE proteins (both types I and II) began only recently. Doyle et al. established that MHD interacts with proteins that possess a really interesting new gene (RING) domain (Doyle et al., 2010). Surprisingly, the MHD does not bind to the RING domain itself but rather to various unrelated protein modules found on binding partners of MAGE proteins. The MHD may be able to do so through internal conformational changes enabled by a flexible linker connecting its two winged helices. Despite this binding

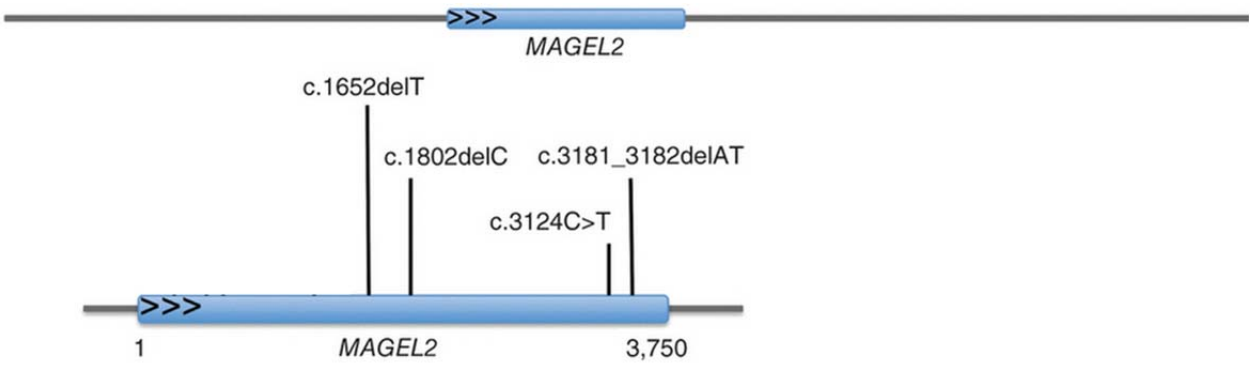

Figure 3. Reported *MAGEL2* mutations. Four human patients with PWS-like characteristics have been identified who have truncating mutations in *MAGEL2*. This gene contains a single exon and no introns. Adapted from (Schaaf et al., 2013).

plasticity, the MHD has high functional specificity and only binds to RING domain-containing proteins, many of which are E3 ubiquitin ligases (Lorick et al., 1999). This protein-protein interaction enhances the activity of E3 RING ubiquitin ligases (Doyle et al., 2010). More recent work reveals a role of *MAGEL2* in endosomal protein recycling, which involves an interaction with an E3 RING ubiquitin ligase (Hao et al., 2013).

Endosomal protein recycling uses retrograde transport to return membrane proteins from endosomes to the trans-Golgi network or the plasma membrane (Fig. 4). An important initiation step in this process is the recognition of retrograde cargo, which occurs through a retromer protein complex (Bonifacino and Rojas, 2006). Next, the retromer subunit VPS35 recruits another protein complex to the endosome— Wiskott-Aldrich syndrome protein and scar homolog (WASH) (Harbour et al., 2012). In the default state, an important motif of WASH is autoinhibited through inter- and intramolecular interactions (Chen et al., 2010). This motif is called VCA (verprolin homologous or WH2, central hydrophobic, and acidic) and to activate it, WASH must be ubiquitinated through K63-linked ubiquitin chains. Once activated, the VCA motif of WASH binds actin and the Arp2/3 complex to stimulate actin filament nucleation, allowing for fission of endosomes during the recycling process (Derivery et al., 2009). MAGEL2 is involved in this process through its interaction with the E3 RING ubiquitin ligase TRIM27. This protein-protein interaction enhances the enzymatic activity of TRIM27, which enables the latter to ubiquitinate WASH thereby activating the VCA motif (Hao et al., 2013). Without MAGEL2, endosomal F-actin nucleation is highly inefficient and reduced to levels achieved with WASH-RNAi, which greatly impairs endosomal protein recycling (Hao et al., 2013).

1.1.4 *MAGEL2* expression patterns

To further illuminate the contribution of *MAGEL2* to the clinical phenotype of PWS, several studies examined gene expression patterns of *MAGEL2* and its mouse ortholog, *Magel2*. The human gene shows highest expression levels in the adult brain, which is comparable across the frontal, occipital and temporal lobes, as well as the putamen, medulla and cerebral cortex. Low levels of *MAGEL2* expression were also discovered in the adult spinal cord and cerebellum.

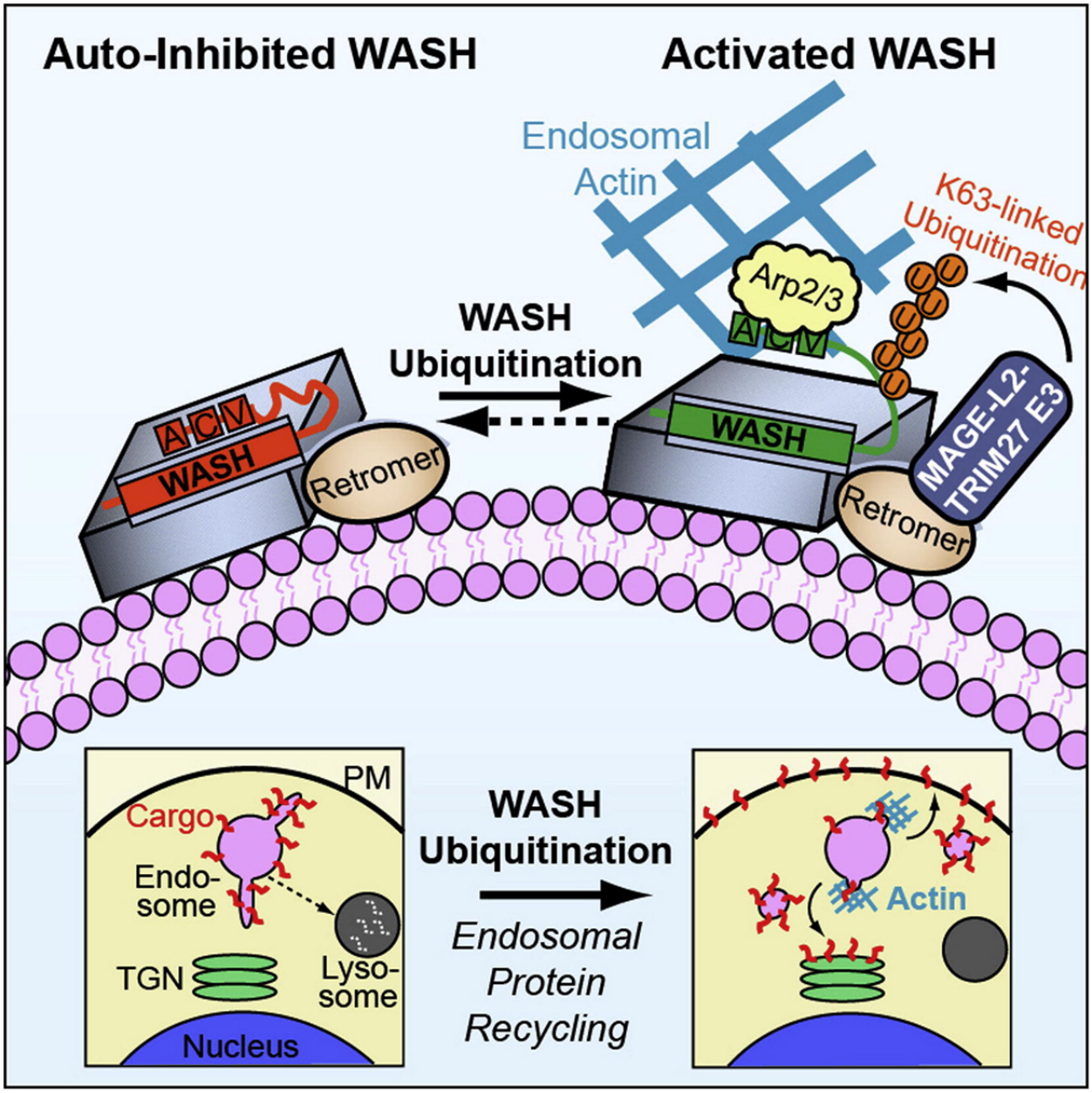

Figure 4. **Role of MAGEL2 in retrograde endosomal transport.** MAGEL2 binds to the E3 ubiquitin ligase TRIM27 to enhance its activity. Subsequent ubiquitination of the WASH complex by TRIM27 activates WASH and leads to Arp2/3-dependent actin filament nucleation. When WASH is inactive, endosomes are targeted for lysosomal degradation but its ubiquitination inhibits this process and activates recycling of endosomes back to the trans-Golgi network (TGN) and the plasma membrane (PM). VCA, verprolin homologous or WH2, central hydrophobic, and acidic motif of the WASH complex. Adapted from (Hao et al., 2013).

Foetal *MAGEL2* expression was detected not only in the brain but also in peripheral tissues: lung, liver and kidney (Lee et al., 2000). The expression pattern of the mouse ortholog *Magel2*, which encodes a protein of 72% amino acid similarity to its human counterpart (Lee et al., 2000), has been explored in some detail. In the adult mouse, *Magel2* expression is mainly restricted to hypothalamic nuclei within the brain, specifically the arcuate (ARC), paraventricular (PVN), ventromedial (VMN), suprachiasmatic (SCN), and supraoptic (SON) nuclei (Fig. 5). There are some neurons with high levels of expression in the external capsule, lateral and triangular septal nuclei, bed nucleus of stria terminalis, lateral geniculate nuclei and amygdala. Interestingly, *Magel2* expression in adult hypothalamic nuclei (ARC, PVN, VMN, SCN) is circadian rhythm-dependent. For instance, *Magel2* mRNA levels in the ARC experience a 5.1-fold change between daily peaks and troughs. Even more striking is that these fluctuations persist (albeit at diminished levels) when mice are isolated from light cues by being kept in total darkness (Kozlov et al., 2007). Embryonic *Magel2* expression is more widespread than in the adult mouse, which resembles findings of human tissue analysis. In mid-gestation embryos, *Magel2* is most highly expressed in the hypothalamus, forebrain, midbrain, and neural tube (Fig. 6). There is also expression in dorsal root ganglia, peripheral neurons innervating limb and trunk muscles, genital tubercle, placenta, and midgut region (Kozlov et al., 2007). At later embryonic stages (E15.5, 18.5) *Magel2* expression declines in the forebrain, the gene remains highly expressed in the ARC and PVN, among other hypothalamic nuclei (Lee et al., 2003).

1.1.5 Mouse model for Prader-Willi syndrome

Like the human PWS region localized to 15q11-q13, mice have an orthologous locus on chromosome 7B, also maternally imprinted. Considering the possibility of multiple gene involvement in PWS etiology, several mouse models have been developed that harbour deletions in specific genes/loci on chromosome 7B. A common theme among many of these models is partial recapitulation of the PWS phenotype combined with perinatal/early postnatal lethality, which limits their usefulness (Muscatelli et al., 2000, Bressler et al., 2001, Tsai et al., 1999). Our

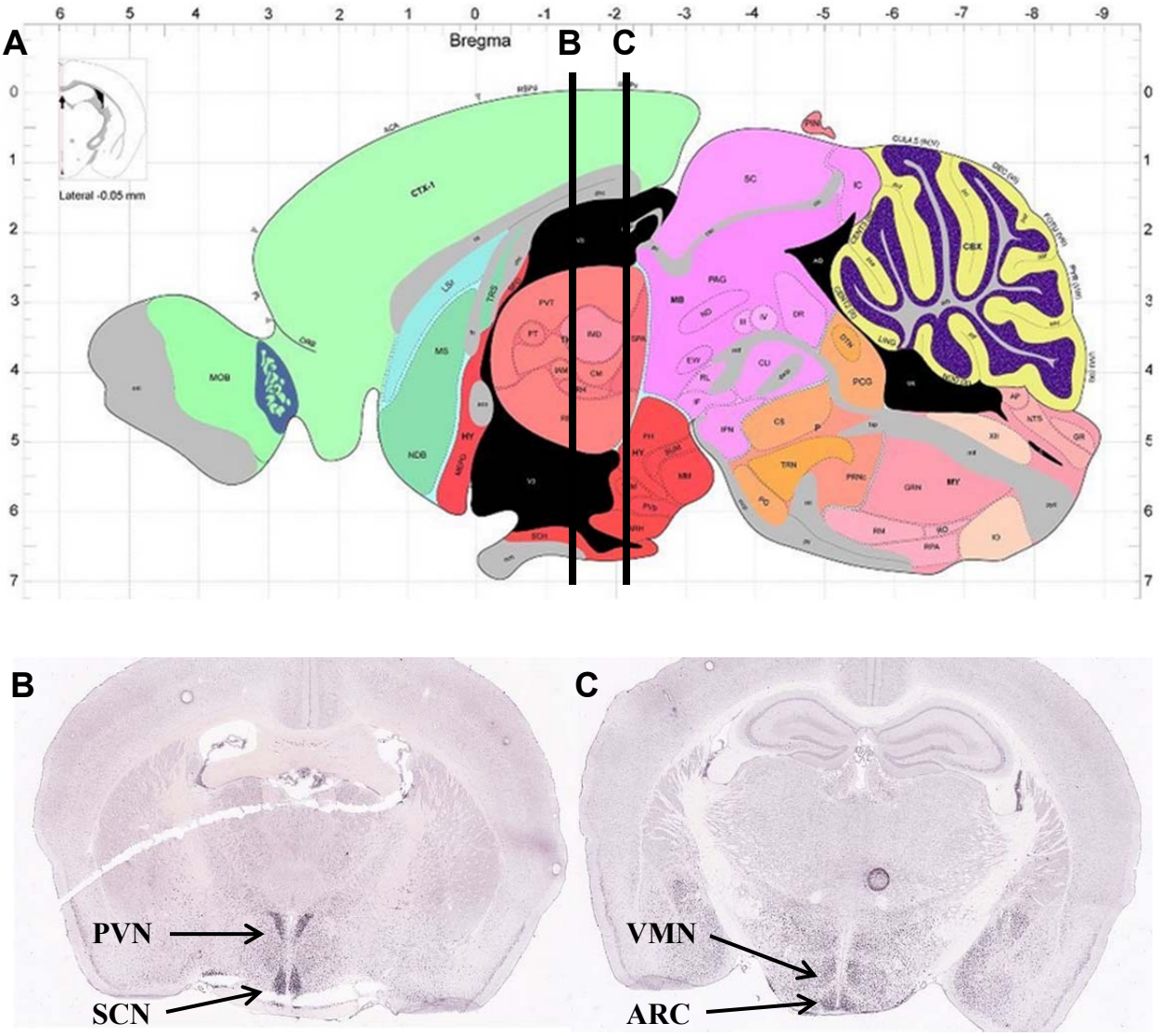

Figure 5. Expression of *Magel2* in the adult mouse brain. A) Midsagittal section showing various brain areas, where hypothalamic nuclei are labelled in red. B-C) Coronal sections corresponding to B and C in A. *Magel2* is found predominantly within hypothalamic nuclei: paraventricular (PVN), suprachiasmatic (SCN), ventromedial (VMN) and arcuate (ARC). Adapted from (Lein et al., 2007).

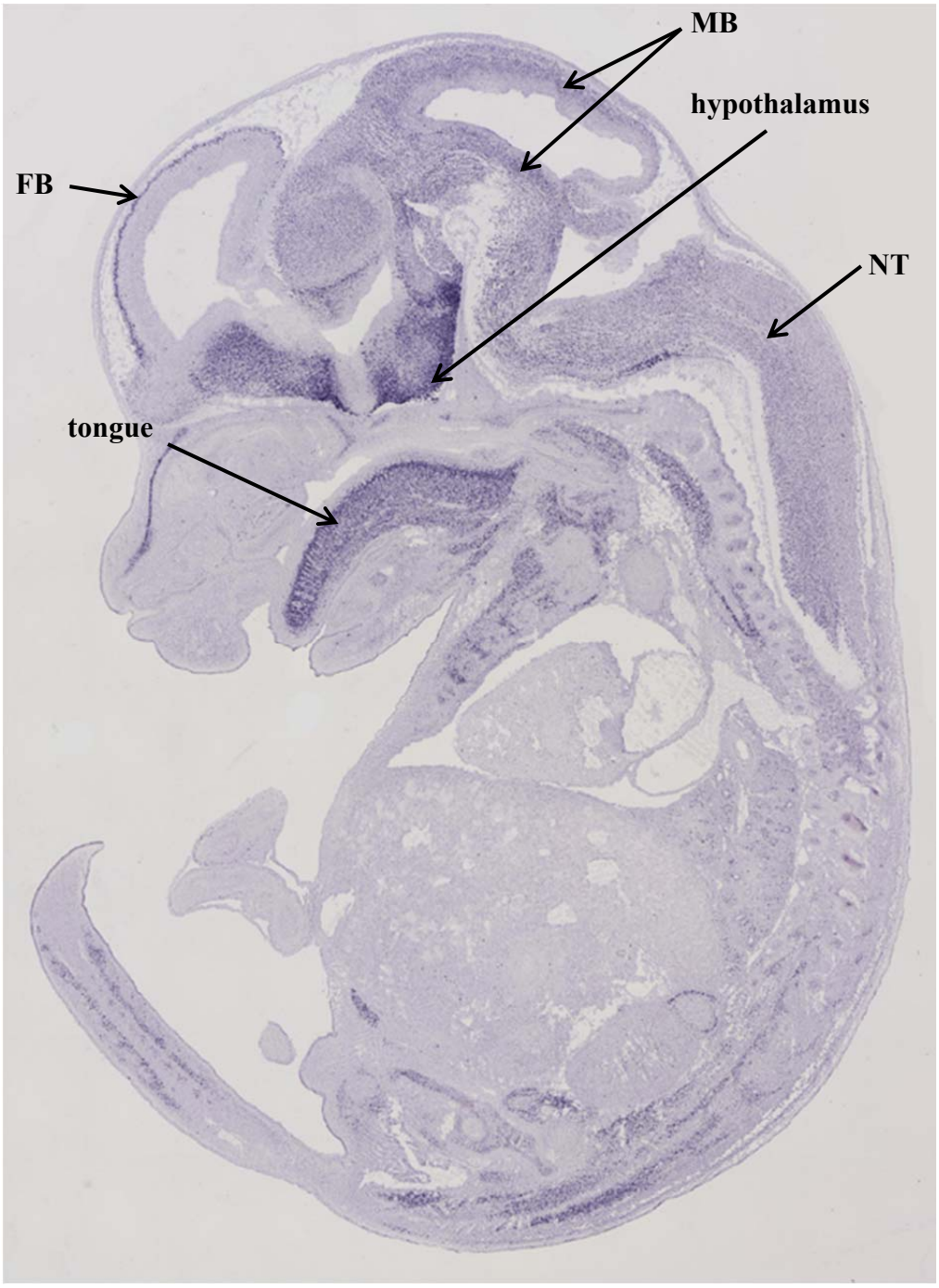

Figure 6. Embryonic expression of *Magel2* in mice. Midsagittal section at E14.5 showing strong expression of *Magel2* in the developing hypothalamus, forebrain (FB), midbrain (MB), neural tube (NT) and tongue. Adapted from (Diez-Roux et al., 2011).

mice carry a maternally-inherited imprinted (silenced) *Magel2* allele and a paternally-inherited (expressed) *Magel2-lacZ* knock-in allele, whereby they produce a β-galactosidase reporter protein instead of Magel2 from paternal allele transcripts, and also lack Magel2 production from the imprinted maternal allele, rendering them null for Magel2 protein. Although these mutant mice are born at a frequency 10% lower than expected, *Magel2*-null pups have postnatal survival rates similar to those expected of wildtype littermates (Kozlov et al., 2007, Mercer and Wevrick, 2009). In addition to high viability, our *Magel2*-null mice display several abnormalities that reflect crucial aspects of the PWS phenotype seen in humans.

Male and female PWS patients typically have hypogonadism, characterized by genital hypoplasia, incomplete pubertal development, and infertility (Eiholzer et al., 2006). Similarly, *Magel2*-null mice have a number of reproductive defects: decreased testosterone levels in males, delayed and lengthened puberty in females, prolonged oestrous cycles, reduced olfactory preference for females odours, and early reproductive termination (Mercer and Wevrick, 2009). Endocrine issues are also common among PWS patients, including central hypothyroidism and impaired glucose tolerance. *Magel2*-null mice have reduced levels of T_4 (suggestive of central hypothyroidism), weakened glucose tolerance, and delayed counterregulatory response to hypoglycaemia, indicating hypothalamic defects (Tennese and Wevrick, 2011). Interestingly, hypothalamic defects have been observed in a number of mouse models for genetic obesity such as the leptin-deficient mouse and mice lacking melanocortin 4 receptor receptors (Oltmans, 1983, Himms-Hagen, 1985, Butler and Cone, 2002).

Obesity—a crucial clinical finding in PWS—significantly contributes to morbidity and mortality of affected individuals but its etiology in PWS remains unknown. Our mouse model recapitulates the obese phenotype. Although *Magel2*-null postnatal day 1 (P1) newborns are of normal weight (unlike human newborns who are underweight at birth), growth retardation occurs in the pups soon after. Between P7 and the age of weaning (P21), *Magel2*-null pups are significantly lighter than wildtypes. After weaning, mutant pups enter a phase where they gain weight more rapidly than their wildtype counterparts. The fastest weight gains are observed between 4 and 6 weeks of age, and by 5-6 weeks, *Magel2*-null mutants and wildtype mice have equal body weights. Moreover, mutants continue to gain weight up until 12 weeks of age and perhaps beyond (Bischof et al., 2007). This excessive weight gain corresponds well with PWS

phase 2a where children progressively gain weight without an increase in appetite or calorie intake (Miller et al., 2011). In humans, true hyperphagia does not develop until later (phase 3), and is not a characteristic of our *Magel2*-null mouse model. Adult mutants have normal crown-to-rump lengths, reduced lean mass but increased fat mass. Whereas the brain, heart, liver and kidneys are of comparable mass between genotypes, adult *Magel2*-null mice have epididymal and retroperitoneal fat pads that are more than twice as heavy compared to those of wildtypes, which helps explain the increased body weight. Their adiposity cannot be due to hyperphagia because mutant adults consume 10% less food than wildtypes (Bischof et al., 2007). Instead, it may be explained by reduced physical activity. In wheel running experiments, *Magel2*-null mutants exercise in more frequent but much shorter bouts than wildtype littermates (Kozlov et al., 2007). These studies characterize the overweight phenotype of *Magel2*-null mutants as being accompanied by reduced energy expenditure, findings consistent with obesity and decreased activity seen in children with PWS (Butler et al., 2007).

1.2 Central nervous system control of energy balance

1.2.1 Neuronal sensing of adiposity signals

As part of an ongoing effort to maintain a steady supply of energy for metabolic processes, the body fine tunes a balance between energy intake and energy expenditure in a process called energy homeostasis. This process tightly regulates the amount of body fuel stored as fat in adipocytes, which constitute white adipose tissue. In normal-weight individuals, homeostatic mechanisms protect a weight set-point from fluctuations inducible by voluntary caloric restriction or overfeeding (Leibel et al., 1995). Notably, the body is better suited to defend its weight during periods of starvation than during excessive caloric consumption (Farias et al., 2011). Obesity results from increased caloric intake and the recalibration of the weight set-point to an elevated level, which the body then vigorously defends to prevent weight loss. If an obese individual attempts to lose weight through voluntary caloric restriction, the body may

upregulate receptors to certain adiposity signals to ensure that this person's energy expenditure matches energy intake, sustaining body weight at the new elevated set-point.

Two types of signals regulate energy homeostasis: short-term and long-term. The short term players are responsible for the perception of satiety and the initiation and termination of a meal as well as meal size (Strubbe and Woods, 2004). Food intake distends the stomach and activates vagal nerve afferents through stretch receptors. Similarly, the presence of long-chain fatty acids and proteins in the small intestine causes mucosal endocrine cell release of cholecystokinin, which in turn stimulates vagal afferents. These nerves transmit satiety signals to the nucleus tractus solitarius (NTS) in the hindbrain, which relays this information to higher regions of the brain and to autonomic motor nuclei for further processing and appropriate efferent output (Solomon et al., 2006). Notably, other short-acting gastrointestinal hormones such as peptide YY3–36 and ghrelin are also involved in energy homeostasis regulation through satiety signalling pathways (Ritter, 2004). In contrast, there are two regulators of long-term energy homeostasis: insulin and leptin. Both of these peptide hormones meet the proposed criteria for negative feedback regulation of adiposity. They: 1) circulate in the blood at levels proportionate to body fat content and enter the brain, 2) act on neuronal systems to stimulate weight loss, and 3) their absence promotes increased food intake and body weight gain (Morton et al., 2006). The level of circulating insulin is directly proportional to adiposity and to blood glucose levels (Woods et al., 1996). Similarly, levels of circulating leptin reflect fat stores but also depend on insulin (Mueller et al., 1998). Nevertheless, meal consumption does not significantly increase levels of leptin in the blood (Considine et al., 1996). Importantly, leptin has a more crucial role in energy homeostasis than insulin, and the subsequent discussion focuses on leptin signalling pathways (Schwartz et al., 2000).

Leptin is a peptide hormone made predominantly by white adipose tissue. Nevertheless, low levels of gene expression are also reported in brain, pituitary, trophoblast, stomach, mammary epithelial cells, liver, chondrocytes, and muscle (Wrann et al., 2012). Larger adipocytes secrete more leptin than smaller adipocytes, which explains the linear relationship between fat stores and plasma leptin (Lonnqvist et al., 1997). Two isoforms of the leptin receptor exist: the short and long form. Although both can transduce leptin signals, the long form (LepRb) is five times more efficient at doing so (Bjorbaek et al., 1997). The short form is found in high

concentration in brain microvasculature and transports leptin across endothelial cells of the blood-brain-barrier (Bjorbaek et al., 1998, Hileman et al., 2002). LepRb, on the other hand, is the main receptor that mediates leptin signal transduction. Throughout the body there are many regions expressing leptin receptors but the most important one for energy homeostasis is the central nervous system. Within the brain, LepRb mRNA is expressed in a number of hypothalamic nuclei including the dorsomedial (DMN), paraventricular (PVN), ventromedial (VMN) and arcuate (ARC) nuclei (Mercer et al., 1996). The coordinated action of these nuclei likely contributes to central regulation of energy homeostasis by leptin. A mouse study found that leptin can act directly on neurons of the DMN to increase sympathetic outflow to brown adipose tissue, which causes it to produce heat through thermogenesis (Enriori et al., 2011). This is one mechanism though which leptin can counteract increased adiposity. It can also stimulate oxytocin neurons of the PVN, which likely inhibits food intake and increases energy expenditure (Perello and Raingo, 2013). In the VMN, leptin activates steroidogenic factor-1-positive neurons, restraining body weight (Dhillon et al., 2006). However, the ARC has garnered the most attention and is widely accepted as leptin's main site of action for control of energy homeostasis.

1.2.2 Hypothalamic control of energy homeostasis

Although the ARC is composed of a diverse population of neurons, two types of first-order neurons play a vital role in leptin-mediated energy homeostasis and produce opposing physiological actions (Fig. 7). The orexigenic neuron, dubbed NPY/AgRP, coexpresses neuropeptide Y (NPY) and agouti-related protein (AgRP) and releases gamma-aminobutyric acid (GABA). The anorexigenic, POMC neuron, expresses pro-opiomelanocortin (POMC). Interestingly, not all NPY/AgRP and POMC neurons have leptin receptors, suggesting heterogeneity within these populations (Williams et al., 2010). Perhaps as an adaptive response to nutrient scarcity, which predictably correlates with low levels of circulating leptin, NPY/AgRP neurons tonically inhibit POMC neuronal firing to promote food consumption and reduced energy expenditure. This occurs through GABAergic inhibition as well as the action of

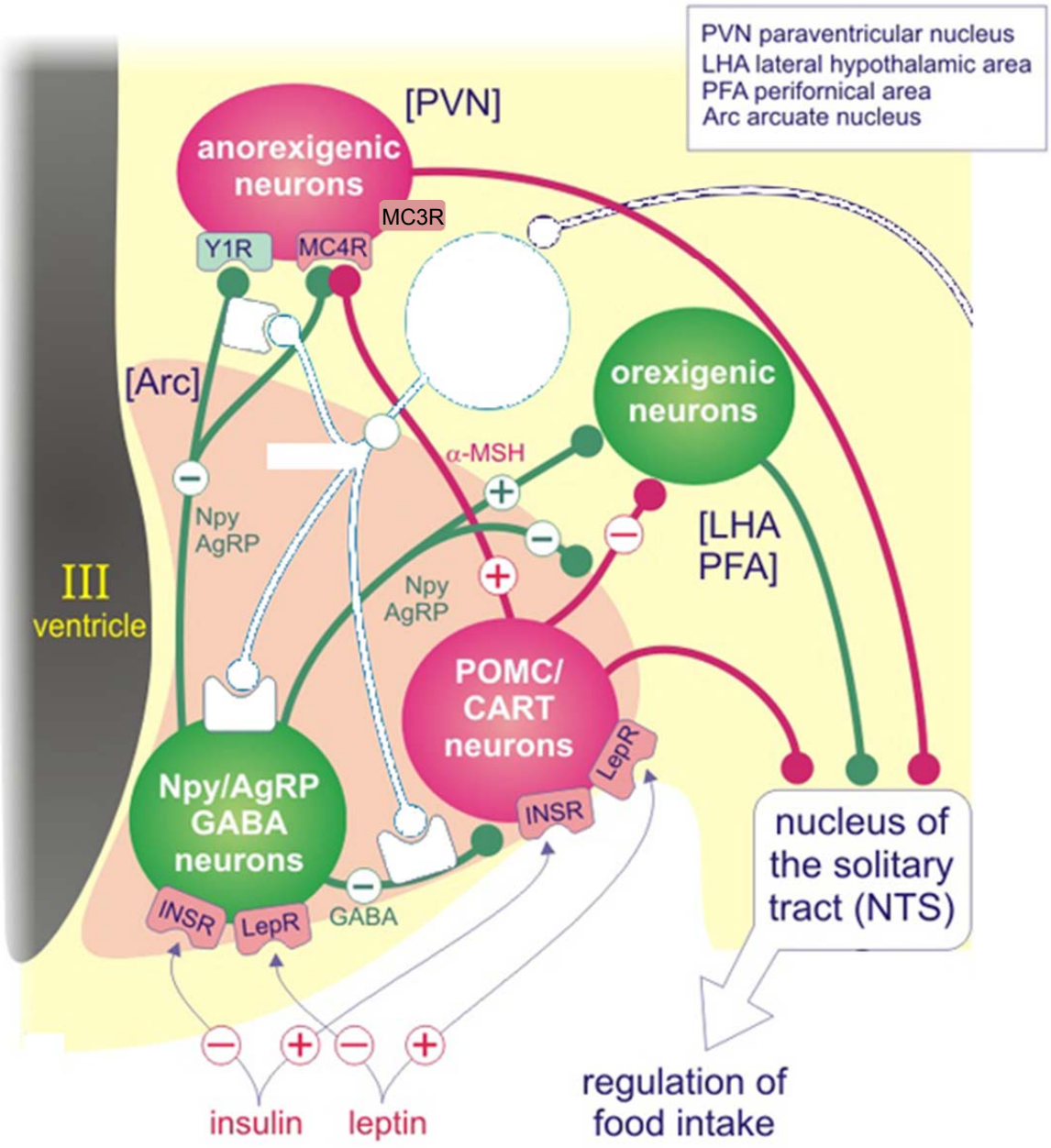

Figure 7. Hypothalamic control of energy homeostasis. Leptin and insulin both regulate energy homeostasis through the NPY/AgRP and POMC neurons found in the ARC. NPY/AgRP neurons tonically inhibit POMC neurons though GABA and NPY. High levels of circulating leptin inhibit NPY/AgRP neurons and stimulate α-MSH release from POMC neurons. The ARC neurons have antagonistic actions on MC4R receptors of anorexigenic neurons in the paraventricular nucleus (PVN) and in other brain regions. Adapted from http://www.cellbiol.net/ste/alpobesity2.php.

NPY on NPY-Y1 receptors of POMC cells (Broberger and Hokfelt, 2001, Cowley et al., 2001). A state of caloric surplus increases circulating leptin levels, allowing it to bind ARC LepRb receptors in sufficient quantity to elicit a physiological response. First, leptin hyperpolarizes NPY/AgRP neurons, drastically reducing their basal firing rate. This suppresses NPY and GABA secretion, releasing neighbouring POMC neurons from inhibition rendering them more excitable. Next, leptin directly depolarizes POMC neurons causing them to fire action potentials and release neuropeptides stored in vesicles, many of which are cleavage products of the *POMC* gene (Cowley et al., 2001). The POMC prohormone precursor is synthesized in the rough endoplasmic reticulum and cleaved within cytoplasmic vesicles by prohormone convertase PC1/3 to adrenocorticotropic hormone (ACTH) and several other products (Fig. 8). ACTH is cleaved by prohormone convertase PC2 and this product is further processed to alpha-melanocyte-stimulating hormone (α-MSH) through amidation and acetylation (Mazurkiewicz et al., 2000). In humans but not in rodents, one of the initial POMC cleavage products is processed to β-MSH (Biebermann et al., 2012). Although both α-MSH and β-MSH influence energy homeostasis, the subsequent discussion is restricted to the former because the experiments described in this thesis focus on mice, which lack β-MSH.

The antagonistic action of NPY/AgRP and POMC neurons results from interaction of neuropeptides that they secrete onto downstream targets—second-order neurons. POMC-derived α-MSH is an agonist that stimulates the melanocortin G-protein-coupled receptors MC3R and MC4R on PVN neurons. In contrast, AgRP is an antagonist and inverse agonist for these receptors (Haskell-Luevano and Monck, 2001, Fu and van den Pol, 2008). Both receptors are found in high concentration in the PVN but have different physiological actions. Knockout studies in mice implicate MC3R in the regulation of physical activity and metabolic processes such as oxidation of fats, while MC4R is thought to regulate food intake. Notably, *Mc3r*$^{-/-}$ mice have modest increases in adiposity compared to wildtypes, whereas *Mc4r*$^{-/-}$ mice are severely obese (Butler et al., 2000, Sutton et al., 2006). These findings suggest that MC4R receptors are more crucial for the regulation of food intake and body weight and thus, are of greater interest to obesity research. By stimulating MC4R, the melanocortin α-MSH recruits the stimulatory subunit (Gs), whereas AgRP binding activates the inhibitory subunit (Gi/o) (Breit et al., 2011). At this time, the activity downstream of MC4R is poorly understood. Studies implicate action of single-minded gene 1 and brain-derived neurotrophic factor in the PVN distal to MC4R but the

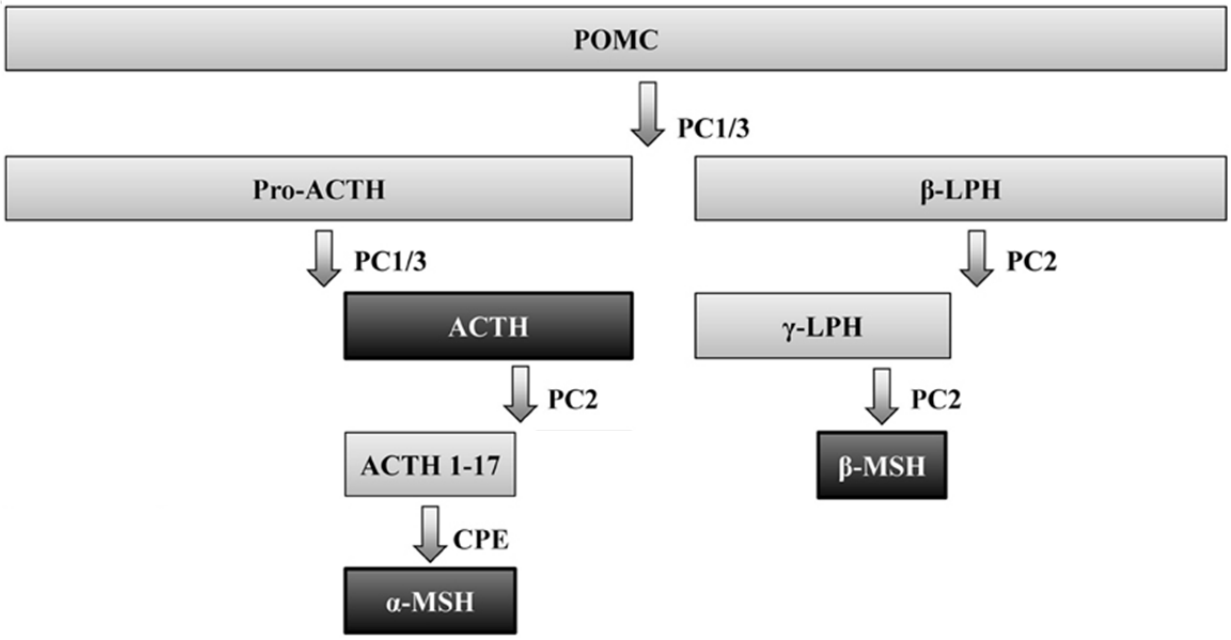

Figure 8. Posttranslational processing of *POMC*. The POMC prohormone precursor is cleaved by prohormone convertase PC1/3 to adrenocorticotropic hormone (ACTH) and beta-lipotropin (β-LPH). Beta-melanocyte-stimulating hormone (β-MSH) is only produced in humans but not in mice. The final product of ACTH cleavage, alpha-melanocyte-stimulating hormone (α-MSH), has profound influence over energy homeostasis regulation in both humans and rodents. Prohormone convertase PC2 and carboxypeptidase (CPE) are involved in the final production of α-MSH. Adapted from (Olney et al., 2014).

remainder of this pathway is yet to be characterized (Kublaoui et al., 2006, Xu et al., 2003, Wang et al., 2010). It is hypothesized that outputs from the PVN integrate with pathways transmitting satiety and food reward signals, and the interplay of all of these systems regulates long-term as well as short-term energy homeostasis (Morton et al., 2014).

1.2.3 POMC signalling and development of hypothalamic melanocortin system

As previously mentioned, the POMC neurons of the ARC are crucial first-order cells of the anorexigenic pathway. Leptin binds the extracellular domain of LepRb, which causes a conformational change in the receptor and subsequent activation of the LepRb-associated Janus kinase 2 (Jak2) (Robertson et al., 2008). Activated Jak2 promotes phosphorylation of several intracellular tyrosine residues on LepRb/Jak2 (Fig. 9). Phosphorylation of Tyr_{1138} stimulates Jak2-mediated phosphorylation of signal transducer and activator of transcription 3 (STAT3) to pSTAT3. A transcription factor, pSTAT3 dimerizes and translocates into the nucleus where it upregulates *POMC* transcription in POMC neurons (Gao et al., 2004). A neural-specific knockout of *Stat3* leads to severe obesity, whereas a POMC-specific Stat3 deficiency results in mild obesity (Gao et al., 2004, Xu et al., 2007). Thus, the LepRb→pSTAT3 signalling pathway is important for leptin-regulated energy homeostasis but is not the only transduction pathway for leptin signals. Indeed, Tyr_{985} phosphorylation of the LepRb receptor recruits tyrosine-protein phosphatase non-receptor type 11 (SHP2), which activates the extracellular signal-regulated kinase (ERK) pathway, resulting in upregulation of immediate early gene/transcription factor *c-fos* (Banks et al., 2000). The downstream targets of *c-fos* in POMC neurons are currently unknown. Nevertheless, pharmacological blockade of ERK1/2 in the ARC diminishes leptin's ability to reduce food intake and body weight (Rahmouni et al., 2009). Thus, leptin regulates energy homeostasis through the combined action of pSTAT3 and ERK signalling pathways in POMC neurons. Other pathways involving pSTAT5 and phosphatidylinositol 3′-kinase are implicated in leptin signal transduction but the significance of their contribution to the regulation of energy homeostasis is less clear (Hill et al., 2008, Ladyman et al., 2012).

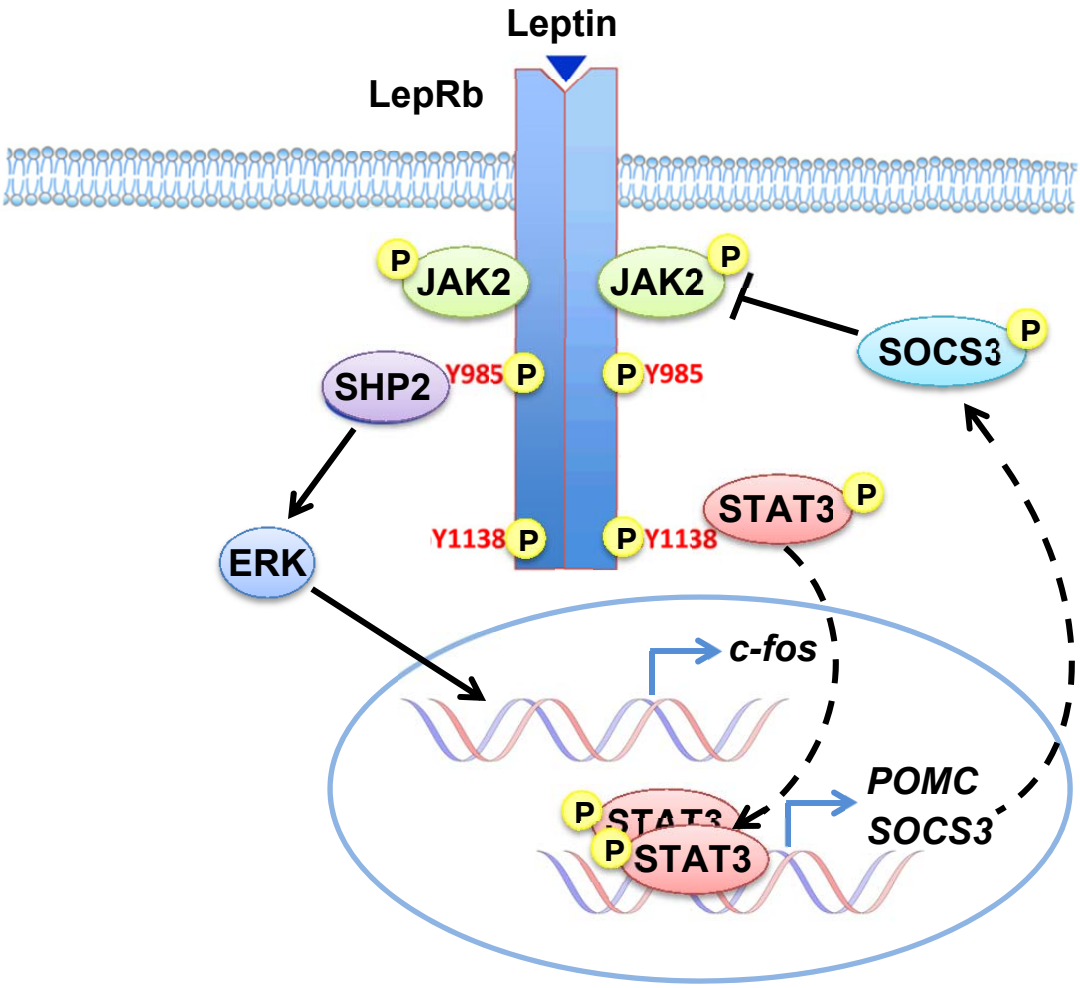

Figure 9. Leptin signalling pathway in POMC neurons. Binding of leptin to the long isoform leptin receptor (LepRb) activates Janus kinase 2 (Jak2) through phosphorylation. In turn, JAK2 phosphorylates several tyrosine residues on LepRb (Y985 and Y1138). This pathway activates extracellular signal-regulated kinase (ERK) through tyrosine-protein phosphatase non-receptor type 11 (SHP2), which leads to increased transcription of *c-fos*. Phosphorylation of signal transducer and activator of transcription 3 (STAT3) causes it to dimerize and translocate into the nucleus where it serves as a transcription factor to produce pro-opiomelanocortin (POMC) and suppressor of cytokine signalling-3 (SOCS3) mRNA. SOCS3 is a negative feedback regulator of LepRb/Jak2 signal transduction.

In addition to the ARC, POMC neurons are also found in the NTS—the nucleus that relays satiety signals. Predictably, the former population controls long-term energy balance whereas the latter participates in short-term regulation of meals (Zhan et al., 2013). The overall function of ARC POMC neurons is to reduce food intake and increase energy expenditure, which is achieved through efferent neural signals to other brain areas including the PVN, DMN, lateral hypothalamic area (LHA), and the ventral tegmental area (King and Hentges, 2011). POMC neurons link leptin with the melanocortin system, which includes but is not limited to: α-MSH, AgRP and their receptors MC3R and MC4R.

The development of the melanocortin system involves neurogenesis, differentiation and formation of functional circuitry. In mice, the majority of POMC neurons are born during E11-E12 but some may also first arise as late as E13. Despite these cells first expressing POMC mRNA at E10-E12, half of them acquire a non-POMC cell fate in the adult mouse. Interestingly, some early *Pomc*-expressing precursors can even become NPY/AgRP neurons (Padilla et al., 2010). To communicate with second-order neurons later in life, ARC neurons develop axonal projections in early postnatal life. The DMN is innervated first at P6, followed by the PVN between P8-P10, and LHA last at P12 (Fig. 10). One study found that a synthetic α-MSH analog administered to rat pups robustly reduces body weight as early as P16, which is around the time a mature pattern of innervation comparable to that of adult rodents first appears (Glavas et al., 2007, Bouret et al., 2004). Also, there are age-dependent changes in PVN neuron responses, which plateaus at P28-P35, suggesting that the α-MSH-MC4R system in PVN is not fully mature till then (Melnick et al., 2007). This is consistent with the finding that leptin is first able to inhibit food intake at P28, just after the age of weaning (Mistry et al., 1999). Since POMC neurons can respond to leptin as early as P10 through the pSTAT3 and ERK pathways but a behavioural response does not appear until this neural circuitry is mature, proper establishment of projections from the ARC is crucial for leptin homeostatic signalling (Bouret et al., 2012).

Proper development of ARC projections to effector nuclei is leptin-dependent. In the absence of LepRb activation, mice have a greatly reduced α-MSH fibre density in the PVN (Bouret and Simerly, 2007). However, leptin administration in the first two weeks of life rescues this phenotype (Bouret et al., 2004). Importantly, axonal growth is mediated through the

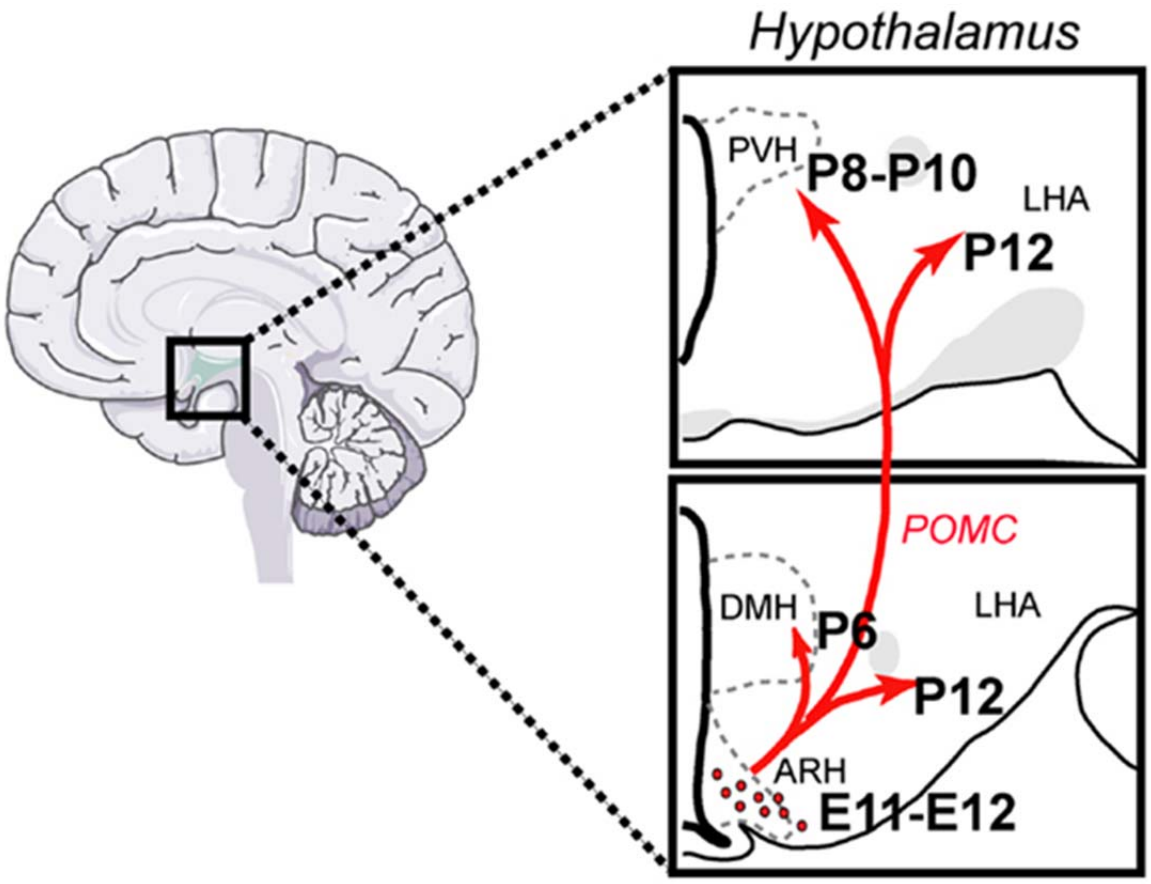

Figure 10. Development of murine POMC neural system. The arcuate nucleus (ARC or ARH) contains first-order pro-opiomelanocortin (POMC) neurons that send projections to second-order neurons in the dorsomedial (DMN or DMN) and paraventricular nuclei (PVN or PVH) of the hypothalamus and to the lateral hypothalamic area (LHA). Neurogenesis of POMC neurons predominantly occurs at E11-E12, and these neurons innervate target nuclei during the first two weeks of postnatal life (P6-P12). Adapted from (Coupe and Bouret, 2013).

LepRb→STAT pathway but not the LepRb→ERK pathway (Bouret et al., 2012). POMC cell axonal guidance is also likely dependent upon the interaction between neuropilin 1 receptors on POMC neurites and semaphorin SEMA3A ligand released by the PVN (Coupe and Bouret, 2013). Additionally, cell adhesion molecules play a role in the development of ARC projections. A mouse model lacking contactin was found to have a lower density of α-MSH fibres in the PVN (Fetissov et al., 2005). Another important process implicated in neurite outgrowth is autophagy, which promotes growth and development, and recycles cellular components within double-membrane bound vesicles (Levine and Klionsky, 2004, Maiuri et al., 2007, Cecconi and Levine, 2008). Membrane for these vesicles—autophagosomes—is synthesized *de novo*, and could conceivably contribute to the cytoplasmic remodelling that occurs during growth of axons (Pereira et al., 2012). In support of this theory, autophagy is constitutively active in POMC perikarya and processes during mouse development (Coupe et al., 2012). Moreover, deletion of autophagy genes in POMC neurons of mice reduces α-MSH fibre density in targets of the ARC nucleus including PVN, DMN and LHA (Coupe et al., 2012). Thus, defects in any of the aforementioned processes involving the development of ARC projections would greatly perturb leptin signalling through the melanocortin system and impair regulation of energy homeostasis.

1.2.4 Leptin resistance

In theory, the negative feedback regulation of adiposity by leptin should prevent any long-term body weight gains. However, an examination of the rising global prevalence of obesity as well as existence of diet-induced obese (DIO) mice argues otherwise. Leptin stimulation of a neuron expressing LepRb creates another negative feedback loop, this time inside the cell. In addition to ERK signalling, phosphorylation of Tyr_{985} recruits the suppressor of cytokine signalling-3 (SOCS3), which inhibits LepRb/Jak2 signal transduction (Fig. 9). Additionally, increased pSTAT3 activation promotes transcription and accumulation of SOCS3, thereby attenuating leptin signalling (Banks et al., 2000, Bjorbak et al., 2000). The inability of significantly elevated levels of leptin (as in obese individuals) to reduce body weight due to this negative feedback loop is termed leptin resistance. In genetic disorders such as PWS, the

mechanism of leptin resistance is different. A disruption of any cellular or molecular process in the leptin-melanocortin system, as well as abnormal development of this pathway could result in leptin resistance or insensitivity by blocking signal transduction. Many discoveries in the field of obesity were first made in murine models and later confirmed in humans—a testament to their utility in studying human obesity. In fact, there seems to be substantial homology in the organization of energy homeostasis mechanisms across mammals (Schwartz et al., 2000). Our *Magel2*-null mouse model of PWS does not respond physiologically to leptin injection, indicating leptin insensitivity. Despite elevated plasma leptin, injections of exogenous leptin induce a robust increase in pSTAT3 in the ARC, arguing against obesity as a causative factor for the leptin insensitivity that we see (Mercer et al., 2013). However, it is yet to be determined whether this leptin insensitivity may contribute to obesity pathogenesis.

1.3 Hypothesis and aims

Previous work with the *Magel2*-null mouse not only identifies impaired leptin signalling, but also implicates POMC neurons as the culprits, which fail to respond to leptin on a cellular level. The NPY/AgRP neurons on the other hand are unaffected by the lack of Magel2 (Mercer et al., 2013). We hypothesize that *Magel2* is essential for leptin responses in the hypothalamus in the POMC neuronal population. In turn, a lack of leptin responses is predicted to impair the release of melanocortins, namely α-MSH, from affected neurons. If we can ascertain the onset of these defects (provided they are not congenital), the results may offer a window of opportunity for therapeutic intervention. This project aims to: 1) examine when neonatal mice lacking *Magel2* become leptin-insensitive, and 2) determine whether melanocortin agonist therapy can treat obesity in *Magel2*-null mice.

Chapter 2. Methods

2.1 Mouse strains

These experiments used the *Magel2*-null mouse originally developed by Serguei V Kozlov (Kozlov et al., 2007), which is now also available from The Jackson Laboratory (C57BL/6-Magel2tm1Stw/J, stock 009062). This mouse has a maternally-inherited imprinted *Magel2* allele and a paternally-inherited *Magel2-lacZ* knock-in allele, which abrogates endogenous *Magel2* function by replacing the open reading frame of *Magel2* with *lacZ*. The knock-in expresses a β-galactosidase (*lacZ*) fusion protein under regulation of upstream promoter/enhancer elements. Expression patterns of β-galactosidase in the knock-in are very similar to expression levels of the wildtype *Magel2* gene. The knock-in was derived by electroporating Bruce4 embryonic stem cells (derived from C57BL/6 mice) with a targeting vector containing a *lacZ* transgene and a neo cassette flanked by loxP sites. The initial colony was established by introducing correctly targeted embryonic stem cells into donor blastocysts and subsequently breeding chimeric progeny onto a C57BL/6J background. Our lab breeds wildtype C57BL/6J females with Magel2$^{-m/+p}$ carrier males to obtain *Magel2*-null progeny, which inherit a silenced wildtype allele from their mother and knock-in allele from their father.

To identify POMC neurons, our lab crosses Magel2$^{-m/+p}$ carrier males to homozygous POMC^{EGFP} females (The Jackson Laboratory, C57BL/6J-Tg(Pomc-EGFP)1Low/J, stock 009593), harbouring an enhanced green fluorescent protein (eGFP) transgene driven by the *Pomc* promoter/enhancer regions (Mercer et al., 2013). Transcripts from this construct express eGFP but not any of the *Pomc* gene products. These mice were originally developed by Dr. Malcolm J Low, who inserted an eGFP cassette containing a polyA signal into exon 2 of the P27*3delta cloning vector, and introduced the clone into a pronucleus of one-cell-stage C57BL/6J mouse embryos. The mouse progeny derived from our Magel2$^{-m/+p}$ x POMC^{EGFP} cross allowed me to study POMC neurons in the ARC of wildtype and *Magel2*-null mice. In experiments where this POMC^{EGFP} reported was used, mice that carry a wildtype *Magel2* allele and the eGFP transgene are designated as “wildtype”. Wildtype and mutant mice were differentiation through genotyping (section 2.2). The University of Alberta Animal Care and Use Committee in accordance with the guidelines of the Canadian Council on Animal Care approved all procedures involving animals.

2.2 Genotyping

Ear notches obtained from mice at weaning were used to distinguish *Magel2*-null mutants from wildtypes. Once collected, notches were stored in 1.5 mL eppendorf tubes at -20°C until further processing. DNA from frozen tissue was extracted using the DNeasy Blood & Tissue Kit (Qiagen) following the manufacturer's instructions. Next, DNA was amplified in a polymerase chain reaction (PCR) in a Veriti 96 well thermal cycler (Applied Biosystems) using reagents listed in Table 1 and conditions listed in Table 2. The primer sequences (Gibco BRL) are as follows: forward common primer (ATGGCTCCATCAGGAGAAC), mutant reverse primer (GGGATAGGTCACGTTGGTGT), and wildtype reverse (GATGGAAAGACCCTTGAGGT). This reaction resulted in 233 bp amplicons for wildtype mice, and 233 bp + 336 bp amplicons for mutants. PCR products were loaded onto a 2% agarose gel precast with 0.1x GelRed Nucleic Acid Gel Stain (Biotium, Hayward, CA) and run at 100 V for 60 minutes. ImageMaster VDS (Pharmacia Biotech, Sweden) was used to visualize bands and produced images such as the one shown in Fig. 11.

2.3 Melanocortin sensitivity

Pups were housed together with parents and littermates until the weaning age of P20. They were housed on ventilated racks on a 12h:12h light:dark cycle with food (PicoLab Rodent Diet 5001) and water administered *ad lib*., and ear notched for genotyping at weaning (Mercer et al., 2013). Pups were divided into four groups: wildtype + vehicle, wildtype + MTII, *Magel2*-null + vehicle, and *Magel2*-null + MTII.

A cohort of mice was initially tested for their ability to respond physiologically to a single intraperitoneal (ip) melanotan II (MTII) injection at P21 (n = 6-10). Pups were weaned at P20 and housed individually for 24 h to acclimatize them to a novel environment. Although housing mice individually for at least 3 days prior to experimentation while injecting them with saline reduces the effect of stress on physiological measurements, weaning mice prior to P20 to

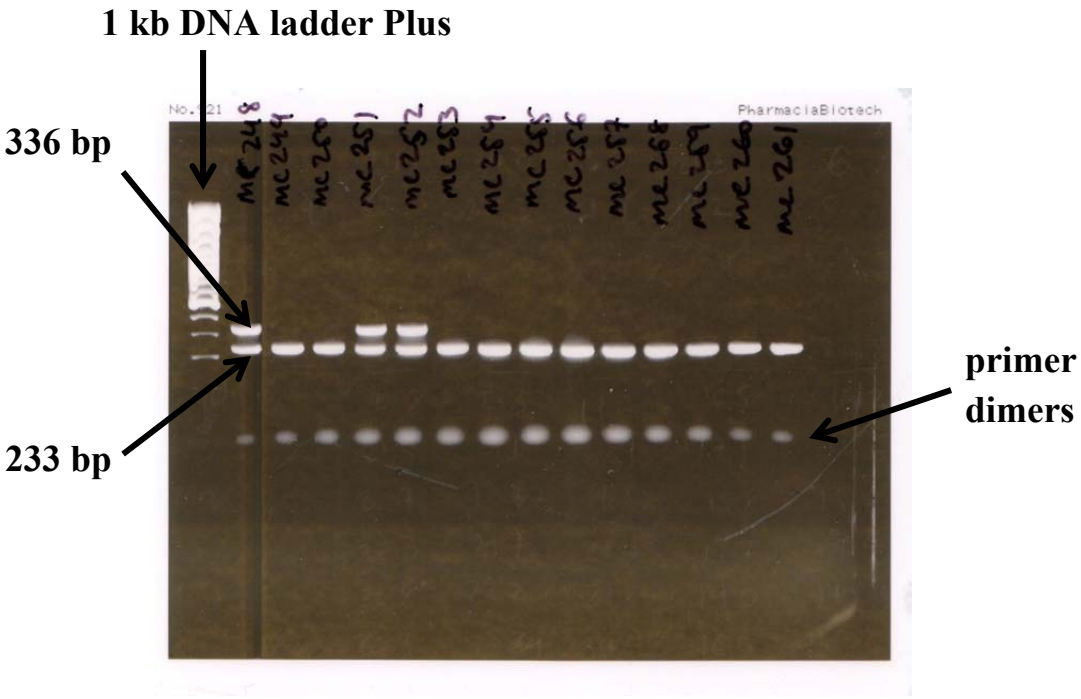

Figure 11. Genotyping of mice. Agarose gel electrophoresis showing mouse *Magel2* and *lacZ* DNA amplicons following PCR amplification. Gel (2% agarose) is stained with GelRed Nucleic Acid Gel Stain. Two bands denote mutants (maternal *Magel2* and paternal *Magel2-lacZ* knock-in alleles) while one band corresponds to wildtype mice (maternal and paternal *Magel2* alleles only).

accomplish this is detrimental to their survival. At P21, pups were weighed at 14:00 and these weights were used to determine injection volume. Mouse food, including any pellet residue found in the bedding, was removed from their cages at 15:00. After a 1 h fast, which eliminates variation between animals that have recently eaten versus ones that have not, food was reintroduced into their cage tops and mice were injected intraperitoneally (ip) with MTII (2.5 mg/kg) or vehicle alone (sterile PBS pH=7.4). Food weight (including any pellet residue) was measured and recorded at 16:00, 18:00, 20:00 h and on the following day at 8:00 and 16:00 h. I chose these time points because mice ingest variable amounts of food throughout the day with peak consumption at 18:00 h (Bischof et al., 2007). Also, MTII is known to produce a strong effect on food intake levels 2 h following administration (Mercer et al., 2013). Thus, choosing 16:00 h for MTII administration maximized my chances of detecting differences in food intake levels between *Magel2*-null and wildtype mice.

The experiment conducted on P21 mice was repeated on a new cohort of mice followed at 4, 5 and 6 weeks of age (n = 8-9). These mice were weaned and ear notched at P20, and housed together with mixed genotype but same sex littermates (up to a maximum of 5 per cage) until 3 days prior to experimentation. Mice were housed individually starting at P25 to acclimatize them to a novel environment and to reduce the effect of stress on physiological measurements. I conducted pilot tests to determine whether daily injections of vehicle alone would further reduce the effect of injection stress on physiological measurements but found no difference between treated and untreated mice. Injections and measurements were performed on the same animals at 4, 5 and 6, weeks of age as previously described.

To examine any long-term benefit of MTII treatment, repeated ip MTII injections were administered to *Magel2*-null and wildtype mice (n = 4-6) and changes in food intake and body weight were measured. Several research groups previously reported that prolonged MTII administration reduces food intake but the effect attenuates within 5 days from initial injection (Pierroz et al., 2002, Zhang et al., 2010). Thus, I administered MTII or vehicle alone to both genotypes once daily for 5 days as previously described. Food intake was measured during the first 24 h as previously described and at 12 h intervals henceforth. Body weight was measured 24 h before the first injection at 16:00 h, then once per day for 5 days. At the completion of each

melanocortin sensitivity experiment, mice were euthanized with sodium pentobarbital (1.92 g/kg). Food intake and body weight were statistically analysed using a two-way ANOVA (GraphPad, La Jolla, CA). P-values of <0.05 were considered statistically significant.

2.4 Immunohistochemistry

Prior to immunohistochemical analysis, tissues were prepared as previously described (Caron et al., 2010). First, 2% paraformaldehyde (PFA) fixative solution was made fresh by dissolving PFA powder in sterile phosphate buffered saline (PBS) pH 8.0. The mixture was heated to 50-60°C, adjusted to pH 8.0 and cooled on ice for 10-15 minutes. Then, it was filter sterilized and stored at 4°C. The mouse was deeply anesthetised with sodium pentobarbital (0.96 g/kg) and pinned to a dissecting tray in the supine position as soon as it lost its toe pinch withdrawal reflex. The mouse was quickly dissected with iris scissors by making a straight incision from the middle of its abdomen to the diaphragm. From there, two more incisions were made—one towards each shoulder blade, cutting through the ribcage—to expose the heart in its entirety. The tissue flap between these two incisions was pinned to the dissecting tray. A BD Vacutainer Safety-Lok Blood Collection Set (Becton Dickinson, East Rutherford, NJ) attached to the perfusion apparatus was inserted into the left ventricle of the beating heart and the right atrium was cut open with iris scissors to start the perfusion. Mice were gravity perfused at 3 mL per minute to ensure good fixation and preserve tissue morphology. First, blood was flushed with 15 mL of ice cold PBS pH 8.0, followed by 30 mL 2% PFA fixative. Next, the carcass was decapitated and skin on the top half of the cranium pulled back to expose the skull. Iris scissors were used to make an incision along the sagittal suture from the brainstem to just past the coronal suture. Two small lateral incisions, one across each parietal bone, were made. Rongeurs were used to peel away the top half of the skull, exposing the brain underneath. An incision along the coronal suture and one severing the optic tract freed the brain, allowing it to be removed without deformation. The brain was transferred onto moist Whatman paper (GE Healthcare, United Kingdom) on top of a petri dish that was filled with ice, and cut down to a smaller block. It was then transferred to a 20% sucrose solution in PBS pH 8.0 containing 2%

PFA for a 2 h postfix at 4°C. The brain block was subsequently cryoprotected in 20% sucrose solution at 4°C overnight. Next, it was placed in a 22 mm x 22 mm square mould (Electron Microscopy Sciences, Hatfield, PA) filled with optimal cutting temperature compound (OCT; Thermo Fisher Scientific, Waltham, MA) and acclimated to the OCT for 2 minutes. The mould was gently lowered into isopentane solution precooled on liquid nitrogen. Once frozen, it was wrapped in tinfoil, transported on dry ice and stored at -80°C until further processing.

Frozen samples were acclimated to -13°C inside the cryostat and the sample temperature was also set to -13°C. I found this temperature to be optimal slicing temperature for fixed brain tissue using the Leica CM1900 cryostat. The OCT block containing brain tissue was affixed to the specimen disk to produce coronal sections, with the hypothalamus facing to the side. From my experience, this orientation is least likely to result in tissue crumbling near the middle where the hypothalamus is found. During slicing, 60 µm sections were used to locate the ventral triangle of the third ventricle at Bregma -0.10 mm according to the Mouse Brain atlas (Keith Franklin, 3rd). From there, sections were counted until Bregma -1.06 mm. To confirm the location, a single section was dipped into 1% thionin for 30 seconds and examined at 2.5 X under a Leica MZ 8 light microscope. The image was compared to the Mouse Brain atlas (Keith Franklin, 3rd) to identify its location. When a section resembling Bregma -1.22 mm was found, containing visible ventromedial hypothalamic nuclei, it marked the rostral segment of the ARC. The following 1.5 mm, which constitutes the ARC in its entirety, was sectioned at 30 µm intervals and adhered to Fisherbrand Superfrost Plus glass slides at room temperature. These slides were kept inside the cryostat until they could be transferred to -80°C for long-term storage.

A thionin stain was used to identify sections for immunohistochemistry. Staining solution was prepared by mixing 10 mL of 35 mM thionin acetate with 60 mL of 17.4 N glacial acetic acid (Fischerbrand ACS grade) and 40 mL of 100 mM sodium acetate trihydrate. The mixture was stirred on low heat for 1 h and filter-sterilized. Slides were warmed in an incubator at 37°C for 30 minutes to dry them prior to staining. They were then immersed in a series of solutions in coplin jars: 50% ethanol (1 min), dH_2O (1 min), thionin (10 min), dH_2O (3 quick dips), 50% ethanol (3 quick dips), 75% ethanol (3 quick dips), 95% ethanol (2 min), 100% ethanol (2 min), 100% ethanol (2 min), xylene (3 min), xylene (4 min). Slides were mounted with VectaMount (Vector Labs, Burlingame, CA), coverslipped and dried at room temperature. They were

examined under a light microscope and matched to precise brain regions within the ARC according to the Mouse Brain atlas (Keith Franklin, 3rd). Sections corresponding to Bregma -1.46, -1.58 and -1.70 mm were identified and adjacent sections were stained with the antibody of interest.

For pSTAT3 and eGFP double immunofluorescence staining, I chose sections at and near Bregma -1.58 mm because this location within the ARC was previously shown to contain the largest number of pSTAT3 positive neurons (Mercer et al., 2013). Additionally, this plane also contains many POMC neurons (Mercer et al., 2013), which are labeled with eGFP in our mouse model. Slides were warmed in an incubator at 37°C for 30 minutes to dry them prior to staining and washed in PBS pH 8.0 for 3 x 10 min. For optimal anti-pSTAT3 antibody penetration, sections were subjected to the following pretreatment: 0.5% NaOH + 0.5% H_2O_2 in PBS pH 8.0 (20 min), PBS wash (5 min), 0.3% glycine in PBS pH 8.0 (10 min), PBS wash (5 min), 0.03% SDS in PBS pH 8.0 (10 min), PBS wash (2 x 10 min). This treatment did not adversely affect eGFP staining but greatly improved the signal-to-noise ratio for the pSTAT3 stain. After pretreatment, sections were blocked in 4% normal goat serum (NGS) + 1% bovine serum albumin (BSA) + 0.4% Triton X-100 in PBS for 1 h at room temperature in a humidified chamber. Next, sections were incubated with rabbit anti-pSTAT3 primary antibody (1:500, Cell Signaling 9131, Beverly, MA) in 1% NGS + 1% BSA + 0.4% Triton X-100 in PBS for 16 h at 4°C in a humidified chamber. Sections were washed 6 x 10 min in 0.25% BSA + 0.02% Triton X-100 in PBS and incubated with goat-anti-rabbit AF564 (1:500, Life Technologies, Carlsbad, CA) in 1% BSA + 0.4% Triton X-100 in PBS for 2 h at room temperature in a humidified chamber. Finally, sections were washed 6 x 10 min in 0.25% BSA in PBS and 3 x 10 min in PBS. Next, slides were blocked in 10% NGS in PBS for 1 h at room temperature and subsequently incubated with chicken anti-eGFP primary antibody (1:1000, Abcam 13970, Cambridge, United Kingdom) in 10% NGS + 0.1% Triton X-100 in PBS for 16 h at 4°C in a humidified chamber. Sections were washed 6 x 10 min in 0.02% Triton X-100 in PBS and incubated with goat-anti-chicken AF488 (1:1000, Life Technologies, Carlsbad, CA) in 0.1% Triton X-100 in PBS for 2 h at room temperature in a humidified chamber. Sections were then washed 9 x 10 min in PBS and coverslipped with prolong gold antifade reagent + 4',6-diamidino-2-phenylindole (DAPI) (Life Technologies, Carlsbad, CA). Sections were dried at room temperature overnight and stored at -20°C until imaging.

Slides were imaged using the Zeiss LSM 510 confocal microscope and Leica Application Suite Advanced Fluorescence (LAS AF) software. Frame averaging (3 x) and slow scan rate (100 Hz) was employed to enhance image quality. Z-stacks containing 24 planes were collected for each hemisection in the red, green and blue channels simultaneously. Using Image J software, Z-stacks were then compressed into maximum intensity 2-D projections and adjusted for brightness and contrast. To account for slight variations in staining time and to ensure comparability between images taken on different days, images were thresholded. Briefly, the mean intensity and standard deviation value of each image was measured, and intensity was thresholded based on a predetermined number of standard deviations which was kept constant between images. Next, images were transformed using a binary scale so that any pixel value which met or exceeded the threshold cutoff was given a value of 1 (black) and any pixel which fell short of the threshold (background) was given a value of 0 (white). Cells were counted manually using Image J—anything greater than 4 pixels was considered a cell. The number of pSTAT3-IR and eGFP-IR cells was counted using this method. The number of cells with colocalized pSTAT3-IR and eGFP-IR signals was counted using the same procedure, except that images were not transformed using a binary scale, retaining their color throughout the analysis. Differences in the number of immunoreactive cells between genotypes and between treatment conditions were statistically analysed using a Student's unpaired *t*-test (GraphPad, La Jolla, CA). P-values of <0.05 were considered statistically significant.

2.5 Electrophysiology

Slice solution was prepared from 10X stock (Table 3) by adding glucose (final concentration = 10 mM), $NaHCO_3$ (final concentration = 26 mM), $CaCl_2$ (final concentration = 1.5 mM) and kynurenate (final concentration = 1 mM) (Mercer et al., 2013). Slice solution was stored at 4°C overnight and used the next day. Bath solution was prepared from 10 X stock (Table 4) by adding glucose (final concentration = 2.5 mM), sucrose (final concentration = 7.5 mM), $NaHCO_3$ (final concentration = 26 mM), and $CaCl_2$ (final concentration = 2.5 mM) and used on the day of the experiment. Mice were euthanized by decapitation and brains were

removed as previously described (section 2.4). The freshly dissected brain was placed in carbogenated ice-cold slice solution for 1 minute and cut down into a smaller block as previously described (section 2.4). The block was glued onto a specimen chamber, resting against a 3% agar block. The chamber was filled with fresh carbogenated ice-cold slice solution and affixed to a Slicer HR2 vibratome (Sigmann Electronik, Hüffenhardt, Germany). Slices from the ARC were obtained at 250 μm thickness and incubated in carbogenated room-temperature bath solution for 1 h prior to recording.

Patching was accomplished with a Zeiss FS2 microscope and changes in voltage from POMC neurons were recorded using a MultiClamp 700B amplifier and pclamp 9.2 software. During the recording, slices were continually gravity-perfused with fresh carbogenated bath solution warmed to 34°C. $POMC^{EGFP}$ neurons were initially identified with epifluorescence illumination, and infrared-differential interference contrast imaging was used to visualize cell morphology for cell patching. Whole-cell patching was accomplished with a thin-walled glass patch pipette filled with pipette solution containing: 126 mM K-gluconate, 4 mM KCl, 10 mM HEPES, 5 mM MgATP, 0.3 mM NaGTP, 1 mM EGTA and 0.3 mM $CaCl_2$. (pH adjusted to 7.25 with KOH, 280 mOsm/L). Cells were patched in voltage clamp mode and recorded from in current clamp mode. Their holding potential was adjusted immediately after patching to -50 mV to ensure cell viability throughout the recording. Prior to drug administration, cells were allowed 10 minutes to stabilize. Drugs were administered by mixing with carbogenated bath solution (34°C) and applied using the gravity-perfusion apparatus. After administration of 10mL leptin (100 nM), the slice was washed with bath solution for 10-15 min to remove any traces of leptin activity. NPY was subsequently administered (300 nM, 10mL) and washed with bath solution for 20 min. Images were captured before and after each trial, recording glass pipette's location within the brain.

Recordings were exported to Clampfit and analyzed for changes in membrane potential. Cursors were used to demarcate areas within the recording and calculate average voltage for those regions. The change in membrane potential between baseline and maximum drug response was compare and any voltage change exceeding 2 mV was considered significant.

2.6 Calcium imaging

Slices and solutions were prepared exactly as for electrophysiology (section 2.5). Recordings were performed with a confocal microscope equipped with an argon (488 nM) laser and filters (20× XLUMPlanF1-NA-0.95 objective; Olympus FV300, Markham, Ontario). Slices were perfused with bath solution (34°C) at 5 mL/min using a 405U/VM2 50 RPM pump. A thin-walled glass pipette was broken off on the sharp end to create an opening of roughly 10 μm, and filled with 3 μL of 0.5 mM fluo-4 AM dye. First, a Z-stack was obtained through a portion of the ARC at 600 X magnification using two-photon microscopy to visualize POMC neurons. The laser power was set at 4% to detect weak native eGFP fluorescence. Next, laser power was reduced to 1.5% and the slice injected with the fluo-4 AM dye for 10 min at a pressure of 35-40 mmHg. The dye was injected roughly 100 μM below the slice surface and adequately stained the entire field of view under 600 X magnification. The best-stained area was localized roughly 50 μM below slice surface and this region was used for subsequent recordings. The best plane for recordings was identified by matching up images from the pre-injected Z-stack recording with live recordings from the stained slice. Under light illumination, cell morphology was visualized and unusual features as well as light and dark patterns were used to identify the same cells before and after dye injection. Next, a Z plane containing the largest number of well-stained $POMC^{EGFP}$ neurons was identified by comparing the pre- and post-stained images. To ensure that the final video recording contained this plane, the video was set up so that the microscope scanned three planes at 1.1 s intervals throughout the recording. Adjacent planes were 5 μm apart, covering a total distance of 10 μm. Since a POMC neuron has a diameter of roughly 10 μm, a 10 μm spread would capture a plane transecting each POMC neuron near the center, maximizing the area of each cell available for recording (Meister et al., 2006). Imaging videos were recorded for 20 min. Leptin (100 nM, 10 mL) was applied exactly 1 minute after the initiation of each recording and allowed to wash out for 10-15 minutes. Glutamate (0.1 mM, 3 mL) was subsequently administered and allowed to wash out until the end of the recording. Still images were captured after each recording to keep track of specific areas used for each trial.

Video recordings were analyzed using FluoView v4.3 software. Briefly, $POMC^{EGFP}$ neurons were identified in a calcium recording by matching a still frame containing maximal

glutamate effect with a Z plane from the Z-stack collected prior to dye injection. Initially, light illumination images were used to match cells of uncommon shape/contrast between the two sets of images. Next, fluorescent images were compared from the two sets planes and $POMC^{EGFP}$ neurons were identified by morphology and distance from one another. Regions of interest were placed over $POMC^{EGFP}$ neurons in the video recordings, which were then used to compute fluorescent signal intensity throughout the recording. Careful manual examination ensured that slight drift within the plane did not shift regions of interest onto adjacent cells and that the signals recorded were not due to artifacts. Since three planes were acquired for each video recording, to avoid double counting each cell was analyzed in only one plane—the one that showed the brightest and most robust signal. Depending on initial cell brightness, which was influenced by quality of staining as well as plane focus, cell responses to leptin and glutamate had varying magnitudes. Any change in dye intensity in excess of 10% of baseline was considered significant. Differences between genotypes in the number of leptin-responsive neurons were analysed using a Fisher's exact test (GraphPad, La Jolla, CA). P-values of <0.05 were considered statistically significant.

Table 1. PCR reagents, volumes and concentration used in mouse genotyping.

Reagent	**Source**	**Volume (µL)**
10X PCR Buffer –$MgCl_2$	Invitrogen	2
$MgCl_2$ (50 mM)	Invitrogen	0.6
dNTPs (2 mM)	Invitrogen	2
Forward primer (10 mM)	Invitrogen	2
Reverse primer (10 mM)	Invitrogen	1
Control primer R (10 mM)	Invitrogen	1
Taq DNA polymerase (5 U/µL)	Invitrogen	0.1
MilliQ water	-	9.3
DNA sample (50mg/L)	-	2
Total volume	-	20

Table 2. PCR conditions used in mouse genotyping.

Step	**Temperature (°C)**	**Number of Cycles**
Initial denaturation	95	1
Denaturation	95	35
Annealing	60	
Extension	72	
Final extension	72	1

Table 3. 10X stock slice solution preparation.

Chemical	**Concentration (mM)**
NaCl	1180
KCl	30
$MgSO_4*7H_2O$	13
NaH_2PO_4	14
$MgCl_2*6H_20$	5

Table 4. 10X stock bath solution preparation.

Chemical	**Concentration (mM)**
NaCl	1240
KCl	30
$MgSO_4*7H_2O$	13
NaH_2PO_4	14

Chapter 3. Results

3.1 Young *Magel2*-null mice have a normal number of ARC POMC neurons

A previous study from the Wevrick lab found a reduced number of POMC neurons in the ARC of *Magel2*-null adult mice (Mercer et al., 2013). I wanted to determine whether this observation also holds true for younger mutants. Thus, I performed immunohistochemical analysis of P10 mouse brain sections (n = 3 animals, per genotype). I amplified eGFP fluorescence in POMC neurons of Magel2$^{-m/+p}$ x POMC^{EGFP} mouse progeny using an AlexaFluor 488-labelled anti eGFP antibody and counterstained with DAPI (Fig. 12A). I obtained confocal images of stained tissue and manually quantified the number of POMC^{EGFP} neurons in each section (note: these are not volumetric count estimates of the total number of neurons within the brain). Only sections at Bregma -1.46, -1.58 and -1.70 mm were examined (3 sections per animal, one at each coordinate) because this region was previously shown to contain a large density of POMC neurons (Mercer et al., 2013). Unlike previous reports from adult mice (Mercer et al., 2013), I found no statistically significant differences in the number of POMC neurons between *Magel2*-null and wildtype mice at P10 (Fig. 12B). I concluded that *Magel2*-null mice at P10 have a normal number of ARC POMC neurons.

3.2 No defect is apparent in the ability to sense leptin at the LepRb receptor by POMC neurons of young *Magel2*-null mice

The high levels of circulating leptin and excess adipose tissue in *Magel2*-null mice (Bischof et al., 2007) suggest that these mice have defects in behavioural responses to endogenous leptin. Previous work revealed that 6-week-old wildtype mice reduce 24 h food intake by 35% following ip leptin administration (2.5 mg/kg) (Mercer et al., 2013). However, age-matched *Magel2*-null mutants fail to respond to the peripherally administered leptin. An examination of 6 week old mouse brains uncovered a reduced number of leptin-induced pSTAT3-IR neurons in the ARC of *Magel2*-null mice when compared to wildtypes (Mercer et al., 2013).

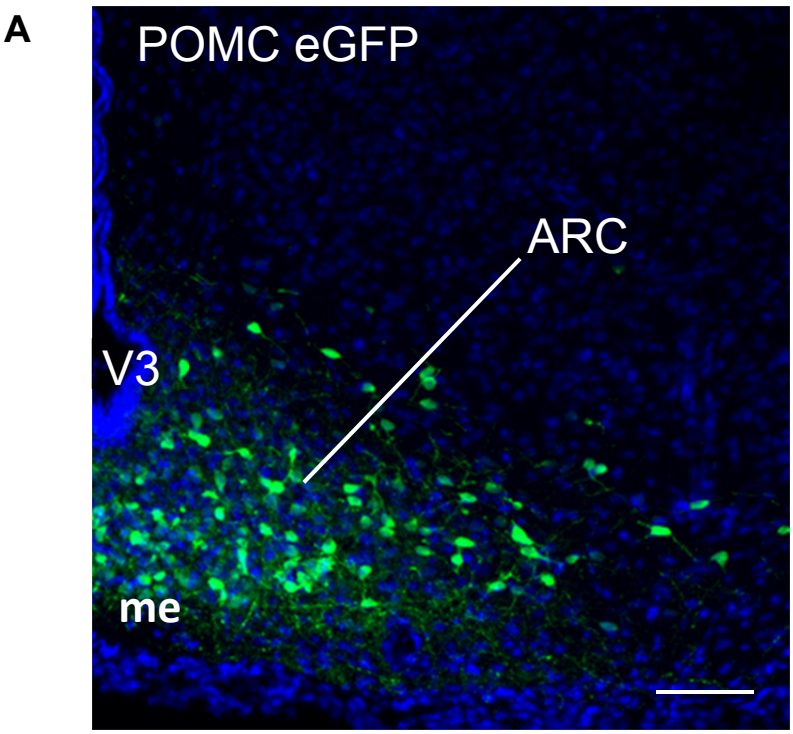

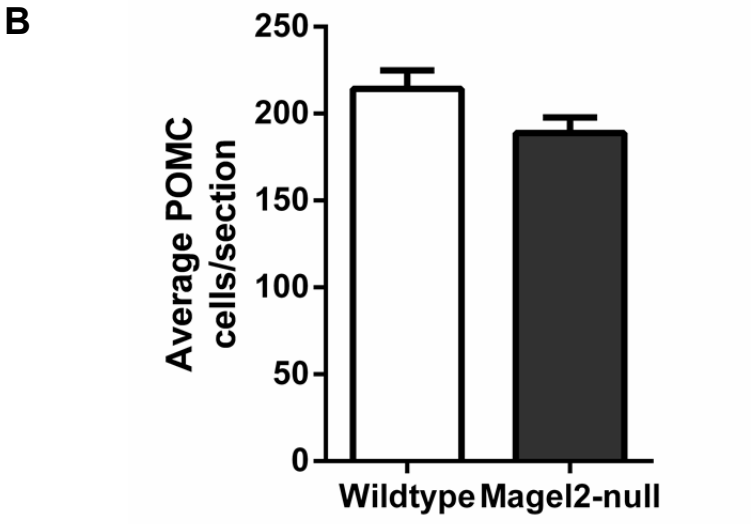

Figure 12. Quantification of POMC^{EGFP} neurons in the P10 ARC. A) Confocal image showing eGFP-labeled POMC neurons (green) of P10 mouse pups counterstained with DAPI (blue). Scale bar, 100 μm. B) P10 *Magel2*-null mice had the same number of POMC^{EGFP} neurons in the arcuate nucleus (ARC) as did wildtypes. Values are means ± SEM. ARC, arcuate nucleus; me, median eminence; V3, third ventricle.

I divided mutant and wildtype P10 mice from Magel2$^{-m/+p}$ x POMC^{EGFP} crosses into two groups (n = 3 animals, per group): one received ip injections of saline while the other received ip leptin (2.5 mg/kg). I euthanized the mice 45 minutes after injection, performed intracardial perfusion with ice-cold PBS and processed brains for immunohistochemistry. I stained for leptin-induced pSTAT3-IR in the ARC at Bregma -1.46, -1.58 and -1.70 mm (3 sections per animal, one at each coordinate) and quantified immunoreactive neurons (Fig. 14A-B). I chose P10 as the earliest time point for examination of pSTAT3 immunoreactivity because mice first show robust pSTAT3 responses in the hypothalamus at P10 (Caron et al., 2010). I found that leptin-injected animals had three times as many ARC pSTAT3-IR neurons as did saline-injected controls (Fig. 13C), which agrees with previous studies (Bouret et al., 2012). However, unlike previous findings in 6 week-old mice (Mercer et al., 2013), I found no difference between the number of pSTAT3-IR neurons in the ARC of *Magel2*-null and wildtype mice at P10 in either the saline- or leptin-treated groups. Since these mice carry an eGFP transgene driven by the *Pomc* promoter/enhancer regions, I was able to visualize POMC neurons of the ARC by amplifying the eGFP signal using immunohistochemistry (Fig. 14 A-B). This allowed me to determine whether *Magel2*-null mice have leptin-dependent pSTAT3 signalling defects specifically in their POMC neurons. Thus, I reanalyzed the same set of sections for pSTAT3+eGFP immunoreactivity to identify double-labeled neurons in the ARC. I compared the four groups (wildtype + vehicle, wildtype + leptin, *Magel2*-null + vehicle, and *Magel2*-null + leptin) and found no statistically significant differences between genotypes in either the saline- or leptin-injected groups (Fig. 14C). I concluded that ARC POMC neurons of P10 *Magel2*-null mice undergo normal activation of pSTAT3 in response to peripherally applied leptin.

3.3 POMC neurons of young *Magel2*-null mice may depolarize in response to leptin stimulation

Although pSTAT3-IR is indicative of LepRb stimulation and activation of downstream signalling, it does not correlate with the actual release of peptides from stimulated cells. It is the release of a-MSH from POMC neurons and their subsequent action in the PVN that ultimately

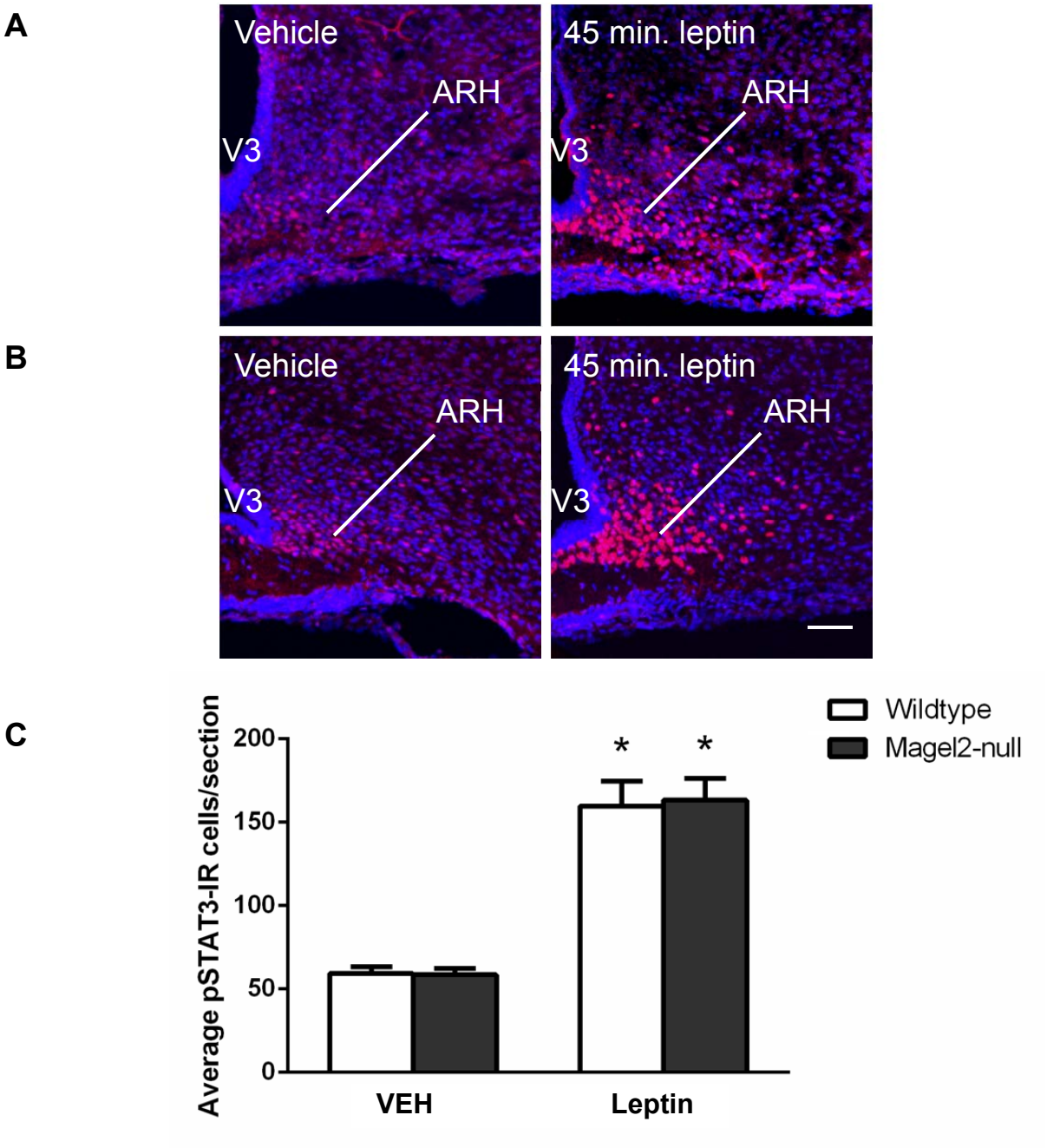

Figure 13. Quantification of pSTAT3-IR neurons in the P10 ARC. A-B) Confocal images showing pSTAT3 immunoreactivity (red) counterstained with DAPI (blue) 45 min after intraperitoneal injection of either leptin (2.5 mg/kg) or vehicle alone on P10 pups (A: wildtype, B: *Magel2*-null). Scale bar, 100 μm. C) Both genotypes have an increased number of pSTAT3 immunoreactive cells following leptin injection compared to vehicle alone. Values are means ± SEM. *P < 0.05 (* denotes significantly different from saline treated, same genotype). ARC, arcuate nucleus; me, median eminence; V3, third ventricle.

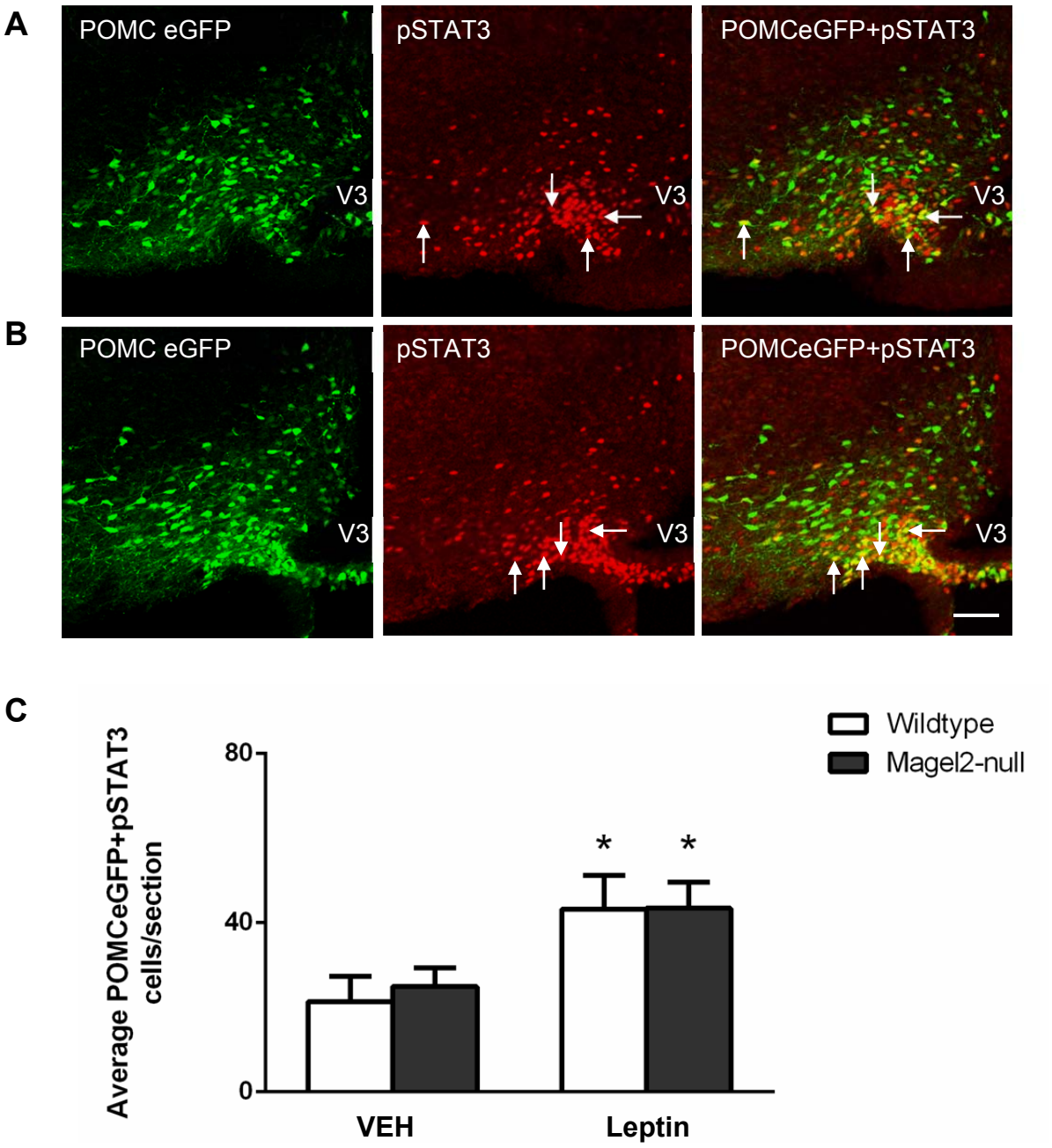

Figure 14. Quantification of pSTAT3-positive POMC neurons in the P10 ARC. A-B) Confocal images showing pSTAT3 (red) 45 min after intraperitoneal injection of leptin (2.5 mg/kg) on P10 pups (A: wildtype, B: *Magel2*-null). POMC neurons labeled with eGFP. Arrows point to double-labeled neurons. Scale bar, 100 um. C) There were more double-labeled neurons in the leptin-injected group compared to the saline-injected group in both genotypes. Values are means ± SEM. *P < 0.05 (* denotes significantly different from saline treated, same genotype). me, median eminence; V3, third ventricle.

results in behavioural response of reduced food intake and increased energy expenditure. The release of α-MSH from POMC neurons is dependent upon calcium oscillations within neurons, which result from calcium influx into cells (Kolk et al., 2002). Thus, cellular depolarization that involves transmembrane movement of many ions in addition to calcium, correlates with α-MSH release. A previous study examined changes in membrane potential in response to leptin by whole-cell electrophysiology recording. Leptin stimulation (100 nM) of POMC neurons in ARC in live brain slices failed to produce depolarization responses in adult *Magel2*-null mice, but the same cells of wildtype mice responded with a mean membrane potential change of +5 mV (Mercer et al., 2013).

I repeated this experiment in P10 mice. Briefly, I euthanized mice from Magel2$^{-m/+p}$ x POMC^{EGFP} crosses by decapitation, extracted their brains, and placed them in ice-cold carbogenated slice solution. I then used whole-cell patching to obtain electrophysiology recordings from 250 μM-thick coronal brain slices. Throughout the recordings, slices were continually perfused with fresh carbogenated bath solution warmed to 34°C. To identify ARC POMC neurons, I used a microscope equipped with epifluorescence illumination that was capable of detecting native fluorescence of the eGFP transgene protein product (Fig. 15A-B). Leptin (100 nM, 10 mL) was administered directly into the bath solution and changes in membrane potential were recorded (Fig. 15C). After a washout period (10-15 min), NPY (300 nM, 10 mL) was administered in a similar fashion to leptin (Fig. 15D), and served as a positive control to rule out leptin-unresponsive neurons that fail to respond to other drugs as well, due to poor cellular health. Any membrane potential change exceeding 2 mV was considered significant. This study used 2-3 animals per genotype and 3-5 slices per animal. Each slice was used to record from only one neuron and then discarded. It is important to note that many neurons that I recorded from produced uninterpretable recordings and very few cells could be properly analyzed. I discovered leptin-responsive neurons in both *Magel2*-null and wildtype P10 mice (Fig. 15F). Moreover, the magnitude of leptin-induced depolarization was comparable for *Magel2*-null mice (7.9 ± 1.8 mV) and wildtypes (7.5 ± 2.5 mV). This finding agrees with the average magnitude of depolarizing leptin responses in POMC neurons published in a previous study (Mercer et al., 2013). NPY administration produced a robust hyperpolarizing response in POMC neurons in both genotypes, with average magnitudes of -15.2 ± 4.1 mV and -14.5 ± 4.2 mV for mutants and and wildtypes, respectively (Fig. 15E). It is important to note that the resting

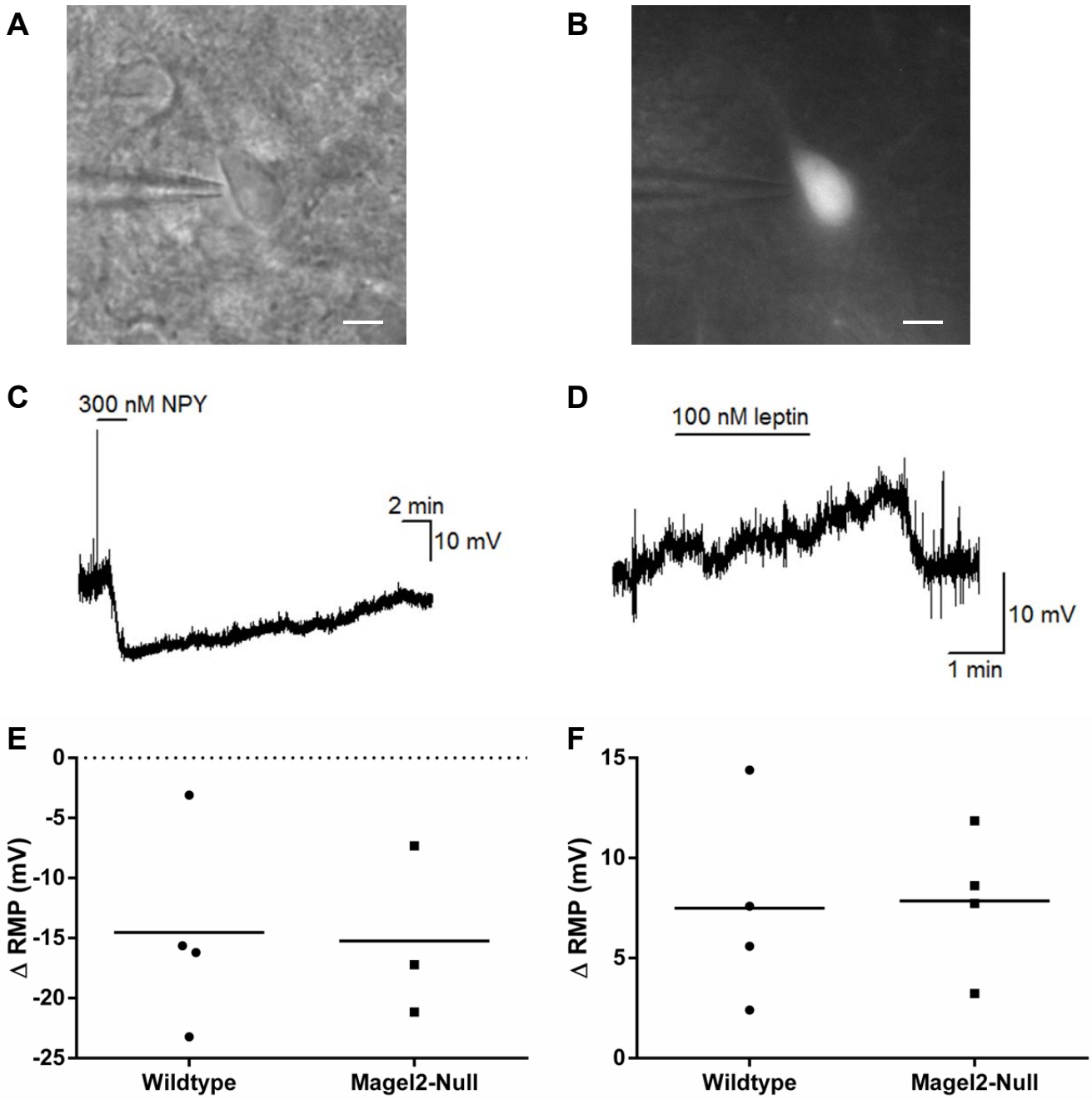

Figure 15. Electrophysiology responses of ARC POMC neurons at P10. POMC^{EGFP} neuron under A) infrared-differential interference contrast imaging and B) epifluorescence. Scale bar, 10 μm C-D) Whole-cell recording from a POMC neuron showing C) the hyperpolarizing effect of 300 nM NPY, and D) the depolarizing effect of 100 nM leptin. E-F) NPY (E) and leptin (F) produced responses of comparable magnitude in POMC neurons of wildtype and *Magel2*-null P10 mouse pups. Circles and squares represent individually tested neurons.

membrane potential was unstable and highly variable in P10 brain slices of all mice tested. Thus, it was difficult to determine whether the leptin responses that were identified are true responses or natural fluctuations of baseline activity. Although these results suggest that POMC neurons of *Magel2*-null mice may be responsive to leptin at P10, other studies were necessary to confirm this preliminary finding.

3.4 *Magel2*-null mice have leptin-responsive POMC neurons at birth but lose this functionality by adulthood

Due to the unreliable nature of electrophysiology recordings obtained at P10, I used a different method—calcium imaging—to examine cellular responses to leptin in the ARC. This not only eliminated a highly variable baseline, but also allowed me to measure activity due to leptin stimulation in many cells simultaneously versus one cell at a time in electrophysiology. Similar to the electrophysiology experiment, this study also used mouse progeny from the Magel2$^{-m/+p}$ x POMC^{EGFP} cross. Coronal brain slices of 250 μM thickness were obtained as previously described (section 3.3) at P21, P28, P42 and P84-P98. Slices were continually perfused with fresh carbogenated bath solution warmed to 34°C throughout each recording. I visualized ARC POMC neurons by detecting fluorescence of the eGFP transgene protein product using a two-photon microscope with laser power set to 4% and obtained a Z-stack of images (Fig. 16A). I then reduced laser power to 1.5% and injected a calcium sensitive fluo-4 AM dye (0.5 mM) into the ARC of each slice. At reduced laser power (1.5%), native eGFP fluorescence is almost not visible (Fig. 16B) but calcium signals are very apparent (Fig. 16C), allowing for the use of a green dye and identification of eGFP-positive cells. The eGFP neurons showed no activity prior to dye infusion but had spontaneous calcium oscillations after taking up the dye. I recorded a video from each slice simultaneously in three planes that were 5 μm apart from each other. This technique maximized the area of each cell available for recording and increased the amount of data generated. During each recording, leptin (100 nM, 10 mL) was applied directly

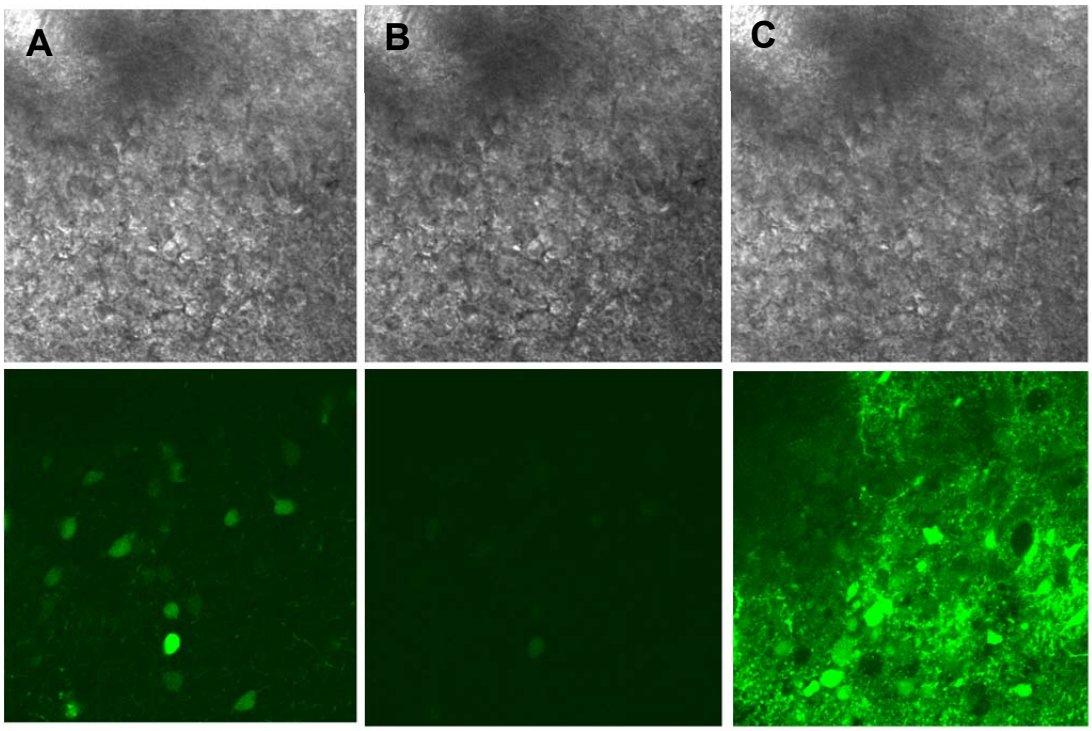

Figure 16. Staining eGFP-positive neurons with a green calcium-sensitive dye. A-C) Arcuate neurons in the same brain slice and Z plane under infrared-differential interference contrast imaging (top panels) and two photon microscopy (bottom panels). A) Native eGFP fluorescence in POMC cells under 4% laser power. B) Native eGFP fluorescence in POMC cells under 1.8% laser power. C) Brain slice after 10 minutes of Fluo-4AM calcium-sensitive dye infusion.

into the bath solution and after a washout period (10-15 min), glutamate (0.1 mM, 3 mL) was administered. Glutamate served as a positive control to rule out leptin-unresponsive neurons that fail to respond to other drugs as well, due to poor cellular health or inadequate staining (Fig. 17B-C). I identified POMC neurons in video recordings by comparing cell morphology in the previously acquired Z-stack (showing only POMC neurons in native eGFP fluorescence) to a still frame demonstrating maximal glutamate effect from live video (Fig. 17A). I used regions of interest placed over ARC POMC neurons to compute fluorescent signal intensity throughout each recording. From the three planes acquired during each recording, I only used one to collect data for each cell—the one that showed the brightest and most robust signal. Due to small fluctuations in baseline, any change in dye intensity in excess of 10% of baseline was considered significant. This study used 2-3 animals per genotype and 2-3 slices per animal. Each slice was injected with dye only once and after a single leptin + glutamate administration it was discarded. Unlike the electrophysiology experiments, every slice used for calcium imaging produced interpretable data for analysis.

I observed spontaneous fluorescence intensity changes in every slice at every age tested in both, wildtype and *Magel2*-null mice. ARC cells displayed considerable heterogeneity of baseline calcium signals: most cells had weak regular or irregular baseline calcium oscillations while some had no baseline activity but nevertheless responded to drug treatment. Activity was comparable across younger ages but greatly diminished in slices from 12-14 week-old animals. There did not appear to be any obvious patterns of baseline activity or synchronous oscillations among the POMC neurons studied. There were no apparent differences between genotypes in terms of baseline cellular activity or magnitude of glutamate response (not quantified). Despite this activity, responses to leptin (100 nM) greatly exceeded baseline fluctuations (Fig. 17E). To validate calcium imaging for examination of leptin responses, I used adult *Magel2*-null mice and wildtypes (12-14 weeks old, n = 3 per genotype). Similar to what has been previously shown by electrophysiology (Mercer et al., 2013), I found leptin-induced increases in calcium intensity (which correspond to depolarizations) in 12 of 39 POMC neurons in wildtype mice (pooled from all slices collected at this age). However, only 1 of 52 POMC neurons was leptin-responsive in *Magel2*-null mice (Table 5). A Fisher's exact test revealed that at this age, the genotypes were significantly different ($p < 0.05$) and I concluded that at this age, the proportion of leptin-responsive neurons differed between genotypes.

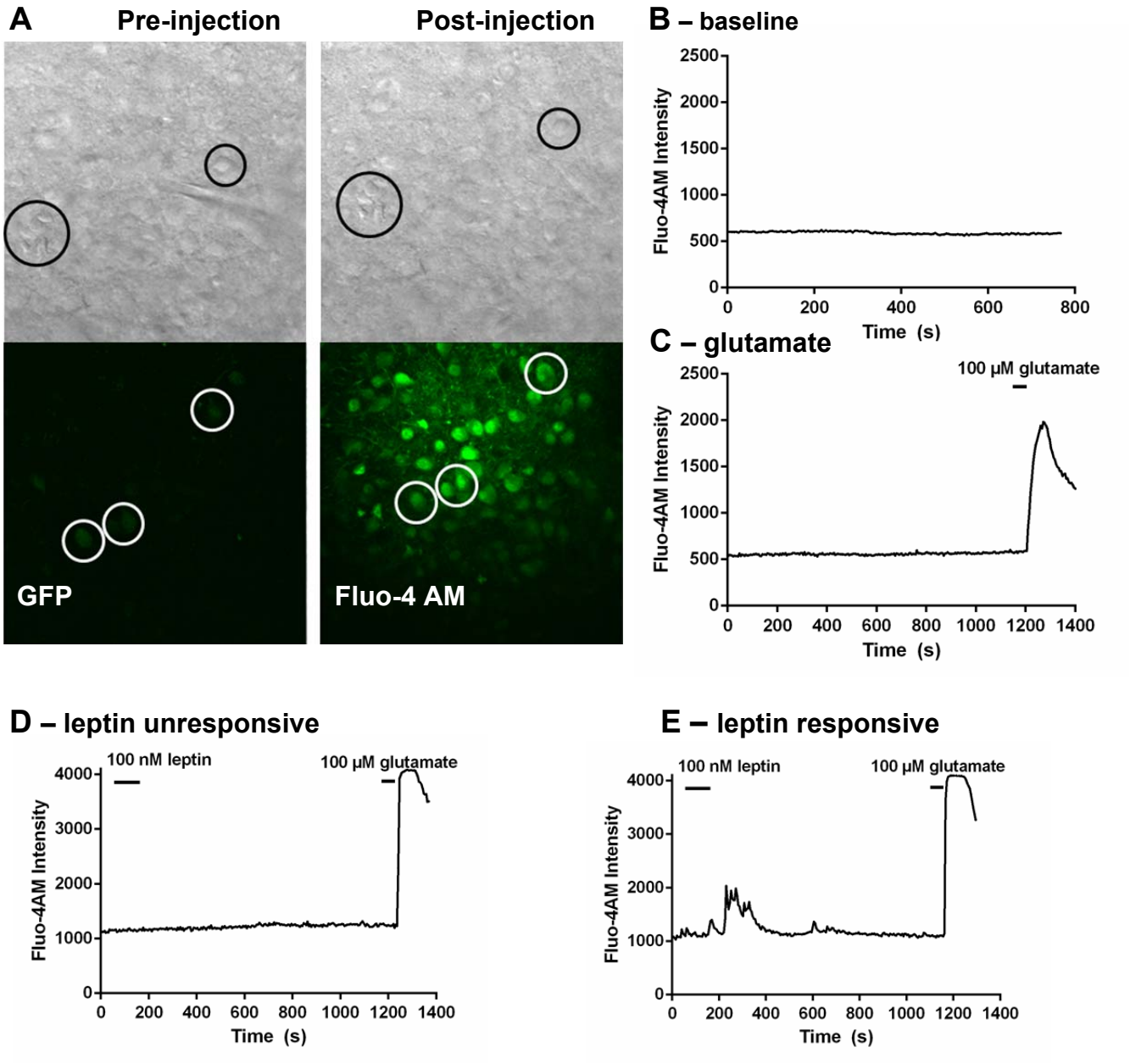

Figure 17. Calcium imaging: leptin responses in ARC POMC neurons. A) Arcuate neurons in the same brain slice and Z plane under infrared-differential interference contrast imaging (top panels) and two photon microscopy (bottom panels). The same POMC neurons are circled in images taken before and after Fluo-4 AM injection. B) baseline and C) glutamate-induced (100 µM) calcium signal profile for the same $POMC^{EGFP}$ neuron. D) Typical calcium signal profile of a $POMC^{EGFP}$ neuron that fails to respond to 100 nM leptin but responds to 100 µM glutamate. E) Typical calcium signal profile of a $POMC^{EGFP}$ neuron that responds to both, 100 nM leptin and to 100 µM glutamate.

Next, I examined mice of both genotypes starting at P21 to determine the earliest time point where mutant POMC neurons differ from those of wildtypes in their ability to respond to leptin (Table 5). At P21, I found leptin-induced increases in calcium intensity in 17 of 121 POMC neurons of wildtype mice and in 15 of 55 POMC neurons of *Magel2*-null mice. At P21, both genotypes had a comparable number of leptin-responsive POMC neurons according to the Fisher's exact test ($p > 0.05$). At P28, there were leptin-induced increases in calcium intensity in 13 of 47 POMC neurons of wildtype mice and in 28 of 80 POMC neurons of *Magel2*-null mice. The Fisher's exact test revealed that at P28 wildtypes and mutants had a comparable number of leptin-responsive POMC neurons ($p > 0.05$). However, at P42 I found leptin-induced increases in calcium intensity in 40 of 94 POMC neurons of wildtype mice but only 7 of 69 POMC neurons of *Magel2*-null mice responded to leptin. This difference is significant according to the Fisher's exact test ($p < 0.05$). I concluded that there is a decrease in the proportion of POMC neurons from *Magel2*-null mice that respond to leptin stimulation when the mouse is between 4 and 6 weeks of age.

3.5 *Magel2*-null mice are hypersensitive to MTII by 4 weeks of age

A loss of depolarization of POMC neurons is predicted to impair the release of α-MSH release from axon terminals of neurons due to the coupling of peptide release with calcium influx (Kolk et al., 2002). Administration of endogenous α-MSH or synthetic analog normally produces a reduction in food intake over 24 hours in mice. Several studies previously showed that administration of α-MSH or the synthetic analog MTII produces an exaggerated response in the *Magel2*-null as well as other animal models of leptin insensitivity (Hansen et al., 2001, Mercer et al., 2013, Scarpace et al., 2003, Li et al., 2004). Thus, I examined whether MTII administration to young *Magel2*-null mice would also produce an exaggerated behavioral response as measured by food intake. Since the leptin-melanocortin signalling pathway does not fully develop until after weaning (Mistry et al., 1999) and because food intake cannot be reliably measured until after weaning, I chose P21 as the earliest time point for studying the behavioural responses to melanocortin administration (i.e. food intake) in mice.

Table 5. Calcium imaging: leptin responses in ARC POMC neurons at different ages. Counts of arcuate POMC neurons, which are responsive and unresponsive to leptin stimulation. At P21 and P28, there is no difference in the number of leptin-responsive neurons between genotypes (Fisher's exact test). In young adults (6 week-old animals) and old adults (12-14 week-old animals), there is a statistically significant difference between genotypes in the number of leptin-responsive POMC neurons. WT, wildtype; M, mutant.

POMC neurons	**# Responsive**	**# Unresponsive**	**Sample Size**	**P-value**
P21 (WT)	17	104	3	
P21 (M)	15	40	2	>0.05
P28 (WT)	13	34	2	
P28 (M)	28	52	3	>0.05
Young adult (WT)	40	54	3	
Young adult (M)	7	62	3	0.0001
Old adult (WT)	12	27	3	
Old adult (M)	1	51	3	0.0001

I divided pups into four groups: wildtype + vehicle, wildtype + MTII, *Magel2*-null + vehicle, and *Magel2*-null + MTII. I administered an ip injection of MTII or vehicle alone (saline) at 15:00, fasted mice for 1 h to reduce variability between nutritional states, and recorded weight of food pellets in cage tops at 16:00, 18:00, 20:00 h and on the following day at 8:00 and 16:00 h. Differences between genotypes were ascertained using a two-way ANOVA. At P21 (n = 6-10), a single MTII ip injection (2.5 mg/kg) produced a robust 50% decrease in food intake 2 h after injection in both, wildtype and *Magel2*-null mice (Fig. 18A). However, P21 *Magel2*-null mice were not hypersensitive to MTII at 2 h, 4 h, 16 h or 24 h following injection. At 4 weeks of age (n = 8-9), *Magel2*-null mice consumed half as much food 2 h following MTII injection compared to wildtypes but the food intake of MTII-treated mutants normalized to vehicle-injected control levels by 16 h after injection (Fig. 18B). However, this hypersensitivity of MTII-treated mutants was not evident in the same mice at 5 or 6 weeks of age (Fig. 18C-D). I concluded that *Magel2*-null mice are first hypersensitive to MTII administration at 4 weeks of age.

3.6 Long-term MTII treatment does not reduce long-term food intake or body weight

Prolonged 5-day administration of MTII was previously shown to reduce long-term food intake. In rats, daily central administration of MTII (1 mg/kg) reduced food intake by more than 50% on day 1, and this response gradually attenuated by day 5 after which no further reduction was observed (Zhang et al., 2010). Another study tested the effect of MTII (2.5 mg/kg) administered ip four times daily to DIO mice and reported a 50% reduction in food intake 1.5 days after the first injection, with gradual attenuation by day 5 (Pierroz et al., 2002). Daily doses as low as 2.5 mg/kg proved to be equally effective when administered ip (Mercer et al., 2013). Thus to investigate long-term effect of MTII, I administered the drug to adult (6 week old) mice (n = 4-6) at a concentration of 2.5 mg/kg, daily for 5 days. Preliminary data from this pilot study showed a reduction in food intake for MTII-treated wildtype and mutant mice at 2 and 4 h post injection. Food intake returned to saline-treated baseline levels at 16 h and showed no further

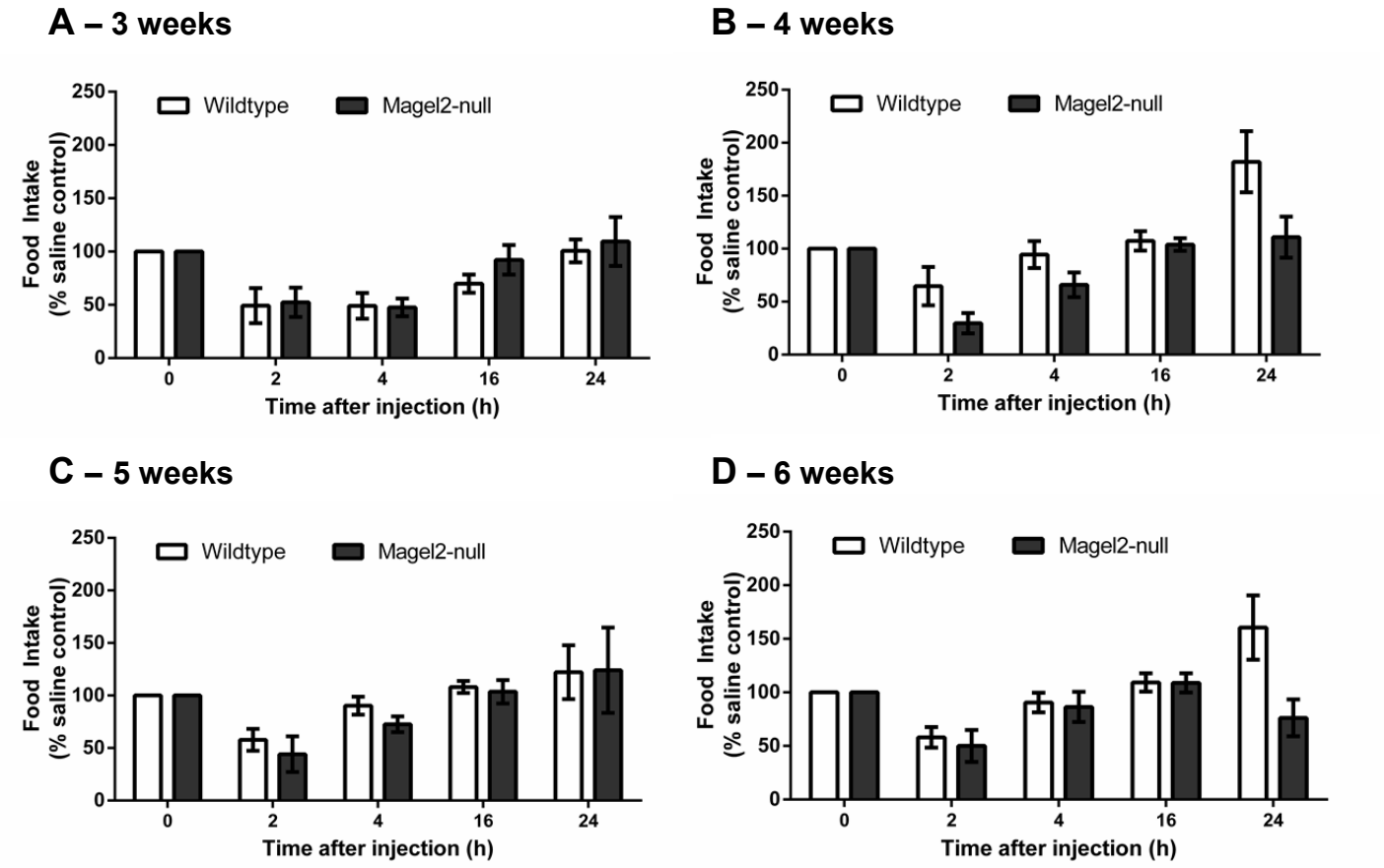

Figure 18. Food intake following MTII injection at various ages. A-D) Food intake after a single intraperitoneal injection of MTII (2.5 mg/kg) following a 1 hour fast in wildtype and *Magel2*-null mice at A) 3 weeks, B) 4 weeks, C) 5 weeks, and D) 6 weeks of age. MTII reduced food intake in wildtypes 2 h following injection to a similar degree at all ages tested. Food intake was restored to baseline levels by 16 h after injection. *Magel2*-null mice were hypersensitive to MTII administration at the 2 h time point at 4 weeks of age. Values are means ± SEM.

reduction from this time point onward (Fig. 19A). *Magel2*-null mice were also not hypersensitive to MTII administration. Unlike previous studies that report a progressive reduction in body weight of rodents following multiple MTII administrations (Pierroz et al., 2002, Zhang et al., 2010), I found that daily ip administration of MTII (2.5 mg/kg) did not reduce body weight of *Magel2*-null mice when compared to saline-injected controls throughout the 5 day pilot study (Fig. 19B). All of the results presented in this thesis as well as previous characterization of the *Magel2*-null mouse phenotype are summarized in Table 6.

A

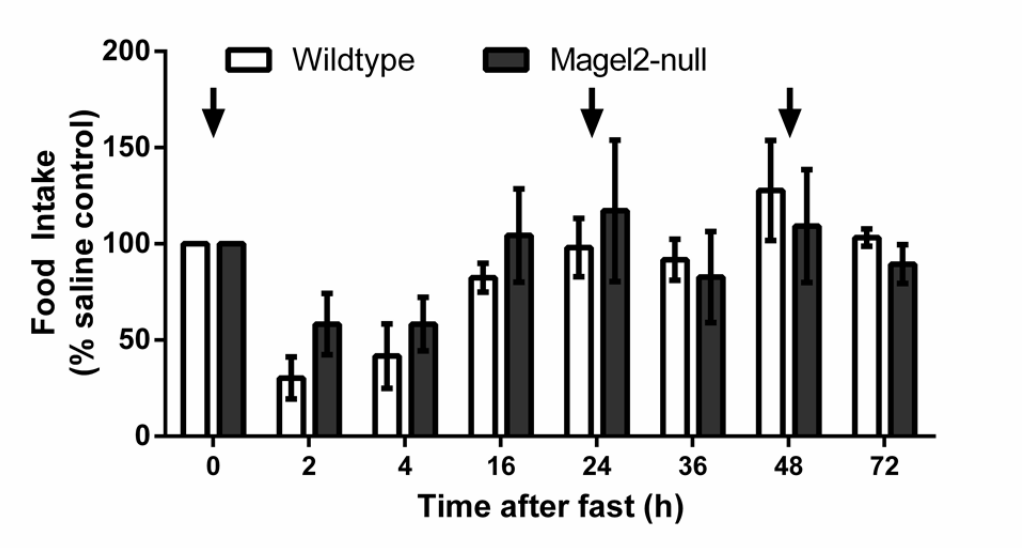

B

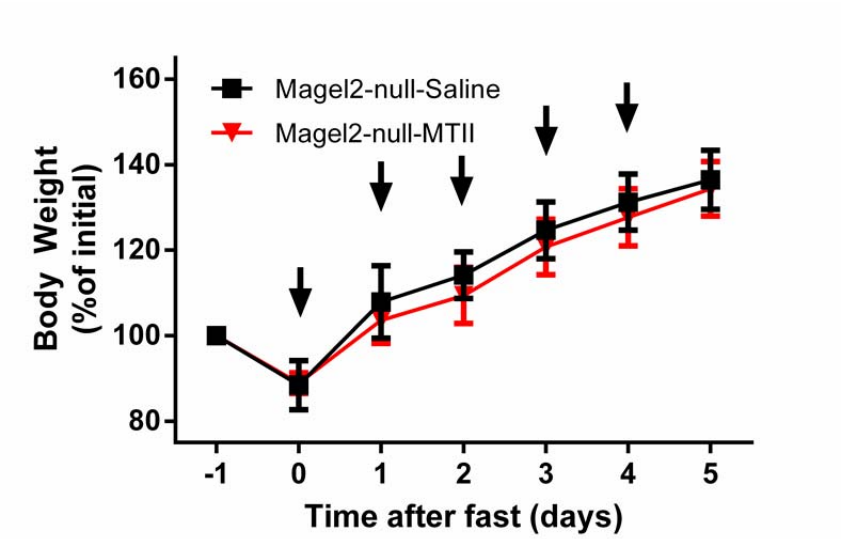

Figure 19. Food intake and body weight following long-term MTII treatment. A) Food intake after 3 intraperitoneal injections of MTII (2.5 mg/kg) given on consecutive days, following a 24 h fast of wildtype and *Magel2*-null mice at 6 weeks of age. MTII reduced food intake 2 h following injection but did not lead to long term suppression of food intake in either genotype. B) Body weight after 5 intraperitoneal injections of MTII (2.5 mg/kg) or vehicle alone given on consecutive days, following a 24 h fast of *Magel2*-null mice at 6 weeks of age. Arrows represent MTII administration. Values are means ± SEM.

Table 6. Summary of results and characterization of the *Magel2*-null mouse phenotype. Results presented in this thesis have sample sizes associated with them in this table whereas previous findings do not. *Too much spontaneous activity.

***Magel2*-null mouse:**	**P10**	**3 week-old**	**4 week-old**	**6 week-old**	**Older adult**
pSTAT3 activation	Normal (n = 3)	-	-	-	Reduced
POMC cell count	Normal (n = 3)	-	-	-	Reduced
POMC leptin response (electrophysiology)	Responsive* (n = 2)	-	-	-	Unresponsive
POMC leptin response (calcium imaging)	-	Responsive (n = 2-3)		Unresponsive (n = 3)	
MTII response (food intake)	-	Normal (n = 6-10)	Hypersensitive (n = 8-10)		Hypersensitive

Chapter 4. Discussion

4.1 ARC POMC neurons of the *Magel2*-null mouse can sense leptin

In characterizing the *Magel2*-null mouse model for PWS, our group uncovered defects in many areas, including reproduction, endocrine function, circadian rhythm, behaviour and body weight regulation. The latter is particularly intriguing given that obesity and related complications are responsible for the 3% annual mortality rate of PWS patients (Butler et al., 2002). Importantly, ours is the only mouse model created to date that partially recapitulates increased adiposity seen in PWS patients, allowing us to study the etiology of this vital clinical component on a cellular and molecular level (Chamberlain and Lalande, 2010). Previous work with the *Magel2*-null mouse identified defects in signalling of leptin—a peptide hormone crucial to hypothalamic control of energy metabolism. These mice have increased circulating leptin, suggesting reduced sensitivity to this hormone (Bischof et al., 2007). Support for this hypothesis emerges from the finding that adult mutant mice, unlike wildtypes, fail to reduce food intake in response to peripherally-administered leptin (Mercer et al., 2013). To further ascertain the cause of this leptin insensitivity, our group examined whether leptin is able to bind its receptor (LepRb) in the ARC and initiate a downstream signalling cascade by phosphorylating the transcription factor STAT3, thereby activating it. Although leptin treatment increased the number of ARC pSTAT3-IR neurons in adult animals of both genotypes, leptin-treated adult mutants had fewer pSTAT3-IR neurons than did leptin-treated wildtypes (Mercer et al., 2013). In determining when this defect is first apparent in the *Magel2*-null mouse, I examined pSTAT3-IR at P10 and found that both mutant and wildtype mice responded to leptin with increased phosphorylation of STAT3 in the ARC when compared to saline-injected controls. However, there was no difference in the number of pSTAT3-IR neurons between leptin-injected mutants and wildtypes, which indicates normal leptin sensitivity at LepRb in the ARC of young mutant animals. Although it is not possible to measure pSTAT3 activation at birth because of low LepRb expression in the ARC (Bouret et al., 2012), it is likely that *Magel2*-null neonates are born with a normal number of leptin-sensing ARC neurons.

The reduced pSTAT3 activation that we see in adult *Magel2*-null mice could be due to: 1) decrease in the number of leptin-responsive neurons in the ARC, and/or 2) loss of leptin sensitivity at the leptin receptor in a subpopulation of ARC neurons. Immunohistochemical

analysis revealed that adult *Magel2*-null mice have a reduced number of POMC neurons in the ARC when compared to wildtypes (Mercer et al., 2013). Although it supports the former hypothesis, this finding does not rule out the possibility that some remaining ARC POMC neurons may also lose the ability to initiate pSTAT3 signalling. To explore this hypothesis in P10s, I performed immunohistochemical double-labelling with pSTAT3+eGFP on ARC neurons of our Magel2$^{-m/+p}$ x POMC^{EGFP} cross progeny. Cell counting revealed that an equal proportion of POMC neurons responded to ip leptin with pSTAT3 activation in *Magel2*-null and wildtype pups. Thus, the proportion of ARC POMC neurons that sense leptin and initiate the appropriate signalling cascade downstream of LepRb is the same in mutant mice and age-matched wildtype mice at P10.

4.2 Apoptosis may be responsible for the decline in the POMC neuronal population of the ARC

Mutant and wildtype pups have a comparable number of ARC POMC neurons at P10, but in adulthood mutants have a reduced number of these cells. Given that POMC neurogenesis is complete by E13 and that these neurons acquire terminal phenotype at E15, it is highly unlikely that this reduction in *Magel2*-null POMC cell number results from decreased proliferation or impaired differentiation postnatally (Khachaturian et al., 1985, Padilla et al., 2010). Thus, it is likely that apoptosis is occurring, which in theory could be investigated with a quantitative measurement of cell death (e.g. by a TUNEL assay) but in practice, it would be very difficult to execute for the following reasons. If the apoptotic wave is brief, on the order of hours or several days, we would need to examine mice at many individual time points between P10 and 6 weeks of age (adulthood). Even if apoptosis is gradual, the observed reduction in POMC cells count is only 30%, which necessitates an examination of many mice at each time point to reveal any statistically significant differences between genotypes. This question should be addressed, but at a later date when we know more about cellular and molecular processes underlying loss of *Magel2* in relation to hypothalamic energy circuits, which would focus our search for apoptosis to a narrower developmental time frame.

4.3 Impairment of POMC-mediated anorexigenic drive that is first apparent between 4 and 6 weeks of age in *Magel2*-null mice causes adiposity and reduced energy expenditure

The aforementioned hypothalamic impairments seen in *Magel2*-null mice prompted our research group to focus on neuronal subpopulations within the ARC. A previous electrophysiology study showed that no ARC POMC neurons of adult mutant mice depolarize in response to leptin stimulation. Since depolarization is coupled to peptide release at their axon terminal, these defective POMC neurons are predicted to lack secretion of α-MSH, a crucial anoroxigenic peptide (Kolk et al., 2002). On the contrary, the antagonistic AgRP neurons of adult *Magel2*-null mice respond to leptin as expected, suggesting that orexigenic peptide release from these cells is normal (Mercer et al., 2013). To see if these findings hold true in younger animals, I repeated the experiment on P10 mice. Interestingly, POMC neurons of young mutants depolarize in response to leptin. Moreover, the magnitude of depolarization is comparable to that of wildtype POMC neurons and coincides with a previously-reported mean membrane potential change of -5mV (Mercer et al., 2013). Unfortunately, the reliability of this result is questionable because baseline membrane potential fluctuated much more at P10 than it did in adult brain slices, which made it difficult to determine whether the responses I saw were real or simply a by-product of an unsteady baseline. Since electrophysiology could not reliably show when POMC neurons of *Magel2*-null mice lose their ability to respond to leptin's anorixegenic effects, I used a different method to answer this question.

Calcium imaging is a technique that visualizes intracellular Ca^{2+} influx using calcium-sensitive dyes and may use two-photon confocal microscopy. This method is usually restricted to cell cultures and slices of neonatal tissue because many adult tissues do not load well with bulk-applied membrane-permeant dyes (Stosiek et al., 2003). An abundance of glial cells which preferentially absorb the dye limits its availability to adjacent neurons. Surprisingly, I was able to load ARC neurons from animals as old as 14 weeks of age with Fluo-4AM dye. The mice used for these experiments came from my $Magel2^{-m/+p}$ x $POMC^{EGFP}$ crosses. This unusual technical finding may reflect a general property of the ARC. Implicit is the idea that our mice can be used to study fully developed neuronal networks involving the ARC to uncover yet-unidentified macroscopic features of processing networks within this nucleus. The lack of discernible patterns

in the baseline activity of ARC POMC neurons studied suggests that these cells act independently of one another. The heterogeneity of baseline oscillations seen in this neuronal subpopulation agrees with the previous finding that distinct POMC neuronal populations exist (Sohn et al., 2011).

To validate the calcium imaging method for my experiment, I replicated previous electrophysiology findings using this complimentary technique (Mercer et al., 2013). Unlike wildtypes, adult (12-14 week old) *Magel2*-null mice have no (or very few) leptin-responsive POMC neurons in the ARC. Upon careful examination of calcium responses at various ages, I found that POMC neurons of mutant mice are leptin-responsive at 3 and 4 weeks of age but lose this ability by 6 weeks of age. The inability of POMC cells to respond to leptin and secrete α-MSH onto downstream PVN targets ablates a major component of the anorexigenic drive in *Magel2*-null animals (Mercer et al., 2013). Since the NPY neuronal function seems to be unperturbed, the orexigenic drive is likely still present. The lack of antagonism that would normally be supplied by POMC neurons would allow the orexigenic drive to dominate. Strikingly, the age at which *Magel2*-null mice first display impaired energy homeostasis coincides with the period of fastest weight gain (Bischof et al., 2007). Thus, the loss of ARC POMC signalling that leads to an impaired anorexigenic drive is the likely reason why our mutant mice have diminished physical activity, increased adiposity and higher body weight.

Since *Magel2*-null mice are not born with this anorexigenic defect but develop it in late adolescence/early adulthood, we can hope to therapeutically delay, arrest or even reverse the loss of leptin responsiveness of POMC neurons. Importantly, I narrowed down the onset of this defect to a 2 week period between 4 and 6 weeks of age. Therapeutic intervention may be most useful during this age gap or at an earlier time point, depending on underlying pathology. Thus, further efforts to pinpoint the age at which *Magel2*-null POMC neurons lose their ability to respond to leptin may not be warranted. Nevertheless, before effective therapeutic agents can be developed it is important to understand the underlying defect that causes loss of function in ARC POMC neurons of mutant mice. We know that these neurons have functional leptin receptors but fail to secrete a major peptide product—α-MSH in response to leptin administration. It follows that mutant ARC POMC cells are defective in leptin signalling somewhere downstream of LepRb activation but upstream of α-MSH release. Points of interest include: POMC transcription

and translation, POMC cleavage, α-MSH anterograde transport and secretory vesicle formation and release. Given that POMC neurons fail to depolarize and that depolarization is coupled to α-MSH release, secretory vesicles are likely not released in *Magel2*-null mice perhaps due to impaired intracellular signalling. This hypothesis could be tested by culturing neuronal explants and measuring α-MSH release into culture media (Wren et al., 2002). Even if this hypothesis is supported by experimental evidence, it would still be important to investigate any potential defects in α-MSH production, transport and vesicle packing. This is because therapies would need to ensure that α-MSH is not only effectively secreted but also properly synthesized and transported.

4.4 Onset of melanocortin hypersensitivity parallels timing of development of the leptin-melanocortin system

The *Magel2*-null mouse has a defect in the leptin signalling pathway, predicted to result in a lack of α-MSH secretion onto target PVN neurons. However, we have reason to believe that downstream leptin-dependent anorexigenic brain circuitry is largely unperturbed. It follows that acute administration of α-MSH or a similar compound which activates MC4R receptors in the PVN should induce an anorexigenic response in our mutant mice. Indeed, a previous study found that ip administration of MTII, a synthetic analog of α-MSH, causes a pronounced reduction in food intake in *Magel2*-null and wildtype mice (Mercer et al., 2013). MTII belongs to a class of compounds known as melanocortin receptor agonists. Although MTII binds both, MC3R and MC4R receptors, it elicits its behavioral response primarily through MC4R (Marsh et al., 1999, Chen et al., 2000). This compound is a useful research tool for studying murine melanocortin responses because it has a longer half-life than α-MSH and cell culture experiments show that MTII is over 100 times more potent than its endogenous analog in activating the murine MC4R receptor (Mock et al., 2002, Adan et al., 1999, Wright and Wilson, 1983).

A peculiar abnormality of the melanocortin system in *Magel2*-null mice was previously noted and prompted my investigation of mutant mice at different ages to determine when it first occurs. Two hours following MTII administration adult *Magel2*-null mice reduce their food

intake by roughly twice as much as MTII-injected wildtypes. As the drug is excreted from the system in the hours to come, this disparity between genotypes diminishes and is no longer apparent 24 h following treatment (Mercer et al., 2013). We hypothesized that this hypersensitivity to MTII results from loss of melanocortinergic tone from ARC POMC neurons, which is predicted to manifest itself in an increased number of MC4R on target cells in the PVN. Other studies involving leptin-insensitive rodent models also found exaggerated responses to MTII, providing support for this hypothesis (Scarpace et al., 2003, Li et al., 2004). In addition, chronic lack of receptor stimulation by its agonist results in compensatory upregulation of the receptor in many biological pathways (Pokk et al., 1996, Sutton et al., 2003, Ghisi et al., 2009). Nevertheless, it would be beneficial to address this question directly by quantifying MC4R in the PVN of *Magel2*-null mice and wildtypes. My study analyzed melanocortin responses starting at weaning age (P21)—the earliest time point at which leptin signalling begins to mature and food intake can be measured reliably. At this age, *Magel2*-null mice respond to MTII with a reduction in food intake; however, no melanocortin hypersensitivity is apparent when comparing mutants to wildtypes. In contrast, starting at P28 mutants begin to show the same melanocortin hypersensitivity pattern as the *Magel2*-null adults. This is not surprising, given that physiological leptin-melanocortin responses (such as food intake) first appear at P28, and that the PVN neurons are less excitable before P28 (Mistry et al., 1999, Melnick et al., 2007). Thus, if MC4R upregulation is indeed taking place, it must happen between 3 and 4 weeks of age. I originally predicted that the loss of ARC POMC depolarization and concomitant abrogation of α-MSH release would trigger MTII hypersensitivity of the PVN in *Magel2*-null mice. However, this cannot be true because the onset of hypersensitivity precedes loss of depolarizing responses in POMC neurons. A plausible alternate hypothesis involves a confounding variable that is responsible for both of the aforementioned observations. This confounder may be a crucial developmental biology process underlying the pathology of *Magel2* loss.

4.5 Developing and testing alternative therapies for PWS patients

Few treatments for PWS have been developed so far, the most promising of which is growth hormone (GH) therapy. Benefits of the FDA-approved GH treatment for individuals with PWS include normalized height, increased lean muscle mass and reduced body fat (Carrel et al., 2002, Angulo et al., 2007). While GH treatment is particularly beneficial to PWS patients with short stature, it can induce diabetes mellitus in children who are already obese. Once GH-induced diabetes mellitus develops, physicians recommend cessation of GH administration, which leaves few treatment options for the patient. Additionally, although GH therapy reduces body fat, it has no effect on hyperphagia; thus, there exists a need to develop other treatment options. My project continued to test the feasibility of melanocortin agonists (namely MTII) as novel PWS therapeutic agents. In a pilot study, I administered ip MTII once a day for 5 days to mutant and wildtype adult mice. Similar studies in rats and diet-induced obese (DIO) mice showed that comparable doses of MTII reduce food intake by 50% a day after initial injection, but this effect attenuates 4 days later (Zhang et al., 2010, Pierroz et al., 2002). Both of these groups also reported progressive reduction in body weight across the 5 day period and beyond. I was unable to detect a similar MTII-induced reduction in food intake or body weight in our mutant and wildtype mice. This may be attributed to differences in animal models. Both rats and DIO mice are significantly heavier than the mice used in my study and heavier animals have more adipose tissue that they can lose. A more probable explanation is the contention that my experiment was a pilot study involving a small sample size, which is unable to allow for detection of small differences between groups. A small sample size is also the likely reason that hindered my ability to detect MTII hypersensitivity in these *Magel2*-null adult mice. As a preclinical study, this effort may have been somewhat premature. A major issue with MTII treatment is that it produces hypertension, diminishing its clinical utility (Fani et al., 2014). Nevertheless, safer α-MSH analogs are currently being developed and this long-term pilot study may be repeated in the future, with major modifications. First, it will likely require a significantly larger sample size. Second, we may need to record food intake more precisely. Instead of using a weight scale with a precision of ± 0.1 g, we may need to measure food intake in a metabolic chamber. However, metabolic chambers may present a confounding variable

because *Magel2*-null mice experience increased anxiety in novel environments. If switched from pellet chow to powdered chow, wildtype mice consume less food for the first two days but increase food intake to normal levels thereafter. In contrast, mutant mice reduce intake of powdered food in this "novel" environment and never regain normal levels of food consumption (Mercer et al., 2009). Nevertheless, weaning mutants directly into metabolic chambers may greatly diminish their anxiety response. Third, since *Magel2*-null mice are not grossly overweight but instead have significantly more adipose tissue but proportionately less lean mass, it may also be important to measure adiposity and lean mass in addition to body weight. Last, the timing of drug administration must be considered. Still, melanocortin agonists are promising therapeutic agents for treating obesity. An MC4R receptor agonist, RM 493, is currently in Phase 2 clinical trials for weight loss. The melanocortin hypersensitivity seen in *Magel2*-null mice can be exploited to allow for administration of lower drug concentration, thereby reducing side effects. My results suggest that therapeutic agents analogous to α-MSH and MTII should be tested on *Magel2*-null mice no earlier than 4 weeks of age. Melanocortin agonists circumvent any upstream defects in the anorexigenic leptin signalling pathway of *Magel2*-null mice by completing the ARC to PVH neural circuit. However, a greater understanding of the underlying pathology in loss of *Magel2* may present the possibility to forgo chronic treatment with melanocortin agonists in lieu of a curative solution.

4.6 A model for understanding Magel2 involvement in PWS etiology

Interaction of Magel2 with the E3 RING ubiquitin ligase TRIM27 has been shown to greatly enhance the enzymatic activity of the latter. Activated TRIM27 is then able to ubiquitinate the WASH complex, activating its VCA motif (Hao et al., 2013). As part of endosomal protein recycling, a retromer complex recognizes retrograde cargo. When activated WASH binds to the VPS35 subunit of the retromer complex, WASH can recruit Arp2/3. This results in actin filament nucleation (F-actin), which is essential for fission of endosomes. Conversely, lack of Magel2 significantly impairs this process, which in turn impairs endosomal function. Interestingly, a rare autosomal-dominant form Parkinson's disease due to a VPS35

mutation not only perturbs endosomal recycling but also autophagy. This finding is first to implicate the WASH complex in autophagy (Zavodszky et al., 2014). Consequently, lack of Magel2 should also lead to impaired autophagy. Since autophagosome membrane is synthesized *de novo*, it could contribute to the cytoplasmic remodelling that occurs during growth of axons (Pereira et al., 2012). In fact, autophagy is not only constitutively active in POMC neurons during mouse development, but the deletion of autophagy genes in these POMC neurons reduces α-MSH fibre density in targets of the ARC nucleus including the PVN (Coupe et al., 2012). I propose that the absence of Magel2 at birth greatly impairs autophagy, which in turn hinders the extension of axons from the ARC to downstream target nuclei during the early postnatal period.

The phenotype that we see in *Magel2*-null mice may be a direct manifestation of this pathology. Since mice show a mature pattern of hypothalamic innervation by P18 but the first behavioural responses to leptin appear at P28, the defect in axonal extension may not be apparent at the gross organismal level until after weaning (Bouret et al., 2004, Mistry et al., 1999). In support of this hypothesis, *Magel2*-null mice are underweight at P7 (likely due to other physiological processes independent of energy homeostasis) but gain weight more rapidly than their wild type counterparts just after weaning (Bischof et al., 2007). The ARC innervates PVN at P8-P10 and begins releasing α-MSH onto the second-order neurons of the PVN. The development of a fully functional leptin-melanocortin system that regulates energy homeostasis requires roughly another two weeks, as demonstrated by lack of behavioural responses to exogenous leptin prior to P28. It is at this age that a lack of α-MSH due to impaired axonal extension from ARC POMC neurons would first affect PVN neurons. Predictably, these neurons would upregulate the MC4R receptors. It is not surprising that hypersensitivity to MTII is non-existent at P21 but becomes readily apparent at P28. This model may also explain the reduction of ARC POMC neurons seen in in *Magel2*-null as they age. It is conceivable that impaired axonal projections from POMC neurons would result in a reduction of trophic support from target nuclei, culminating in apoptosis. The POMC neurons of the ARC that do survive may instead experience cellular changes that render them incapable of stimulated depolarization. This is precisely what we see in 6 week old animals whose POMC neurons fail to depolarize in response to leptin.

This model provides a basis for understanding the relevance of the loss of *Magel2* to the experimental findings of this thesis. To test the hypotheses proposed herein, one could examine the density of α-MSH fibers in the PVN at P18-P28 to determine whether axonal projections from the ARC are indeed impaired. If such is the case, one could then investigate whether autophagy is diminished in POMC neurons using mice from the *Magel2* x $POMC^{EGFP}$ cross. The best age to analyze would be before P10 because ARC to PVN connections should already be formed by then, and any impairment in autophagy occurring after P10 cannot be reliably correlated with a defect in axonal extension.

4.7 Clinical relevance

Today, it is still not known how deletions and mutation on chromosomal region 15q11-q13 translate into the complex and variable phenotype of PWS patients. Through studies such as this one, we can attempt to decipher PWS etiology one clinical finding at a time. This work focused on the role of *MAGEL2* in obesity and provides a potential molecular explanation for the pathology of obesity and dysregulation in energy homeostasis in PWS. Previously it was unknown whether leptin insensitivity of *Magel2*-null mice was a congenital or perhaps a degenerative phenomenon. Results from experiments outlined herein indicate that leptin insensitivity is not congenital and not a consequence of obesity. Moreover, the leptin insensitivity in PWS may actually cause obesity but further research is needed to confirm this link. The existence of a period where POMC neurons are responsive to leptin establishes a therapeutic window of opportunity for treating PWS patients with melanocortin agonists and related compounds. I also suggest potential avenues for future work in developing and testing novel therapies for PWS. The evolutionary conservation of homeostatic mechanisms among mammals lends confidence to the applicability of findings from animal studies in helping us understand disorders affecting the human population.

References

ABREU, A. P., DAUBER, A., MACEDO, D. B., NOEL, S. D., BRITO, V. N., GILL, J. C., CUKIER, P., THOMPSON, I. R., NAVARRO, V. M., GAGLIARDI, P. C., RODRIGUES, T., KOCHI, C., LONGUI, C. A., BECKERS, D., DE ZEGHER, F., MONTENEGRO, L. R., MENDONCA, B. B., CARROLL, R. S., HIRSCHHORN, J. N., LATRONICO, A. C. & KAISER, U. B. 2013. Central precocious puberty caused by mutations in the imprinted gene MKRN3. *N Engl J Med,* 368**,** 2467-75.

ADAN, R. A., SZKLARCZYK, A. W., OOSTEROM, J., BRAKKEE, J. H., NIJENHUIS, W. A., SCHAAPER, W. M., MELOEN, R. H. & GISPEN, W. H. 1999. Characterization of melanocortin receptor ligands on cloned brain melanocortin receptors and on grooming behavior in the rat. *Eur J Pharmacol,* 378**,** 249-58.

ANGULO, M. A., CASTRO-MAGANA, M., LAMERSON, M., ARGUELLO, R., ACCACHA, S. & KHAN, A. 2007. Final adult height in children with Prader-Willi syndrome with and without human growth hormone treatment. *Am J Med Genet A,* 143a**,** 1456-61.

BANKS, A. S., DAVIS, S. M., BATES, S. H. & MYERS, M. G., JR. 2000. Activation of downstream signals by the long form of the leptin receptor. *J Biol Chem,* 275**,** 14563-72.

BIEBERMANN, H., KUHNEN, P., KLEINAU, G. & KRUDE, H. 2012. The neuroendocrine circuitry controlled by POMC, MSH, and AGRP. *Handb Exp Pharmacol***,** 47-75.

BIETH, E., EDDIRY, S., GASTON, V., LORENZINI, F., BUFFET, A., CONTE AURIOL, F., MOLINAS, C., CAILLEY, D., ROORYCK, C., ARVEILER, B., CAVAILLE, J., SALLES, J. P. & TAUBER, M. 2014. Highly restricted deletion of the SNORD116 region is implicated in Prader-Willi Syndrome. *Eur J Hum Genet*.

BISCHOF, J. M., STEWART, C. L. & WEVRICK, R. 2007. Inactivation of the mouse Magel2 gene results in growth abnormalities similar to Prader-Willi syndrome. *Hum Mol Genet,* 16**,** 2713-9.

BJORBAEK, C., ELMQUIST, J. K., MICHL, P., AHIMA, R. S., VAN BUEREN, A., MCCALL, A. L. & FLIER, J. S. 1998. Expression of leptin receptor isoforms in rat brain microvessels. *Endocrinology,* 139**,** 3485-91.

BJORBAEK, C., UOTANI, S., DA SILVA, B. & FLIER, J. S. 1997. Divergent signaling capacities of the long and short isoforms of the leptin receptor. *J Biol Chem,* 272**,** 32686-95.

BJORBAK, C., LAVERY, H. J., BATES, S. H., OLSON, R. K., DAVIS, S. M., FLIER, J. S. & MYERS, M. G., JR. 2000. SOCS3 mediates feedback inhibition of the leptin receptor via Tyr985. *J Biol Chem,* 275**,** 40649-57.

BONIFACINO, J. S. & ROJAS, R. 2006. Retrograde transport from endosomes to the trans-Golgi network. *Nat Rev Mol Cell Biol,* 7**,** 568-79.

BOURET, S. G., BATES, S. H., CHEN, S., MYERS, M. G., JR. & SIMERLY, R. B. 2012. Distinct roles for specific leptin receptor signals in the development of hypothalamic feeding circuits. *J Neurosci,* 32**,** 1244-52.

BOURET, S. G., DRAPER, S. J. & SIMERLY, R. B. 2004. Formation of projection pathways from the arcuate nucleus of the hypothalamus to hypothalamic regions implicated in the neural control of feeding behavior in mice. *J Neurosci,* 24**,** 2797-805.

BOURET, S. G. & SIMERLY, R. B. 2007. Development of leptin-sensitive circuits. *J Neuroendocrinol,* 19**,** 575-82.

BREIT, A., BUCH, T. R., BOEKHOFF, I., SOLINSKI, H. J., DAMM, E. & GUDERMANN, T. 2011. Alternative G protein coupling and biased agonism: new insights into melanocortin-4 receptor signalling. *Mol Cell Endocrinol,* 331**,** 232-40.

BRESSLER, J., TSAI, T. F., WU, M. Y., TSAI, S. F., RAMIREZ, M. A., ARMSTRONG, D. & BEAUDET, A. L. 2001. The SNRPN promoter is not required for genomic imprinting of the Prader-Willi/Angelman domain in mice. *Nat Genet,* 28**,** 232-40.

BROBERGER, C. & HOKFELT, T. 2001. Hypothalamic and vagal neuropeptide circuitries regulating food intake. *Physiol Behav,* 74**,** 669-82.

BUITING, K. 2010. Prader-Willi syndrome and Angelman syndrome. *Am J Med Genet C Semin Med Genet,* 154c**,** 365-76.

BUSH, J. R. & WEVRICK, R. 2010. Loss of Necdin impairs myosin activation and delays cell polarization. *Genesis,* 48**,** 540-53.

BUTLER, A. A. & CONE, R. D. 2002. The melanocortin receptors: lessons from knockout models. *Neuropeptides,* 36**,** 77-84.

BUTLER, A. A., KESTERSON, R. A., KHONG, K., CULLEN, M. J., PELLEYMOUNTER, M. A., DEKONING, J., BAETSCHER, M. & CONE, R. D. 2000. A unique metabolic syndrome causes obesity in the melanocortin-3 receptor-deficient mouse. *Endocrinology,* 141**,** 3518-21.

BUTLER, J. V., WHITTINGTON, J. E., HOLLAND, A. J., BOER, H., CLARKE, D. & WEBB, T. 2002. Prevalence of, and risk factors for, physical ill-health in people with Prader-Willi syndrome: a population-based study. *Dev Med Child Neurol,* 44**,** 248-55.

BUTLER, M. G. 1990. Prader-Willi syndrome: current understanding of cause and diagnosis. *Am J Med Genet,* 35**,** 319-32.

BUTLER, M. G., MEANEY, F. J. & PALMER, C. G. 1986. Clinical and cytogenetic survey of 39 individuals with Prader-Labhart-Willi syndrome. *Am J Med Genet,* 23**,** 793-809.

BUTLER, M. G., THEODORO, M. F., BITTEL, D. C. & DONNELLY, J. E. 2007. Energy expenditure and physical activity in Prader-Willi syndrome: comparison with obese subjects. *Am J Med Genet A,* 143**,** 449-59.

CARON, E., SACHOT, C., PREVOT, V. & BOURET, S. G. 2010. Distribution of leptin-sensitive cells in the postnatal and adult mouse brain. *J Comp Neurol,* 518**,** 459-76.

CARREL, A. L., MYERS, S. E., WHITMAN, B. Y. & ALLEN, D. B. 2002. Benefits of long-term GH therapy in Prader-Willi syndrome: a 4-year study. *J Clin Endocrinol Metab,* 87**,** 1581-5.

CASSIDY, S. B. & DRISCOLL, D. J. 2009. Prader-Willi syndrome. *Eur J Hum Genet,* 17**,** 3-13.

CASSIDY, S. B., SCHWARTZ, S., MILLER, J. L. & DRISCOLL, D. J. 2012. Prader-Willi syndrome. *Genet Med,* 14**,** 10-26.

CECCONI, F. & LEVINE, B. 2008. The role of autophagy in mammalian development: cell makeover rather than cell death. *Dev Cell,* 15**,** 344-57.

CHAMBERLAIN, S. J. & LALANDE, M. 2010. Neurodevelopmental disorders involving genomic imprinting at human chromosome 15q11-q13. *Neurobiol Dis,* 39**,** 13-20.

CHEN, A. S., MARSH, D. J., TRUMBAUER, M. E., FRAZIER, E. G., GUAN, X. M., YU, H., ROSENBLUM, C. I., VONGS, A., FENG, Y., CAO, L., METZGER, J. M., STRACK, A. M., CAMACHO, R. E., MELLIN, T. N., NUNES, C. N., MIN, W., FISHER, J., GOPAL-TRUTER, S., MACINTYRE, D. E., CHEN, H. Y. & VAN DER PLOEG, L. H. 2000. Inactivation of the mouse melanocortin-3 receptor results in increased fat mass and reduced lean body mass. *Nat Genet,* 26**,** 97-102.

CHEN, Z., BOREK, D., PADRICK, S. B., GOMEZ, T. S., METLAGEL, Z., ISMAIL, A. M., UMETANI, J., BILLADEAU, D. D., OTWINOWSKI, Z. & ROSEN, M. K. 2010. Structure and control of the actin regulatory WAVE complex. *Nature,* 468**,** 533-8.

CHOMEZ, P., DE BACKER, O., BERTRAND, M., DE PLAEN, E., BOON, T. & LUCAS, S. 2001. An overview of the MAGE gene family with the identification of all human members of the family. *Cancer Res,* 61**,** 5544-51.

CLARREN, S. K. & SMITH, D. W. 1977. Prader-Willi syndrome. Variable severity and recurrence risk. *Am J Dis Child,* 131**,** 798-800.

CONSIDINE, R. V., SINHA, M. K., HEIMAN, M. L., KRIAUCIUNAS, A., STEPHENS, T. W., NYCE, M. R., OHANNESIAN, J. P., MARCO, C. C., MCKEE, L. J., BAUER, T. L. & ET AL. 1996. Serum immunoreactive-leptin concentrations in normal-weight and obese humans. *N Engl J Med,* 334**,** 292-5.

COUPE, B. & BOURET, S. G. 2013. Development of the hypothalamic melanocortin system. *Front Endocrinol (Lausanne),* 4**,** 38.

COUPE, B., ISHII, Y., DIETRICH, M. O., KOMATSU, M., HORVATH, T. L. & BOURET, S. G. 2012. Loss of autophagy in pro-opiomelanocortin neurons perturbs axon growth and causes metabolic dysregulation. *Cell Metab,* 15**,** 247-55.

COWLEY, M. A., SMART, J. L., RUBINSTEIN, M., CERDAN, M. G., DIANO, S., HORVATH, T. L., CONE, R. D. & LOW, M. J. 2001. Leptin activates anorexigenic POMC neurons through a neural network in the arcuate nucleus. *Nature,* 411**,** 480-4.

CYPESS, A. M., ZHANG, H., SCHULZ, T. J., HUANG, T. L., ESPINOZA, D. O., KRISTIANSEN, K., UNTERMAN, T. G. & TSENG, Y. H. 2011. Insulin/IGF-I regulation of necdin and brown adipocyte differentiation via CREB- and FoxO1-associated pathways. *Endocrinology,* 152**,** 3680-9.

DE SMITH, A. J., PURMANN, C., WALTERS, R. G., ELLIS, R. J., HOLDER, S. E., VAN HAELST, M. M., BRADY, A. F., FAIRBROTHER, U. L., DATTANI, M., KEOGH, J. M., HENNING, E., YEO, G. S., O'RAHILLY, S., FROGUEL, P., FAROOQI, I. S. & BLAKEMORE, A. I. 2009. A deletion of the HBII-85 class of small nucleolar RNAs (snoRNAs) is associated with hyperphagia, obesity and hypogonadism. *Hum Mol Genet,* 18**,** 3257-65.

DERIVERY, E., SOUSA, C., GAUTIER, J. J., LOMBARD, B., LOEW, D. & GAUTREAU, A. 2009. The Arp2/3 activator WASH controls the fission of endosomes through a large multiprotein complex. *Dev Cell,* 17**,** 712-23.

DHILLON, H., ZIGMAN, J. M., YE, C., LEE, C. E., MCGOVERN, R. A., TANG, V., KENNY, C. D., CHRISTIANSEN, L. M., WHITE, R. D., EDELSTEIN, E. A., COPPARI, R., BALTHASAR, N., COWLEY, M. A., CHUA, S., JR., ELMQUIST, J. K. & LOWELL, B. B. 2006. Leptin directly activates SF1 neurons in the VMH, and this action by leptin is required for normal body-weight homeostasis. *Neuron,* 49**,** 191-203.

DIEZ-ROUX, G., BANFI, S., SULTAN, M., GEFFERS, L., ANAND, S., ROZADO, D., MAGEN, A., CANIDIO, E., PAGANI, M., PELUSO, I., LIN-MARQ, N., KOCH, M., BILIO, M., CANTIELLO, I., VERDE, R., DE MASI, C., BIANCHI, S. A., CICCHINI, J., PERROUD, E., MEHMETI, S., DAGAND, E., SCHRINNER, S., NURNBERGER, A., SCHMIDT, K., METZ, K., ZWINGMANN, C., BRIESKE, N., SPRINGER, C., HERNANDEZ, A. M., HERZOG, S., GRABBE, F., SIEVERDING, C., FISCHER, B., SCHRADER, K., BROCKMEYER, M., DETTMER, S., HELBIG, C., ALUNNI, V., BATTAINI, M. A., MURA, C., HENRICHSEN, C. N., GARCIA-LOPEZ, R.,

ECHEVARRIA, D., PUELLES, E., GARCIA-CALERO, E., KRUSE, S., UHR, M., KAUCK, C., FENG, G., MILYAEV, N., ONG, C. K., KUMAR, L., LAM, M., SEMPLE, C. A., GYENESEI, A., MUNDLOS, S., RADELOF, U., LEHRACH, H., SARMIENTOS, P., REYMOND, A., DAVIDSON, D. R., DOLLE, P., ANTONARAKIS, S. E., YASPO, M. L., MARTINEZ, S., BALDOCK, R. A., EICHELE, G. & BALLABIO, A. 2011. A high-resolution anatomical atlas of the transcriptome in the mouse embryo. *PLoS Biol,* 9**,** e1000582.

DOWN, J. L. 1887. *Mental Affections of Childhood and Youth,* London, Churchill.

DOYLE, J. M., GAO, J., WANG, J., YANG, M. & POTTS, P. R. 2010. MAGE-RING protein complexes comprise a family of E3 ubiquitin ligases. *Mol Cell,* 39**,** 963-74.

DUKER, A. L., BALLIF, B. C., BAWLE, E. V., PERSON, R. E., MAHADEVAN, S., ALLIMAN, S., THOMPSON, R., TRAYLOR, R., BEJJANI, B. A., SHAFFER, L. G., ROSENFELD, J. A., LAMB, A. N. & SAHOO, T. 2010. Paternally inherited microdeletion at 15q11.2 confirms a significant role for the SNORD116 C/D box snoRNA cluster in Prader-Willi syndrome. *Eur J Hum Genet,* 18**,** 1196-201.

EIHOLZER, U., L'ALLEMAND, D., ROUSSON, V., SCHLUMPF, M., GASSER, T., GIRARD, J., GRUTERS, A. & SIMONI, M. 2006. Hypothalamic and gonadal components of hypogonadism in boys with Prader-Labhart- Willi syndrome. *J Clin Endocrinol Metab,* 91**,** 892-8.

EINFELD, S. L., KAVANAGH, S. J., SMITH, A., EVANS, E. J., TONGE, B. J. & TAFFE, J. 2006. Mortality in Prader-Willi syndrome. *Am J Ment Retard,* 111**,** 193-8.

ENRIORI, P. J., SINNAYAH, P., SIMONDS, S. E., GARCIA RUDAZ, C. & COWLEY, M. A. 2011. Leptin action in the dorsomedial hypothalamus increases sympathetic tone to brown adipose tissue in spite of systemic leptin resistance. *J Neurosci,* 31**,** 12189-97.

FANI, L., BAK, S., DELHANTY, P., VAN ROSSUM, E. F. & VAN DEN AKKER, E. L. 2014. The melanocortin-4 receptor as target for obesity treatment: a systematic review of emerging pharmacological therapeutic options. *Int J Obes (Lond),* 38**,** 163-9.

FARBER, C., GROSS, S., NEESEN, J., BUITING, K. & HORSTHEMKE, B. 2000. Identification of a testis-specific gene (C15orf2) in the Prader-Willi syndrome region on chromosome 15. *Genomics,* 65**,** 174-83.

FARIAS, M. M., CUEVAS, A. M. & RODRIGUEZ, F. 2011. Set-point theory and obesity. *Metab Syndr Relat Disord,* 9**,** 85-9.

FAROOQI, I. S., KEOGH, J. M., YEO, G. S., LANK, E. J., CHEETHAM, T. & O'RAHILLY, S. 2003. Clinical spectrum of obesity and mutations in the melanocortin 4 receptor gene. *N Engl J Med,* 348**,** 1085-95.

FETISSOV, S. O., BERGSTROM, U., JOHANSEN, J. E., HOKFELT, T., SCHALLING, M. & RANSCHT, B. 2005. Alterations of arcuate nucleus neuropeptidergic development in contactin-deficient mice: comparison with anorexia and food-deprived mice. *Eur J Neurosci,* 22**,** 3217-28.

FU, L. Y. & VAN DEN POL, A. N. 2008. Agouti-related peptide and MC3/4 receptor agonists both inhibit excitatory hypothalamic ventromedial nucleus neurons. *J Neurosci,* 28**,** 5433-49.

GAO, Q., WOLFGANG, M. J., NESCHEN, S., MORINO, K., HORVATH, T. L., SHULMAN, G. I. & FU, X. Y. 2004. Disruption of neural signal transducer and activator of transcription 3 causes obesity, diabetes, infertility, and thermal dysregulation. *Proc Natl Acad Sci U S A,* 101**,** 4661-6.

GHISI, V., RAMSEY, A. J., MASRI, B., GAINETDINOV, R. R., CARON, M. G. & SALAHPOUR, A. 2009. Reduced D2-mediated signaling activity and trans-synaptic upregulation of D1 and D2 dopamine receptors in mice overexpressing the dopamine transporter. *Cell Signal,* 21**,** 87-94.

GLAVAS, M. M., JOACHIM, S. E., DRAPER, S. J., SMITH, M. S. & GROVE, K. L. 2007. Melanocortinergic activation by melanotan II inhibits feeding and increases uncoupling protein 1 messenger ribonucleic acid in the developing rat. *Endocrinology,* 148**,** 3279-87.

GLENN, C. C., DRISCOLL, D. J., YANG, T. P. & NICHOLLS, R. D. 1997. Genomic imprinting: potential function and mechanisms revealed by the Prader-Willi and Angelman syndromes. *Mol Hum Reprod,* 3**,** 321-32.

GLENN, C. C., SAITOH, S., JONG, M. T., FILBRANDT, M. M., SURTI, U., DRISCOLL, D. J. & NICHOLLS, R. D. 1996. Gene structure, DNA methylation, and imprinted expression of the human SNRPN gene. *Am J Hum Genet,* 58**,** 335-46.

GRAY, T. A., SAITOH, S. & NICHOLLS, R. D. 1999. An imprinted, mammalian bicistronic transcript encodes two independent proteins. *Proc Natl Acad Sci U S A,* 96**,** 5616-21.

GUNAY-AYGUN, M., SCHWARTZ, S., HEEGER, S., O'RIORDAN, M. A. & CASSIDY, S. B. 2001. The changing purpose of Prader-Willi syndrome clinical diagnostic criteria and proposed revised criteria. *Pediatrics,* 108**,** E92.

HALL, B. D. & SMITH, D. W. 1972. Prader-Willi syndrome. A resume of 32 cases including an instance of affected first cousins, one of whom is of normal stature and intelligence. *J Pediatr,* 81**,** 286-93.

HANSEN, M. J., BALL, M. J. & MORRIS, M. J. 2001. Enhanced inhibitory feeding response to alpha-melanocyte stimulating hormone in the diet-induced obese rat. *Brain Res,* 892**,** 130-7.

HAO, Y. H., DOYLE, J. M., RAMANATHAN, S., GOMEZ, T. S., JIA, D., XU, M., CHEN, Z. J., BILLADEAU, D. D., ROSEN, M. K. & POTTS, P. R. 2013. Regulation of WASH-dependent actin polymerization and protein trafficking by ubiquitination. *Cell,* 152**,** 1051-64.

HARBOUR, M. E., BREUSEGEM, S. Y. & SEAMAN, M. N. 2012. Recruitment of the endosomal WASH complex is mediated by the extended 'tail' of Fam21 binding to the retromer protein Vps35. *Biochem J,* 442**,** 209-20.

HASKELL-LUEVANO, C. & MONCK, E. K. 2001. Agouti-related protein functions as an inverse agonist at a constitutively active brain melanocortin-4 receptor. *Regul Pept,* 99**,** 1-7.

HERTZ, G., CATALETTO, M., FEINSILVER, S. H. & ANGULO, M. 1995. Developmental trends of sleep-disordered breathing in Prader-Willi syndrome: the role of obesity. *Am J Med Genet,* 56**,** 188-90.

HILEMAN, S. M., PIERROZ, D. D., MASUZAKI, H., BJORBAEK, C., EL-HASCHIMI, K., BANKS, W. A. & FLIER, J. S. 2002. Characterizaton of short isoforms of the leptin receptor in rat cerebral microvessels and of brain uptake of leptin in mouse models of obesity. *Endocrinology,* 143**,** 775-83.

HILL, J. W., WILLIAMS, K. W., YE, C., LUO, J., BALTHASAR, N., COPPARI, R., COWLEY, M. A., CANTLEY, L. C., LOWELL, B. B. & ELMQUIST, J. K. 2008. Acute effects of leptin require PI3K signaling in hypothalamic proopiomelanocortin neurons in mice. *J Clin Invest,* 118**,** 1796-805.

HIMMS-HAGEN, J. 1985. Defective brown adipose tissue thermogenesis in obese mice. *Int J Obes,* 9 Suppl 2**,** 17-24.
HOLM, V. A., CASSIDY, S. B., BUTLER, M. G., HANCHETT, J. M., GREENSWAG, L. R., WHITMAN, B. Y. & GREENBERG, F. 1993. Prader-Willi syndrome: consensus diagnostic criteria. *Pediatrics,* 91**,** 398-402.
HORSTHEMKE, B. & BUITING, K. 2006. Imprinting defects on human chromosome 15. *Cytogenet Genome Res,* 113**,** 292-9.
JANCAR, J. 1971. Prader-Willi syndrome. (Hypotonia, obesity, hypogonadism, growth and mental retardation). *J Ment Defic Res,* 15**,** 20-9.
JONG, M. T., GRAY, T. A., JI, Y., GLENN, C. C., SAITOH, S., DRISCOLL, D. J. & NICHOLLS, R. D. 1999. A novel imprinted gene, encoding a RING zinc-finger protein, and overlapping antisense transcript in the Prader-Willi syndrome critical region. *Hum Mol Genet,* 8**,** 783-93.
KAY, B. K., WILLIAMSON, M. P. & SUDOL, M. 2000. The importance of being proline: the interaction of proline-rich motifs in signaling proteins with their cognate domains. *Faseb j,* 14**,** 231-41.
KHACHATURIAN, H., ALESSI, N. E., LEWIS, M. E., MUNFAKH, N., FITZSIMMONS, M. D. & WATSON, S. J. 1985. Development of hypothalamic opioid neurons: a combined immunocytochemical and [3H]thymidine autoradiographic study. *Neuropeptides,* 5**,** 477-80.
KIM, S. J., MILLER, J. L., KUIPERS, P. J., GERMAN, J. R., BEAUDET, A. L., SAHOO, T. & DRISCOLL, D. J. 2012. Unique and atypical deletions in Prader-Willi syndrome reveal distinct phenotypes. *Eur J Hum Genet,* 20**,** 283-90.
KING, C. M. & HENTGES, S. T. 2011. Relative number and distribution of murine hypothalamic proopiomelanocortin neurons innervating distinct target sites. *PLoS One,* 6**,** e25864.
KISHORE, S. & STAMM, S. 2006. Regulation of alternative splicing by snoRNAs. *Cold Spring Harb Symp Quant Biol,* 71**,** 329-34.
KOLK, S. M., KRAMER, B. M., CORNELISSE, L. N., SCHEENEN, W. J., JENKS, B. G. & ROUBOS, E. W. 2002. Multiple control and dynamic response of the Xenopus melanotrope cell. *Comp Biochem Physiol B Biochem Mol Biol,* 132**,** 257-68.
KOZLOV, S. V., BOGENPOHL, J. W., HOWELL, M. P., WEVRICK, R., PANDA, S., HOGENESCH, J. B., MUGLIA, L. J., VAN GELDER, R. N., HERZOG, E. D. & STEWART, C. L. 2007. The imprinted gene Magel2 regulates normal circadian output. *Nat Genet,* 39**,** 1266-72.
KUBLAOUI, B. M., HOLDER, J. L., JR., GEMELLI, T. & ZINN, A. R. 2006. Sim1 haploinsufficiency impairs melanocortin-mediated anorexia and activation of paraventricular nucleus neurons. *Mol Endocrinol,* 20**,** 2483-92.
LADYMAN, S. R., FIELDWICK, D. M. & GRATTAN, D. R. 2012. Suppression of leptin-induced hypothalamic JAK/STAT signalling and feeding response during pregnancy in the mouse. *Reproduction,* 144**,** 83-90.
LAFONTAINE, J., TCHAKARSKA, G., RODIER, F. & MES-MASSON, A. M. 2012. Necdin modulates proliferative cell survival of human cells in response to radiation-induced genotoxic stress. *BMC Cancer,* 12**,** 234.
LEE, S., KOZLOV, S., HERNANDEZ, L., CHAMBERLAIN, S. J., BRANNAN, C. I., STEWART, C. L. & WEVRICK, R. 2000. Expression and imprinting of MAGEL2

suggest a role in Prader-willi syndrome and the homologous murine imprinting phenotype. *Hum Mol Genet,* 9**,** 1813-9.

LEE, S., WALKER, C. L. & WEVRICK, R. 2003. Prader-Willi syndrome transcripts are expressed in phenotypically significant regions of the developing mouse brain. *Gene Expr Patterns,* 3**,** 599-609.

LEIBEL, R. L., ROSENBAUM, M. & HIRSCH, J. 1995. Changes in energy expenditure resulting from altered body weight. *N Engl J Med,* 332**,** 621-8.

LEIN, E. S., HAWRYLYCZ, M. J., AO, N., AYRES, M., BENSINGER, A., BERNARD, A., BOE, A. F., BOGUSKI, M. S., BROCKWAY, K. S., BYRNES, E. J., CHEN, L., CHEN, L., CHEN, T. M., CHIN, M. C., CHONG, J., CROOK, B. E., CZAPLINSKA, A., DANG, C. N., DATTA, S., DEE, N. R., DESAKI, A. L., DESTA, T., DIEP, E., DOLBEARE, T. A., DONELAN, M. J., DONG, H. W., DOUGHERTY, J. G., DUNCAN, B. J., EBBERT, A. J., EICHELE, G., ESTIN, L. K., FABER, C., FACER, B. A., FIELDS, R., FISCHER, S. R., FLISS, T. P., FRENSLEY, C., GATES, S. N., GLATTFELDER, K. J., HALVERSON, K. R., HART, M. R., HOHMANN, J. G., HOWELL, M. P., JEUNG, D. P., JOHNSON, R. A., KARR, P. T., KAWAL, R., KIDNEY, J. M., KNAPIK, R. H., KUAN, C. L., LAKE, J. H., LARAMEE, A. R., LARSEN, K. D., LAU, C., LEMON, T. A., LIANG, A. J., LIU, Y., LUONG, L. T., MICHAELS, J., MORGAN, J. J., MORGAN, R. J., MORTRUD, M. T., MOSQUEDA, N. F., NG, L. L., NG, R., ORTA, G. J., OVERLY, C. C., PAK, T. H., PARRY, S. E., PATHAK, S. D., PEARSON, O. C., PUCHALSKI, R. B., RILEY, Z. L., ROCKETT, H. R., ROWLAND, S. A., ROYALL, J. J., RUIZ, M. J., SARNO, N. R., SCHAFFNIT, K., SHAPOVALOVA, N. V., SIVISAY, T., SLAUGHTERBECK, C. R., SMITH, S. C., SMITH, K. A., SMITH, B. I., SODT, A. J., STEWART, N. N., STUMPF, K. R., SUNKIN, S. M., SUTRAM, M., TAM, A., TEEMER, C. D., THALLER, C., THOMPSON, C. L., VARNAM, L. R., VISEL, A., WHITLOCK, R. M., WOHNOUTKA, P. E., WOLKEY, C. K., WONG, V. Y., et al. 2007. Genome-wide atlas of gene expression in the adult mouse brain. *Nature,* 445**,** 168-76.

LEVINE, B. & KLIONSKY, D. J. 2004. Development by self-digestion: molecular mechanisms and biological functions of autophagy. *Dev Cell,* 6**,** 463-77.

LI, G., ZHANG, Y., WILSEY, J. T. & SCARPACE, P. J. 2004. Unabated anorexic and enhanced thermogenic responses to melanotan II in diet-induced obese rats despite reduced melanocortin 3 and 4 receptor expression. *J Endocrinol,* 182**,** 123-32.

LONNQVIST, F., NORDFORS, L., JANSSON, M., THORNE, A., SCHALLING, M. & ARNER, P. 1997. Leptin secretion from adipose tissue in women. Relationship to plasma levels and gene expression. *J Clin Invest,* 99**,** 2398-404.

LORICK, K. L., JENSEN, J. P., FANG, S., ONG, A. M., HATAKEYAMA, S. & WEISSMAN, A. M. 1999. RING fingers mediate ubiquitin-conjugating enzyme (E2)-dependent ubiquitination. *Proc Natl Acad Sci U S A,* 96**,** 11364-9.

LUPSKI, J. R. 1998. Genomic disorders: structural features of the genome can lead to DNA rearrangements and human disease traits. *Trends Genet,* 14**,** 417-22.

MACDONALD, H. R. & WEVRICK, R. 1997. The necdin gene is deleted in Prader-Willi syndrome and is imprinted in human and mouse. *Hum Mol Genet,* 6**,** 1873-8.

MAIURI, M. C., ZALCKVAR, E., KIMCHI, A. & KROEMER, G. 2007. Self-eating and self-killing: crosstalk between autophagy and apoptosis. *Nat Rev Mol Cell Biol,* 8**,** 741-52.

MARSH, D. J., HOLLOPETER, G., HUSZAR, D., LAUFER, R., YAGALOFF, K. A., FISHER, S. L., BURN, P. & PALMITER, R. D. 1999. Response of melanocortin-4 receptor-deficient mice to anorectic and orexigenic peptides. *Nat Genet,* 21**,** 119-22.

MAZURKIEWICZ, J. E., CORLISS, D. & SLOMINSKI, A. 2000. Spatiotemporal expression, distribution, and processing of POMC and POMC-derived peptides in murine skin. *J Histochem Cytochem,* 48**,** 905-14.

MEISTER, B., GOMUC, B., SUAREZ, E., ISHII, Y., DURR, K. & GILLBERG, L. 2006. Hypothalamic proopiomelanocortin (POMC) neurons have a cholinergic phenotype. *Eur J Neurosci,* 24**,** 2731-40.

MELNICK, I., PRONCHUK, N., COWLEY, M. A., GROVE, K. L. & COLMERS, W. F. 2007. Developmental switch in neuropeptide Y and melanocortin effects in the paraventricular nucleus of the hypothalamus. *Neuron,* 56**,** 1103-15.

MERCER, J. G., HOGGARD, N., WILLIAMS, L. M., LAWRENCE, C. B., HANNAH, L. T. & TRAYHURN, P. 1996. Localization of leptin receptor mRNA and the long form splice variant (Ob-Rb) in mouse hypothalamus and adjacent brain regions by in situ hybridization. *FEBS Lett,* 387**,** 113-6.

MERCER, R. E., KWOLEK, E. M., BISCHOF, J. M., VAN EEDE, M., HENKELMAN, R. M. & WEVRICK, R. 2009. Regionally reduced brain volume, altered serotonin neurochemistry, and abnormal behavior in mice null for the circadian rhythm output gene Magel2. *Am J Med Genet B Neuropsychiatr Genet,* 150b**,** 1085-99.

MERCER, R. E., MICHAELSON, S. D., CHEE, M. J., ATALLAH, T. A., WEVRICK, R. & COLMERS, W. F. 2013. Magel2 is required for leptin-mediated depolarization of POMC neurons in the hypothalamic arcuate nucleus in mice. *PLoS Genet,* 9**,** e1003207.

MERCER, R. E. & WEVRICK, R. 2009. Loss of magel2, a candidate gene for features of Prader-Willi syndrome, impairs reproductive function in mice. *PLoS One,* 4**,** e4291.

MILLER, J. L., LYNN, C. H., DRISCOLL, D. C., GOLDSTONE, A. P., GOLD, J. A., KIMONIS, V., DYKENS, E., BUTLER, M. G., SHUSTER, J. J. & DRISCOLL, D. J. 2011. Nutritional phases in Prader-Willi syndrome. *Am J Med Genet A,* 155a**,** 1040-9.

MILLER, N. L., WEVRICK, R. & MELLON, P. L. 2009. Necdin, a Prader-Willi syndrome candidate gene, regulates gonadotropin-releasing hormone neurons during development. *Hum Mol Genet,* 18**,** 248-60.

MISTRY, A. M., SWICK, A. & ROMSOS, D. R. 1999. Leptin alters metabolic rates before acquisition of its anorectic effect in developing neonatal mice. *Am J Physiol,* 277**,** R742-7.

MOCK, S., SHEN, X. & TAMVAKOPOULOS, C. 2002. Determination of melanotan-II in rat plasma by liquid chromatography/tandem mass spectrometry: determination of pharmacokinetic parameters in rat following intravenous administration. *Rapid Commun Mass Spectrom,* 16**,** 2142-7.

MORTON, G. J., CUMMINGS, D. E., BASKIN, D. G., BARSH, G. S. & SCHWARTZ, M. W. 2006. Central nervous system control of food intake and body weight. *Nature,* 443**,** 289-95.

MORTON, G. J., MEEK, T. H. & SCHWARTZ, M. W. 2014. Neurobiology of food intake in health and disease. *Nat Rev Neurosci,* 15**,** 367-78.

MUELLER, W. M., GREGOIRE, F. M., STANHOPE, K. L., MOBBS, C. V., MIZUNO, T. M., WARDEN, C. H., STERN, J. S. & HAVEL, P. J. 1998. Evidence that glucose

metabolism regulates leptin secretion from cultured rat adipocytes. *Endocrinology,* 139**,** 551-8.
MUSCATELLI, F., ABROUS, D. N., MASSACRIER, A., BOCCACCIO, I., LE MOAL, M., CAU, P. & CREMER, H. 2000. Disruption of the mouse Necdin gene results in hypothalamic and behavioral alterations reminiscent of the human Prader-Willi syndrome. *Hum Mol Genet,* 9**,** 3101-10.
NEUMANN, L. C., FEINER, N., MEYER, A., BUITING, K. & HORSTHEMKE, B. 2014. The imprinted NPAP1 gene in the Prader-Willi syndrome region belongs to a POM121-related family of retrogenes. *Genome Biol Evol,* 6**,** 344-51.
NEUMANN, L. C., MARKAKI, Y., MLADENOV, E., HOFFMANN, D., BUITING, K. & HORSTHEMKE, B. 2012. The imprinted NPAP1/C15orf2 gene in the Prader-Willi syndrome region encodes a nuclear pore complex associated protein. *Hum Mol Genet,* 21**,** 4038-48.
OHMAN-FORSLUND, K. & NORDQVIST, K. 2001. The melanoma antigen genes--any clues to their functions in normal tissues? *Exp Cell Res,* 265**,** 185-94.
OLNEY, J. J., NAVARRO, M. & THIELE, T. E. 2014. Targeting central melanocortin receptors: a promising novel approach for treating alcohol abuse disorders. *Front Neurosci,* 8**,** 128.
OLTMANS, G. A. 1983. Norepinephrine and dopamine levels in hypothalamic nuclei of the genetically obese mouse (ob/ob). *Brain Res,* 273**,** 369-73.
PADILLA, S. L., CARMODY, J. S. & ZELTSER, L. M. 2010. Pomc-expressing progenitors give rise to antagonistic neuronal populations in hypothalamic feeding circuits. *Nat Med,* 16**,** 403-5.
PEREIRA, L., GIRARDI, J. P. & BAKOVIC, M. 2012. Forms, crosstalks, and the role of phospholipid biosynthesis in autophagy. *Int J Cell Biol,* 2012**,** 931956.
PERELLO, M. & RAINGO, J. 2013. Leptin activates oxytocin neurons of the hypothalamic paraventricular nucleus in both control and diet-induced obese rodents. *PLoS One,* 8**,** e59625.
PIERROZ, D. D., ZIOTOPOULOU, M., UNGSUNAN, L., MOSCHOS, S., FLIER, J. S. & MANTZOROS, C. S. 2002. Effects of acute and chronic administration of the melanocortin agonist MTII in mice with diet-induced obesity. *Diabetes,* 51**,** 1337-45.
POKK, P., KIVASTIK, T., SOBOL, D., LILJEQUIST, S. & ZHARKOVSKY, A. 1996. Is upregulation of benzodiazepine receptors a compensatory reaction to reduced GABAergic tone in the brain of stressed mice? *Naunyn Schmiedebergs Arch Pharmacol,* 354**,** 703-8.
PRADER, A., LABHART, A. & WILLI, H. 1956. Ein syndrom von Adipositas, Kleinwuchs, Kryptorchidismus und Oligophrenie nach Myatonieartigem Zustand im Neugeborenalter. *Schweiz Med Wschr,* 86**,** 1260-1261.
RAHMOUNI, K., SIGMUND, C. D., HAYNES, W. G. & MARK, A. L. 2009. Hypothalamic ERK mediates the anorectic and thermogenic sympathetic effects of leptin. *Diabetes,* 58**,** 536-42.
REN, J., LEE, S., PAGLIARDINI, S., GERARD, M., STEWART, C. L., GREER, J. J. & WEVRICK, R. 2003. Absence of Ndn, encoding the Prader-Willi syndrome-deleted gene necdin, results in congenital deficiency of central respiratory drive in neonatal mice. *J Neurosci,* 23**,** 1569-73.

RITTER, R. C. 2004. Gastrointestinal mechanisms of satiation for food. *Physiol Behav,* 81**,** 249-73.
ROBERTSON, S. A., LEINNINGER, G. M. & MYERS, M. G., JR. 2008. Molecular and neural mediators of leptin action. *Physiol Behav,* 94**,** 637-42.
RUNTE, M., VARON, R., HORN, D., HORSTHEMKE, B. & BUITING, K. 2005. Exclusion of the C/D box snoRNA gene cluster HBII-52 from a major role in Prader-Willi syndrome. *Hum Genet,* 116**,** 228-30.
SAHOO, T., DEL GAUDIO, D., GERMAN, J. R., SHINAWI, M., PETERS, S. U., PERSON, R. E., GARNICA, A., CHEUNG, S. W. & BEAUDET, A. L. 2008. Prader-Willi phenotype caused by paternal deficiency for the HBII-85 C/D box small nucleolar RNA cluster. *Nat Genet,* 40**,** 719-21.
SCARPACE, P. J., MATHENY, M., ZOLOTUKHIN, S., TUMER, N. & ZHANG, Y. 2003. Leptin-induced leptin resistant rats exhibit enhanced responses to the melanocortin agonist MT II. *Neuropharmacology,* 45**,** 211-9.
SCHAAF, C. P., GONZALEZ-GARAY, M. L., XIA, F., POTOCKI, L., GRIPP, K. W., ZHANG, B., PETERS, B. A., MCELWAIN, M. A., DRMANAC, R., BEAUDET, A. L., CASKEY, C. T. & YANG, Y. 2013. Truncating mutations of MAGEL2 cause Prader-Willi phenotypes and autism. *Nat Genet,* 45**,** 1405-8.
SCHRANDER-STUMPEL, C. T., CURFS, L. M., SASTROWIJOTO, P., CASSIDY, S. B., SCHRANDER, J. J. & FRYNS, J. P. 2004. Prader-Willi syndrome: causes of death in an international series of 27 cases. *Am J Med Genet A,* 124a**,** 333-8.
SCHULZE, A., HANSEN, C., SKAKKEBAEK, N. E., BRONDUM-NIELSEN, K., LEDBETER, D. H. & TOMMERUP, N. 1996. Exclusion of SNRPN as a major determinant of Prader-Willi syndrome by a translocation breakpoint. *Nat Genet,* 12**,** 452-4.
SCHWARTZ, M. W., WOODS, S. C., PORTE, D., JR., SEELEY, R. J. & BASKIN, D. G. 2000. Central nervous system control of food intake. *Nature,* 404**,** 661-71.
SHARP, A. J., HANSEN, S., SELZER, R. R., CHENG, Z., REGAN, R., HURST, J. A., STEWART, H., PRICE, S. M., BLAIR, E., HENNEKAM, R. C., FITZPATRICK, C. A., SEGRAVES, R., RICHMOND, T. A., GUIVER, C., ALBERTSON, D. G., PINKEL, D., EIS, P. S., SCHWARTZ, S., KNIGHT, S. J. & EICHLER, E. E. 2006. Discovery of previously unidentified genomic disorders from the duplication architecture of the human genome. *Nat Genet,* 38**,** 1038-42.
SIMPSON, A. J., CABALLERO, O. L., JUNGBLUTH, A., CHEN, Y. T. & OLD, L. J. 2005. Cancer/testis antigens, gametogenesis and cancer. *Nat Rev Cancer,* 5**,** 615-25.
SOHN, J. W., XU, Y., JONES, J. E., WICKMAN, K., WILLIAMS, K. W. & ELMQUIST, J. K. 2011. Serotonin 2C receptor activates a distinct population of arcuate pro-opiomelanocortin neurons via TRPC channels. *Neuron,* 71**,** 488-97.
SOLOMON, A., DE FANTI, B. A. & MARTINEZ, J. A. 2006. The nucleus tractus solitari (NTS) participates in peripheral ghrelin glucostatic hunger signalling mediated by insulin. *Neuropeptides,* 40**,** 169-75.
STEVENSON, D. A., ANAYA, T. M., CLAYTON-SMITH, J., HALL, B. D., VAN ALLEN, M. I., ZORI, R. T., ZACKAI, E. H., FRANK, G. & CLERICUZIO, C. L. 2004. Unexpected death and critical illness in Prader-Willi syndrome: report of ten individuals. *Am J Med Genet A,* 124a**,** 158-64.

STOSIEK, C., GARASCHUK, O., HOLTHOFF, K. & KONNERTH, A. 2003. In vivo two-photon calcium imaging of neuronal networks. *Proc Natl Acad Sci U S A,* 100**,** 7319-24.
STRUBBE, J. H. & WOODS, S. C. 2004. The timing of meals. *Psychol Rev,* 111**,** 128-41.
SUTTON, G. M., TREVASKIS, J. L., HULVER, M. W., MCMILLAN, R. P., MARKWARD, N. J., BABIN, M. J., MEYER, E. A. & BUTLER, A. A. 2006. Diet-genotype interactions in the development of the obese, insulin-resistant phenotype of C57BL/6J mice lacking melanocortin-3 or -4 receptors. *Endocrinology,* 147**,** 2183-96.
SUTTON, M. A., SCHMIDT, E. F., CHOI, K. H., SCHAD, C. A., WHISLER, K., SIMMONS, D., KARANIAN, D. A., MONTEGGIA, L. M., NEVE, R. L. & SELF, D. W. 2003. Extinction-induced upregulation in AMPA receptors reduces cocaine-seeking behaviour. *Nature,* 421**,** 70-5.
TAUBER, M., DIENE, G., MOLINAS, C. & HEBERT, M. 2008. Review of 64 cases of death in children with Prader-Willi syndrome (PWS). *Am J Med Genet A,* 146**,** 881-7.
TENNESE, A. A. & WEVRICK, R. 2011. Impaired hypothalamic regulation of endocrine function and delayed counterregulatory response to hypoglycemia in Magel2-null mice. *Endocrinology,* 152**,** 967-78.
TSAI, T. F., JIANG, Y. H., BRESSLER, J., ARMSTRONG, D. & BEAUDET, A. L. 1999. Paternal deletion from Snrpn to Ube3a in the mouse causes hypotonia, growth retardation and partial lethality and provides evidence for a gene contributing to Prader-Willi syndrome. *Hum Mol Genet,* 8**,** 1357-64.
VAN DER BRUGGEN, P., TRAVERSARI, C., CHOMEZ, P., LURQUIN, C., DE PLAEN, E., VAN DEN EYNDE, B., KNUTH, A. & BOON, T. 1991. A gene encoding an antigen recognized by cytolytic T lymphocytes on a human melanoma. *Science,* 254**,** 1643-7.
WANG, C., GODAR, R. J., BILLINGTON, C. J. & KOTZ, C. M. 2010. Chronic administration of brain-derived neurotrophic factor in the hypothalamic paraventricular nucleus reverses obesity induced by high-fat diet. *Am J Physiol Regul Integr Comp Physiol,* 298**,** R1320-32.
WAWRZIK, M., UNMEHOPA, U. A., SWAAB, D. F., VAN DE NES, J., BUITING, K. & HORSTHEMKE, B. 2010. The C15orf2 gene in the Prader-Willi syndrome region is subject to genomic imprinting and positive selection. *Neurogenetics,* 11**,** 153-61.
WILLIAMS, K. W., MARGATHO, L. O., LEE, C. E., CHOI, M., LEE, S., SCOTT, M. M., ELIAS, C. F. & ELMQUIST, J. K. 2010. Segregation of acute leptin and insulin effects in distinct populations of arcuate proopiomelanocortin neurons. *J Neurosci,* 30**,** 2472-9.
WOODS, S. C., CHAVEZ, M., PARK, C. R., RIEDY, C., KAIYALA, K., RICHARDSON, R. D., FIGLEWICZ, D. P., SCHWARTZ, M. W., PORTE, D., JR. & SEELEY, R. J. 1996. The evaluation of insulin as a metabolic signal influencing behavior via the brain. *Neurosci Biobehav Rev,* 20**,** 139-44.
WRANN, C. D., EGUCHI, J., BOZEC, A., XU, Z., MIKKELSEN, T., GIMBLE, J., NAVE, H., WAGNER, E. F., ONG, S. E. & ROSEN, E. D. 2012. FOSL2 promotes leptin gene expression in human and mouse adipocytes. *J Clin Invest,* 122**,** 1010-21.
WREN, A. M., SMALL, C. J., FRIBBENS, C. V., NEARY, N. M., WARD, H. L., SEAL, L. J., GHATEI, M. A. & BLOOM, S. R. 2002. The hypothalamic mechanisms of the hypophysiotropic action of ghrelin. *Neuroendocrinology,* 76**,** 316-24.
WRIGHT, A. & WILSON, J. F. 1983. Absorption of alpha-MSH from subcutaneous and intraperitoneal sites in the rat. *Peptides,* 4**,** 5-9.

XU, A. W., STE-MARIE, L., KAELIN, C. B. & BARSH, G. S. 2007. Inactivation of signal transducer and activator of transcription 3 in proopiomelanocortin (Pomc) neurons causes decreased pomc expression, mild obesity, and defects in compensatory refeeding. *Endocrinology,* 148**,** 72-80.

XU, B., GOULDING, E. H., ZANG, K., CEPOI, D., CONE, R. D., JONES, K. R., TECOTT, L. H. & REICHARDT, L. F. 2003. Brain-derived neurotrophic factor regulates energy balance downstream of melanocortin-4 receptor. *Nat Neurosci,* 6**,** 736-42.

ZANELLA, S., BARTHELEMY, M., MUSCATELLI, F. & HILAIRE, G. 2008. Necdin gene, respiratory disturbances and Prader-Willi syndrome. *Adv Exp Med Biol,* 605**,** 159-64.

ZAVODSZKY, E., SEAMAN, M. N., MOREAU, K., JIMENEZ-SANCHEZ, M., BREUSEGEM, S. Y., HARBOUR, M. E. & RUBINSZTEIN, D. C. 2014. Mutation in VPS35 associated with Parkinson's disease impairs WASH complex association and inhibits autophagy. *Nat Commun,* 5**,** 3828.

ZHAN, C., ZHOU, J., FENG, Q., ZHANG, J. E., LIN, S., BAO, J., WU, P. & LUO, M. 2013. Acute and long-term suppression of feeding behavior by POMC neurons in the brainstem and hypothalamus, respectively. *J Neurosci,* 33**,** 3624-32.

ZHANG, Y., COLLAZO, R., GAO, Y., LI, G. & SCARPACE, P. J. 2010. Intermittent MTII application evokes repeated anorexia and robust fat and weight loss. *Peptides,* 31**,** 639-43.